ADM80017 – Master Thesis

SWiNBURNE
SWINBURNE UNIVERSITY OF TECHNOLOGY

MECHANICAL PROPERTIES AND ENERGY ABSORPTION CAPABILITY OF FUNCTIONALLY GRADED F2CCZ LATTICE MATERIALS FABRICATED BY SLM

By:

Dheyaa S. J. AL-SAEDI

Student ID: 100035769

Supervised by:

Prof. Syed Masood

A thesis submitted to the Faculty of Science, Engineering & Technology, in partial fulfilment of the requirements for the degree of Master of Engineering Science in Advanced Manufacturing Technology

Swinburne University of Technology

Hawthorn, Victoria, Australia

November 2017

ABSTRACT

Recently, 3D lattice structures have attracted an attention of a large number of applications such as personal protective equipment and packaging due to their distinctive properties, in particular combining the lightweight and high strength. In this research study, mechanical properties and energy absorption capability of uniform and functionally graded lattice structure of F2CCZ style, made of Al-12Si and manufactured by selective laser melting (SLM) process, were investigated. The lattice structures were uniformly and gradually dense with equal relative density. Solution heat treatment (T6) was applied to study the effect on the microstructure and mechanical characteristics of the fabricated SLM-samples. Un-axial compression tests were conducted in build direction to evaluate the mechanical characteristics of the lattice structures. Numerical analysis of compression behaviour was performed using LS-DYNA code of the ANSYS© software to verify the experimental results. In addition, Optical Microscope (OM), Scanning Electron Microscopy (SEM) and X-ray diffraction (XRD) were used to study and investigate the microstructure changes and fracture surface morphology. Lastly, the Gibson and Ashby equations has been established to investigate analytical models for the two-lattice structures.

The experimental investigations have clearly shown that SLM technology can successfully produce the lattice structure such as F2CCZ with good repeatability and high manufacturability. OM and SEM images show that SLM process resulted in an Al-12Si alloy with a characteristically fine microstructure. As-fabricated SLM-microstructure consists different areas, fine grain size of Si and Al in hatch core (melt pool core) and coarse grain sizes at the hatch overlaps (laser scan track). Room tensile tests of as-fabricated SLM-samples exhibited high mechanical properties at the expense of the ductility. Following T6 treatment, the investigations show a significant effect of the heat treatment T6 on the microstructure and the mechanical properties of the Al-12Si material. The results reveal that the yield and fracture strength decrease to about 50% and 43%, while the ductility (fracture strain) has been increased to about 63%. XRD and OM analysis demonstrate that the microstructure of heat-treated SLM-sample have become coarse and homogenous due to grow of Si and Al grain size with complete absence of the microstructure difference regions; dendrites, laser traces, heat affected zones and hatch cores.

The compression tests have shown that functionally graded lattice structures exhibited distinctive and different deformation behaviour than the uniform lattice structures, with the collapse of layers occurring sequentially, starting with a lowest density layer to higher density one in sequence. The uniform lattice structures were found to be homogeneously deformed under compressive loads due to the formation of 45° diagonal shear band along with fracture and flake failures. The experimental investigation of the as-build-lattice structure shows brittle deformation behaviour that is resulting in large decrease and fluctuations in compressive strength. Conducting T6 treatment has significantly eliminated the brittle fracture and low strain failure of as-build lattice structures. The deformation behaviour of the heat-treaded lattice structure exhibited distinct response by providing typical stress strain curve, which includes ideal compressive regions. Finite element analysis results were found to agree well with the empirical findings of the examined heat-treated lattice structures, but these was some discrepancy in comparison with experimental results of as-build lattice structures. Calculation of total energy absorption showed that the gradually dense lattice structure absorbed higher energy than a uniform lattice structure of which 8.03 ± 0.03 MJ/m^3 and 8.336 ± 0.02 MJ/m^3 are the total amount of energy absorbed by heat-treated functionally graded and non-graded lattice structures respectively.

Furthermore, Gibson and Ashby's equations had been established to find out the pre-fectors $C1$, $C5$ and α for functionally graded and uniform lattice structures under the as-fabricated and heat-treated conditions. The determined values of $C1$ and α were found in good agreement with the given range of values by Gibson and Ashby [1], while C5 values were found to be relatively higher.

These results increase the potential that the functionally graded lattice structures of F2CCZ style or other models with of density gradient would be more desirable for an application that required high energy absorption capability. Their deformation response eliminates the conventional failure behaviour, by which they exhibit sophisticated and different collapse behaviour. Consequently, these results give indications that graded lattice structures are more suitable and attractive for applications that required high crush resistance.

ACKNOWLEDGEMENT

DECLARATION

I hereby certify that this document does not contain any material, without consent, used earlier for a degree or diploma certificate; and to the best of our knowledge and belief previously published in any other book or written by another person except where reference is provided. I do consider that using materials and works from other reports and books without providing proper reference may lead to strong disciplinary action may be taken according to Swinburne University of Technology guidelines.

Signed:

Candidate's Full Name: Dheyaa Sabeeh Jasim AL-SAEDI

Student Number: 100035769

Contents

List of Figures

List of Tables

<div align="center">

Chapter 1

INTRODUCTION

</div>

1.1. Overview

This chapter provides an introduction of the research's topic, the main objectives and the problems' statements. Furthermore, it reviews the significance of this research study and the organization of the project.

1.2. Background

Functionally graded lattice structure or functionally graded material (FGM) is a new class of engineered materials that are characterized by changing the composition or structural design gradually over the material volume, resulting in corresponding changes in the properties (mechanical, thermal) in one direction or more directions over the bulk material. FGMs is considered as one of the promising solutions in the science of materials engineering, which has potential applications in various aspects like aerospace, medicine, and engineering devices due to its attractive properties. Traditionally, lattice structure or porosity material has been fabricated using different conventional techniques like melt gas injection [1, 2], investment casting [3], stack and joining the laminated plates [4, 5], physical vapour deposition (PVD) [6] and sheet metal technique [1, 7]. However, these conventional fabrication methods have some limitations such as high cost , limited design freedoms [8], incapability to produce FGMs with structural gradient [9], their effectiveness to the shape complexity [10] and discrepancy in properties of producing cellular structures [11].

Recently, The advancements in additive manufacturing technology, particularly selective laser melting (SLM) process, has shown the ability to manufacture lattice or cellular structures for a wide range of applications due to its ability to overcome the limitations of the conventional techniques. The advantages of metallic additive manufacturing include the ability to fabricate lattice structures in micro scale range, unlimited intricate geometries, high control of internal architecture of voids and solid struts of unit cell and FGMs with structural gradient [9, 12-14].

The use aluminum and aluminum-alloy (Al-12Si) in production of the lattice structure on SLM has been the focus of many researchers because of the distinctive properties of the Al - alloy such as low density, high strength, adequate hardenability, wear and corrosion resistance, and weldability [15].

In this research study, a new approach of designing F2CCZ style functionally graded lattice structures with linearly and continuously changing density gradient throughout the structural layers is proposed for energy absorption applications. Compressive mechanical properties and energy absorption capability of functionally graded F2CCZ lattice structures made of Al-12Si and fabricated by SLM are experimentally investigated and compared to the uniform lattice structure without compromising on the overall volume fraction. The resulted data of the experimental work are verified using finite element analysis (FEA) study. FEA models are developed and conducted using LS-DYNA code of ANSYS© software. The effect of the heat treatment on the compressive behaviour of the uniform and functionally graded lattice structure, dimensional accuracy and surface morphology are also investigated. Further, Gibson and Ashby's equations [1] are empirically applied for examined lattice structures to find out analytical models of these structures for future use.

1.3.   The significance and novelty of this research

The importance of the current study lies with the need to develop a new design approach for functionally graded lattice structures with continuous and linear density gradients to provide novel deformation behaviour for energy absorption applications. The research studies available so far report on lattice structures made with abrupt, step-wise and changed separately in each layer density gradient. To assess the ability of the SLM process to manufacture such designed lattice structure from Al-12Si is another importance. In addition, conducting and developing finite element analysis for this new approach of the lattice structure and verify the experimental results is a novel. Furthermore, there is insufficient data on the effect of solution heat treatment (T6) on the compressive deformation behaviour and thus the energy absorption behaviour of SLM-Al -12Si, which this effect will be provided.

1.4.   The aim and objectives of the research

This research aims to investigate the compressive mechanical properties and energy absorption capability and a new designing approach of F2CCZ functionally graded lattice structure made of Al-12Si and fabricated by SLM technology, considering the effect of heat treatment on the microstructure and its mechanical performance. To achieve this main aim, the research is divided into the following individual objectives.

1.4.1.   The research objectives are:

1. Design functionally graded and uniform lattice structures made of F2CCZ unit cell with equal relative density using PTC^{TM} Creo Parametric 3.0 software.

2. Manufacturing the CAD models of designed lattice structures using SLM process to assess its ability to produce such structures.

3. Evaluating the microstructures and tensile mechanical characteristics of SLM processed Al-12Si test samples in as-build condition and after conducting the solution heat treatment T6 on these samples.

4. Conducting experimental test (compression tests) for investigating the compressive properties and energy absorption capability of as-fabricated and heat-treated F2CCZ lattice structures.

5. Conducting the finite element analysis FEA to study the compressive deformation behaviour of the modelled lattice structures and for comparison with the experimental results.

1.5.   Organisation of thesis structure

This research study consists from of the following distinctive chapters:

The first chapter is an introduction, it provides general information and background about the research's topic, significance and novelty, and the aim and objectives as well as an organisation of the thesis structure.

The second chapter is a literature review, it reviews the relevant previous studies which provide comprehensive knowledge about lattice structures, additive manufacturing technology, selective laser melting, Al-12Si material, heat treatment of Al-Si alloy and functionally graded material. In addition, it presents the summery of what has already

been done in research and development of the lattice structures as well as selection project problem.

The third chapter is a methodology, it describes the material and methods used in implementing this research study. For example, selection unit cell type, material selection, design lattice structures, SLM manufacturing process and etc.

The forth chapter is a mechanical and energy absorption characteristics of lattice structures, it provides methodology to calculate the mechanical properties (modulus of elasticity, plateau stress, onset densification) as well as energy absorption capability. Also, it include the Gibson and Ashby equations and coefficients.

The fifth chapter is an experiments and numerical analyses, it includes comprehensive information about what had been done to assess the mechanical performance of Al-12Si material and compressive properties of the lattice structures.

The sixth chapter is results and discussion, it provides and discuss the obtained results from the experimental procedures and FEA models. Furthermore, it attempts for clarification and interpretation of all results and observations that had happened during the study in order to provide clear picture.

The seventh chapter is conclusions and future work, it concludes the findings and observations as well as suggests the recommended future work.

The final section is an appendix, it provides and explains further information for this research study.

Chapter 2

LITERATURE REVIEW

2.1. Overview

The scope of this chapter is to provide the background and general information of what was found in the literature regarding research on lattice structure, additive manufacturing technology (AM), selective laser melting process, functionally graded material (FGM) and the effect of heat treatment processes on Al-alloy. Towards the end of the chapter, the most relevant studies in research and development of the lattice structures fabricated by AM is reviewed, and the gaps in the literature in the area of lattice structures made of Al-alloy and fabricated by SLM for energy absorption applications that this thesis aims at approaching are pointed out.

2.2. Cellular structure (Lattice structure)

Lattice structure or cellular structure can be defined as a network of cells in a particular shape, in which the cells are assembled and constructed from joining the solid ligaments at node points. Gibson and Ashby [1] have defined the cellular solid as "one made up of an interconnected network of solid struts or plates, which form edges and faces of cells". Lattice structures exist in our life, whether they are natural or manufactured. For example, lotus root, honeycombs and core of bird beak are natural forms of the lattice structures, while, wheels, the core of sandwich panel and building frames are excellent examples of human-made of lattice structures. It is stated that there are two types of cellular solid; two-dimensional cellular solid in which two-dimensional hexagonal cells fill the plane area, and it is called honeycombs. Three-dimensional cellular solid in which three dimension cells fill the space to form the structure, and it is also called foams [1]. Three dimensional-cellular solid can be open-celled or closed-celled, which relies on the existing solid material that the structure is made from. If the solid material is just in the struts edges, it is open-cell structures. If the solid material is in faces and struts of the cells and they are closed by its neighbours, it is a closed-cell structure [1].

Lattice structures have gained a significant attention of many different applications during the last decades, basically due to their attractive properties. The main characteristics of the cellular structures are low relative density, high compressive strength, light weight, thermal and acoustic insulation and high vibration damping according to Gibson and Ashby [1] and Queheillalt et al. [16]. They have mentioned that the main areas of applications that have widely used cellular structures are structural, thermal insulation, energy absorption, packaging, bio-medical for implant, and buoyancy.

It is important to understand the manufacturing techniques of the lattice structures. There are various methods used to produce metallic lattice structures, which completely depend on the phase status of the material that has been processed, as shown in Fig. 2. 1. Banhart [2] & Ryan et al.[17], these start from using liquid metal, solid metal in powdered form, metal vapour or gaseous metallic, metal ion solution.
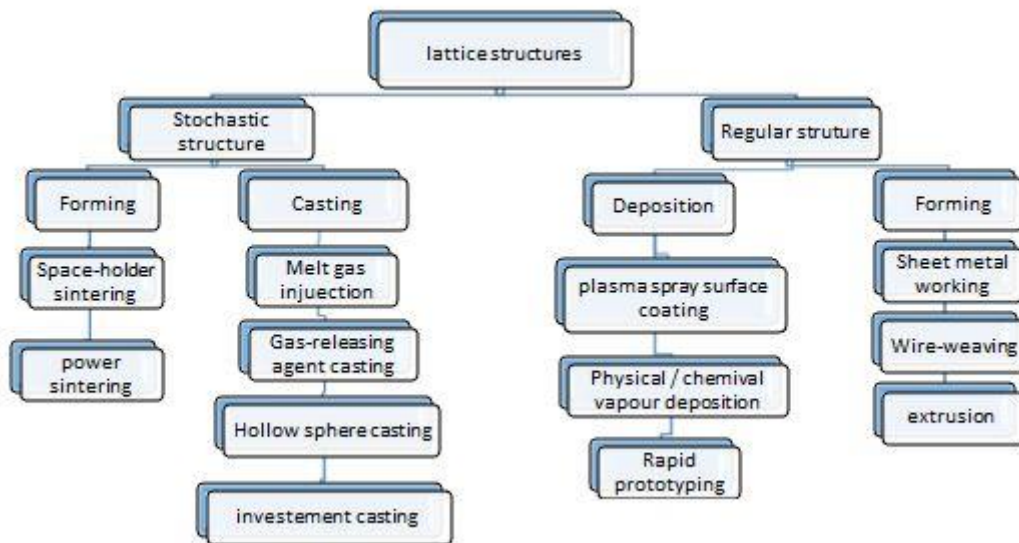
Figure 2.1, Different manufacturing techniques of cellular structures [2].

Ashby et al. [18] and Banhart, [2] mentioned that traditionally, melt gas injection was used to form a metallic foam and then machine it to the desirable shape as shown in Fig 2.2. Other studies Wadley [4, 5] show that cellular structures were made from the stack and join the laminar plates in a periodic manner. Wang et al. [3] explain that investment casting was used to produce cellular solids for use as truss core sandwich panel. On the other hand, thermal spray technologies like physical vapour

deposition (PVD) and chemical vapour deposition (CVD) were used to produce lattice structure with solid struts by deposition of the metals on the polymer templates [18] and [6]. Gibson and Ashby [1] and Zok et al. [7] use the sheet metal technique to fabricate lattice structures in honeycomb form which are widely utilised in the core of sandwich panel structures as can be seen in Fig 2.3.
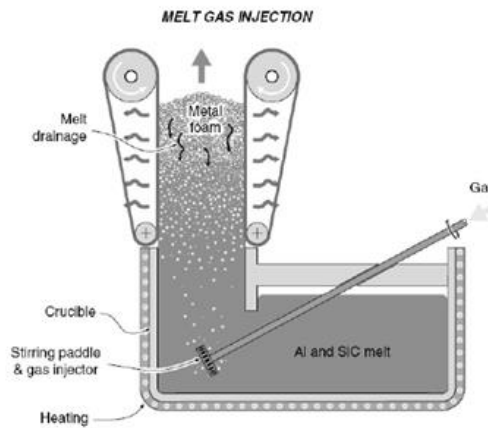
Figure 2.2, Melt gas injection casting process [18]

However, conventional manufacturing processes of lattice structures have some limitations that have been highlighted by other studies. Maskery et al.[9]state that conventional manufacturing techniques are costly and not able to produce lattice structures with complex geometry. On the same way, Wadley [10] the effectiveness of the traditional processes is limited by the shape complexity. Yang [11]states that low production rates and the divergence in properties of lattice structures are the essential limitations of conventional processes.
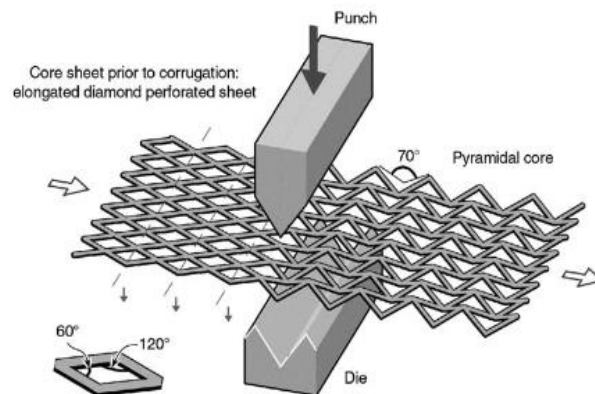
Figure 2.3, fabrication of pyramidal truss core by cutting and bending processes[7]

Recently, the advancement in additive manufacturing technology has led to overcome the problems and limitations that conventional manufacturing processes have in manufacturing lattice structures. Over the last decade, many researchers have investigated and studied the ability of additive manufacturing processes to produce the lattice structures for a range of potential applications. Next section will provide reviews on the additive manufacturing technology in details.

2.3. Additive manufacturing technology (AM)

AM technology is considered last innovation of the manufacturing processes that human have reached until now. In 1986, 3D system company produced the first AM process, which is the Stereolithography (SLA) process. After that, the AM technology has rapidly developed by many companies to become a large family, which consists of many techniques. Rapid manufacturing can be categorized into different groups based on the material type (polymers, metal, ceramic, plastic, etc.), the principle of the operations (extrusion, jetting, deposition, etc.) and material form (liquid, solid, and powder) according to Masood [108]. The most common AM processes, which are widely used today:

1. Stereolithography (SLA)
2. Fused Deposition Modelling (FDM)
3. Selective Laser Sintering (SLS)
4. Selective Laser Melting (SLM)
5. Electron Beam Melting (EBM)
6. Laser Engineered Net Shaping (LENS)
7. Direct Metal Deposition (DMD)
8. Ultrasonic Additive Manufacturing (UAM)

It is worth mentioning that a broad range of applications have utilized AM processes today, because of its unique characteristics, which expands between biomedical, aerospace, automobile, prototyping model, customer demands, entertainment, and repair and reconstruction parts applications. In addition, the main advantages and characteristics of the AM processes are an ability to produce the part with complex geometry which is impossible to manufacture it by conventional production methods.

Also, reduction in the lead time of production, lower cost of the products because it is digitally driven and easy to modify and change, and high precision process with fine resolution to 25 μm are other benefits of AM techniques [11] and [108] .Principally, the work concept of the AM processes is mostly similar in all the techniques. Fig 2. 4 illustrates the sequential steps of the rapid manufacturing processes.
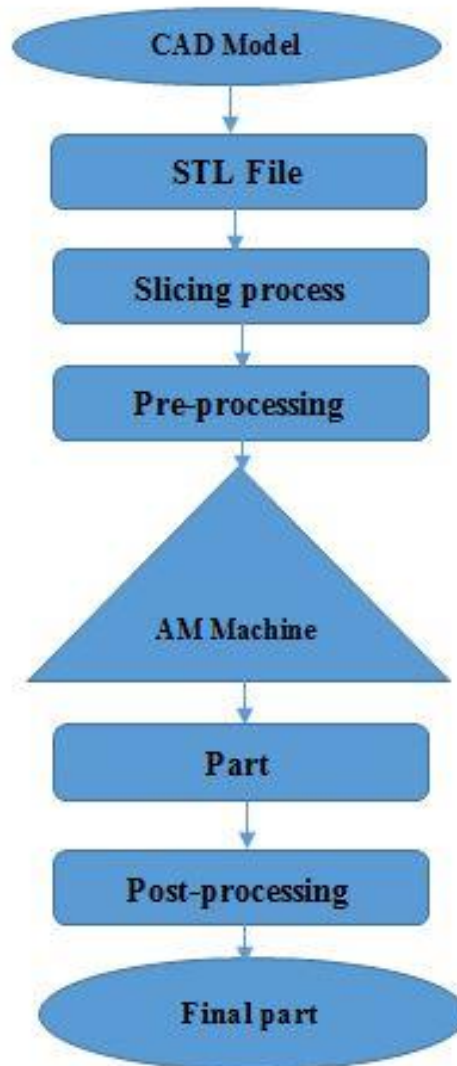
Figure 2.4, procedures of the AM processes

In last decade, the need for the fully dense metallic components with complex internal features have led to development of some of the AM techniques that can be used to process the metal materials. SLM, EBM, LENS, DMD, EBF3, and UAM are the main systems that have been mainly used to produce metal parts today. Table 2.1 shows the comparison between the properties and characteristic of metal processed AM techniques.

9

Table 2.1, additive manufacturing processes for metals

No	process	Power (KW)	Thickness of layers (mm)	Metal materials	Sources
1	Selective Laser Melting (SLM)	0.2 - 0.4	0.02 – 0.1	Steel, Co-Cr, boronze-based alloy, Inconel-718, stainless steel, Ti6Al4V, copper, Al-alloy	Laser
2	Electron Beam Melting (EBM)	4	0.05 – 0.1	Ti6Al4V, H13 tool steel, Co-Cr, Ti-Ni alloy, pure copper, 316 stainless steel	E- beam
3	Leaser Engineering Net Shape (LENS)	1.1	0.38	Ti6Al4V, Inconel-625 and 718, 316 stainless steel, H13 tool steel	Laser
4	Direct Metal Deposition (DMD)	1	0.1 – 1.6	H13 tool steel	Laser
5	Electron Beam Freeform Fabrication (EBF)	42	2	Ti6Al4V, 2219 Al-alloy	Electron beam gun
6	Ultrasonic Additive Manufacturing (UAM)	--	0.5 - 2	Various materials	Ultrasonic actuation

In terms of produce metallic lattice structures by additive manufacturing processes, many researches have been done to examine the ability of metals-AM processes to fabricate cellular structures with desirable mechanical properties. Electron beam melting (EBM) process has received extensive researches in producing porous structures, especially for biomedical application. Parthasarathy et al. [19] studied the ability of EBM technique to fabricate functionally graded cellular structures for bio-medical uses. They have found that EBM was able to make porous structures with suitable density. Furthermore, Morrish et al[20] and Hernández- Nava et al. [21] investigate the size effects of stochastic foams of Ti6Al4V manufactured by EBM in compression response. They have found that changing the manufacturing parameters significantly affect the mechanical characteristics of the various porous structures forms. On the other hand, Laser Engineering Net Shape

(LENS) process has been employed by a number of research studies to evaluate the capability of the process in manufacturing lattice structures for biomedical applications. It is stated that the LENS is capable to produce metallic part with various relative density for implant uses. Also, they add that the LENS techniques is able to fabricate porous structures from composite material and also in a functionally graded manner (Balla et al. [22] and Das et al. [23]).

Selective laser melting (SLM) processes are widely used in studying and developing the metals-lattice structures for different fields of applications. The next section will show the SLM process in details from background information, the principle of the process, properties and characteristics, and the applications.

1.4.2. Selective Laser Melting Technology (SLM)

SLM is one of the most important metal-AM processes that has been developed for producing fully dense parts with mechanical characteristics similar to the basic material. SLM process was developed and marketed by SLM solutions company- Germany in 2000 [108]. In general, SLM process is a powder bed system that uses fibre laser beam to selectively melt and fuse the metallic powder on the substrates in a shielded chamber to create the part, layer by layer until the whole metal part is complete. Since the SLM process has been commercially available, many researchers have focused to study and explore the capability of production metal components with intricate geometries without the need of a particular cutting tool, directly from CAD model data. The principle of SLM process as we mentioned above is similar to other AM technologies. Fig 2.5 illustrates the schematic of the SLM process.
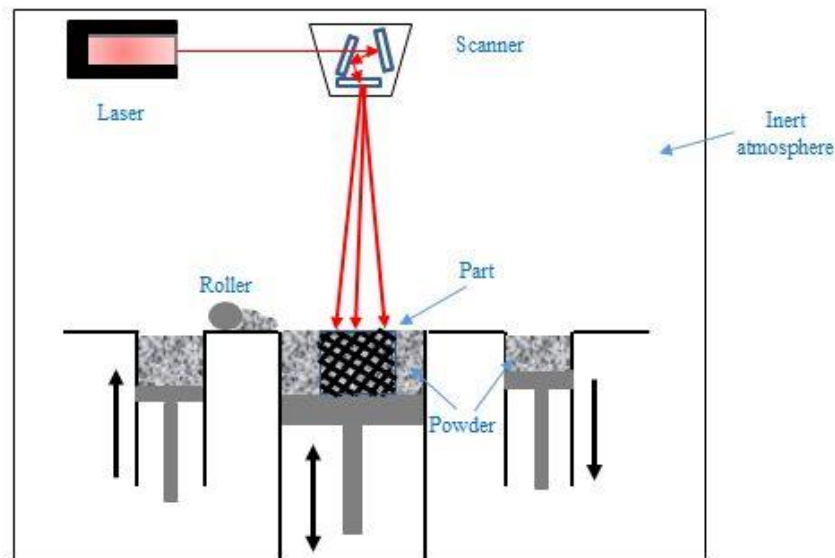
Figure 2.5, schematic of SLM process

Selective Laser Melting has a large number of advantages and characteristics that have enabled it to be used in various applications such as aerospace, automotive and biomedical. Masood [108] and Aboulkhair [24] pointed out in details the main benefits of SLM system:

1. almost 100% density of part
2. complex external / internal features can be made
3. good production quality
4. high strength similar to the basic material
5. ability to reuse and recycle the powder
6. infiltration and post heat treatment not required
7. wide range of material can be processed

Nowadays, SLM processes have been significantly used in production and exploration of lattice structures, porous solids, and scaffold structures due to its distinctive characteristics as shown above. Not only that, the use of SLM has been extended to new approach of lattice structures and metallic components like functionally graded material and structures. Next section will theoretically review the concept of FGMs, its types, the conventional fabrication techniques and influence of AM technology on FGM – fabrication.

1.4.3. Aluminium alloys and selective laser melting

Aluminium and aluminium alloys are widely used in many applications especially in aerospace, automotive, packaging, food and beverage and building construction industries and etc, due to the distinctive properties. Lightweight (low density), thermal properties, electric conductivity, high strength to weight ratio and low recycling costs are the main advantages of aluminium and its alloy [15, 24, 25]. It is stated that the Al-12Si is one of the important aluminium-silicon alloys that is processed by SLM beside many other metallic materials due to the fact that the variation in its temperature between the melting and solidification is highly convergent. [25, 26].

The other importance of using Al-12Si is its ability to transfer its mechanical properties and microstructures into a wide range of desirable properties for specific requirements by using heat treatment techniques. Many research studies have investigated the effect of such heat treatment on the characteristics of SLM - Al-12Si parts. Section 2.5 in this chapter will provide in detail the heat treatment processes of SLM – parts in general and SLM-Al alloys parts in particular.

2.4. Functionally graded material (FGMs)

Functionally graded material is an advanced engineering material that can be characterized by spatial gradation in composition or structure, designed for specific requirements or functions. Technically, it is not a separate class of the homogenous materials, but it represents an engineering approach that is used to modify the chemical composition or structural unit cell of the material /and or structure to provide the desirable properties[27]. Miyamoto et al. [28] have defined the FGMs as a graded material in which both the composition and structure gradually change over the volume, resulting in corresponding change in the properties of the material. FGMs exist in various materials in nature such as bamboo, teeth and bones as shown in Fig 2.6. These materials have naturally designed to be able to withstand in different environmental working conditions that are subjected to them, such as wear resistance and shock absorption [29-31]. In engineering application, the first idea of the functionally graded material was introduced in early 1972 [27, 28, 31]. Bever et al. [32, 33] have theoretically investigated the graded structures of polymeric and composite materials and suggested various models of graded structures to different possible applications.

However, due to the limitation of manufacturing processes at that time, more development and investigation on the functionally graded materials had been delayed. In 1980s, the FGMs concept was proposed in Japan on the composite material, this time the concept was proposed to reduce the thermal stress concentration at the interface of the traditional composite material for aerospace applications. The high temperature gradient between inside and outside the body plane is the main cause of failure of the traditional composite materials. The point of failure was found to be at the interface or joint point of where the two dissimilar materials of the composite were linked. Functionally graded composite material was developed to overcome this issue by gradient interface of the two materials in traditional composite material as shown in Fig. 2.7.
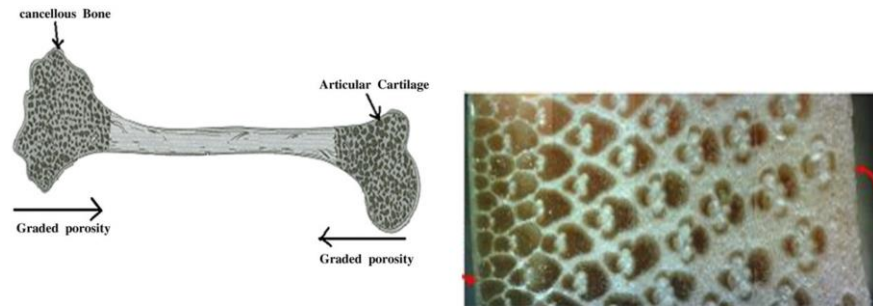
Figure 2.6, Schematic of human bone shows the FGM [30](a), image of bamboo structure shows the FGM[34]

The first comprehensive research program on FGMs "Fundamental studies on the relaxation of the thermal stress by tailoring graded structure" was started in Japan in 1987. The program was mainly focus on the development of the FGMs, resulted in publish the concept of the FGMs worldwide[27, 28]. Nowadays, the research and development of the FGMs has significantly increased due to ability to produce various material with tailored properties for many fields of applications such as bioengineering, aerospace industries etc.
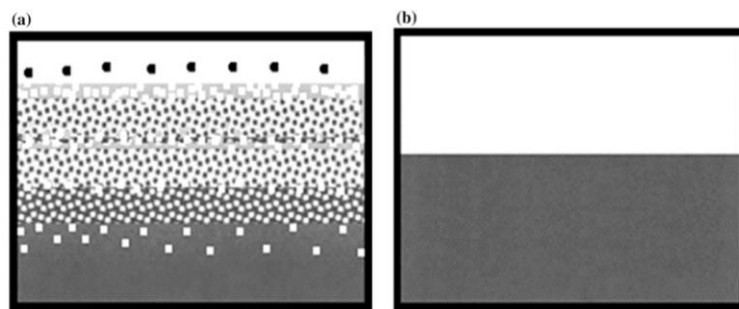
Figure 2.7 Schematic shows composite material (a) FGM, (b) traditional laminate[30]

14

The interest in FGMs let to increase the number of research studies for various applications. Annually, the number of the publications on the FGMs research has been increased significantly. Figure 2.8 shows the number of publications provide by Scopus research engine on FGMs subject in the last decades[31].
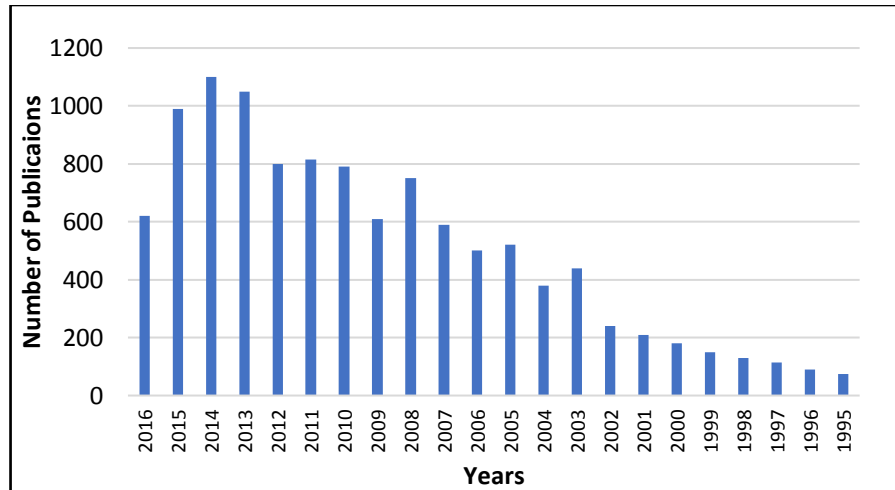
Figure 2.8 Shows the number of publications annually on FGMs, as provided by the search engine of Scopus (as of July 2016) [31]

The main concept of the functionally graded material is due to the gradual change in the chemical composition, microstructure, or the pore distribution over the volume of the bulk material. This results in changing the properties of the material which depend on the spatial position of the material. FGMs materials are designed in two different ways of gradual change of the composition, or structural design within the bulk material. Figure 2.9 demonstrates the two methods of the functionally graded material, continuous material gradients and stepwise material gradients (discontinuous). In continuous graded material, the composition, porosity, or microstructure changes continuously with spatial position providing smooth change. In contrast, in stepwise graded material, the gradual change of the composition, porosity, or microstructure occur in stepwise manner resulting in layer boundaries (interface) between the discrete layers in the structure.
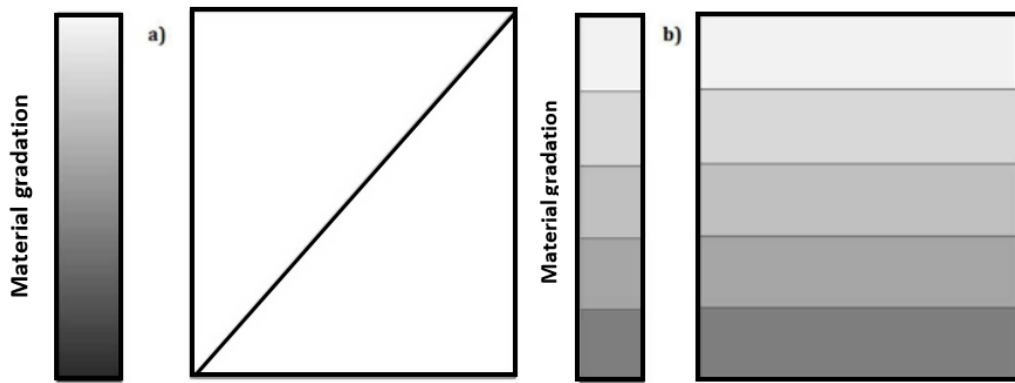
Figure 2.9 Schematic of FGM types (a) continuous, (b) discontinuous

1.4.4. Types of the functionally graded material (FGMs)

The inception of the introducing of the functionally graded material concept was due to the problem of thermal stress concentration at the interface of the joint dissimilar materials in conventional composite material. This problem resulted in introducing the graded composite material with gradually changing interface of the chemical composition. Since that, the increasing interest in the FGMs has led to produce various kinds of functionally gradient materials. There are different ways of classification the FGMs based on the nature of gradients. Generally, the all types of the FGMs have mainly determined based on the application requirement such as bone replacement, aerospace, defence industries etc. Cherradi et al.[35] and Wessel [27]have classified the functionally graded material based on the processing techniques while, Varghese et al.[36] and El-Wazery et al. [37] classified the FGMs based on volume fraction, size, orientation and shape of material gradients as shown in Fig. 2.10.
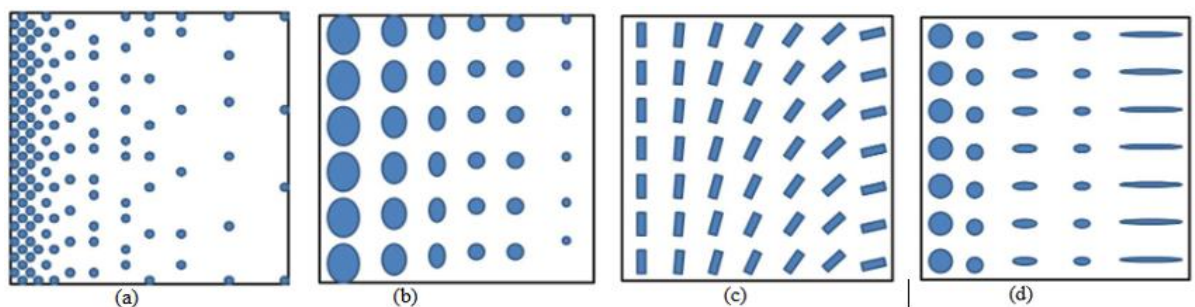
Figure 2.10 Types of functionally graded materials (a) Gradient with Fraction (b) Gradient with Size, (c) Gradient with Orientation, (d) Gradient with Shape [36, 37]

The one of the comprehensive classification of the FGMs that can be applied whether FGMs is graded material or graded structure, provides by Mahamood et al.[30]:

1- Chemical Composition Gradient Functionally Gradient Materials
2- Porosity Gradient Functionally Gradient Materials
3- Microstructure Gradient Functionally Gradient Materials

In chemical composition gradient FGMs type, the chemical composition of the materials (chemical elements) are designed to change through the entire material as seen in Fig. 6. As the chemical composition is varied from one material into the other, it will result in changing of the material properties that would help to achieve the intended application, for which the FGMs is designed for. While in the porosity gradient FGMs type, the porosity in the material is designed to vary with the change in the spatial position in the entire material resulting in the required properties of FGMs as shown in Fig. 2.11. The FGMs with porosity gradation can be designed either by porosity density gradient or pore size gradient.

The FGMs with microstructure gradient can be created from processing the microstructure of the material, such as solidification process, controlled heat treatment process, which will result in different microstructures in the bulk material.

However, all types of the FGMs can be designed, manufactured in the form of thin film, which is applied on the surface of the materials in order to improve the surface properties, or in the form of bulk material in which the properties change gradually over the volume of the entire material. It is important to understand the processing techniques of the FGMs. Next section will briefly explain the main processing techniques of the FGMs.
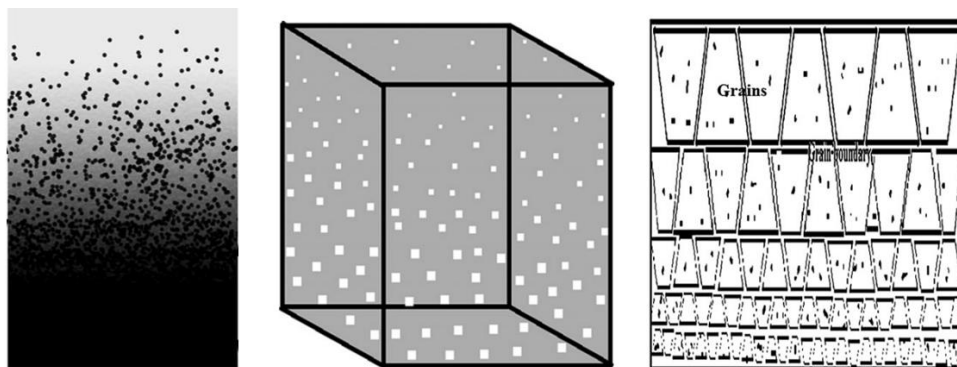
Figure 2.11 Types of functionally graded materials (a chemical composition gradient (b), porosity gradient (c), microstructure (structural) gradient [30].

1.4.5. The processing techniques of FGMs

The increased interest in the FGMs due to their distinctive properties has led to a significant increase in the number of the inventive manufacturing techniques to produce the FGMs. There are numerous studies and reviews have been conducted on the manufacturing part of FGMs [28, 30, 31, 36-39]. Basically, these manufacturing processes can be categorized into two different techniques namely constructive (building) and transported based techniques (consolidation) [30, 36, 39]. In constructive techniques, FGMs is made by stacking the starting materials layer by layer selectively unit the layered component is completed, which provide highly control on compositional gradient. In the transported based techniques, FGMs is made depending on the natural transport phenomena of the materials to make the composition, porosity, and microstructure gradients types of the FGMs through the manufacturing.

This section will focus on the traditional processing techniques that have been used to produce different FGMs for range of applications. While, the next section, which is more related to current research study, will review the using additive manufacturing technologies to create the FGMs. Traditionally, all the processing techniques of FGMs can be classified into three groups [30, 31, 36]:

1- Gas state (Vapour Deposition) processes

There are many different deposition processes that are used to produce thin – film FGMs, which is applied on the surface of the materials to improve the surface properties such as wear resistance, corrosion resistance, thermal connectivity and electrical connectivity. These processes such chemical vapour deposition (CVD) [40, 41], physical vapour deposition (PVD)[42], thermal spray processes[43-45] are most commonly used.

2- Liquid state processes

FGMs has been widely produced from liquid state of the materials. Centrifugal methods or centrifugal casting processes[37] are the most important processes to create the FGMs from the liquid state, in addition to other techniques like Tape casting, Slip casting, Combustion and Gel-casting[31]. In centrifugal casting processes, gravity force and materials densities are the main factors to produce the FGMs by this way.

For example, Watanabe et al. [46], Gao et al.[47] and Prabhu [48] have successfully employed the centrifugal processes to create FGMs for various applications.

3- Solid state processes

For bulk – FGMs type, solid state processes such as powder metallurgy and spark plasma sintering (SPS) (sintering techniques) are the most common processes to fabricate the various types of FGMs. There are a large number of research studies have been conducted to investigate the ability of the SPS to fabricate the FGMs, for example Hong et al.[49], Pellizzari et al.[50] and Eriksson et al. [51]. Their results showed that different FGMs for range of applications were successfully manufactured with tailored properties. On the other hand, powder metallurgy techniques are broadly employed to produce the bulk FGMs for various fields of uses. For instance, Jin et al.[52] and Chenglin et al. [53] have used powder metallurgy to produce multilayered mullite /Mo and Hydroxyapatite–Ti of FGMs for biomaterials applications.

1.4.6. Additive manufacturing technology for FGMs

FGMs is a new class of advanced material that provides gradual change of its properties over the material volume by changing the material composition or structural design. Manufacturing the FGMs using traditional fabrication techniques, which is explained in previous section, is successfully done, but there are some limitations and difficulties. Choy et al.[8] have done comprehensive review on the manufacturing techniques of the FGMs. They concluded that FGMs with composition gradient can be achieved using traditional processing methods, but the FGMs with structural design gradient (porosity) could be done but with some limitations such as simple geometries, limited design freedoms, and consequently lack advanced functionality to meet the requirements. Also, Bobbio et al. [54] mentioned that the conventional fabrication methods of FGMs like deposition methods, fusion weld, powder metallurgy, and centrifugal methods can only create the FGMs in short length scale of gradient (less 1 mm).

Recently, development in additive manufacturing technology has attracted much attentions of different industry sectors because of the distinctive properties. An additive manufacturing technology is a process of making component by adding layer upon layer directly from the CAD digital model and it is opposite to the conventional subtractive manufacturing processes.

Fabrication of the FGMs using additive manufacturing processes has received intensive studies due to their advantages like high control and flexible to provide structural design gradient, porosity gradient and density gradient[8, 54]. Using additive manufacturing technologies able to fabricate to two types of FGMs, composition gradient and structural design gradient.

1- FGMs with composition gradient

Soodi et al. [55] successfully fabricated the functionally graded of 316 SS and 420 SS and wafer-layered of AlBrnz and 420 SS materials using laser direct metal deposition (LDMD) process to investigate the thermal expansion coefficients. They have found that the fabricated FGMs and Wafer-layered materials exhibited lower thermal expansion than those of the original alloys. Schneider et al. [56] used directed energy deposition process (DED − CLAD) to create the FGM of Ti6Al4V-Mo alloy. Five samples of FGM-composition gradient from 0 − 100 % wt of MO manufactured and their results showed chemical composition gradient of mixed powders were clear along the deposition direction. Durejko al el.[57] manufactured the FGM of thin wall tube with Fe3Al/SS316L using laser engineered net shaping process. Their results revealed that FGM structure was characterized by continuous and smooth gradation between the both materials (the 316L steel and the Fe3Al alloy). Chung et al. [58] pointed out that selective laser sintering (SLS) was used to fabricate FGM from nylon 11 filled by nanoparticles of the silica material in order to increase the mechanical properties in desirable direction of the component. Laser engineering net shape process (LENS) was utilized by Zhang et al. [59] to manufacture thin walls from functionally graded titanium carbide in pure titanium material. The results of the experimental tests clearly showed the functional gradient material with high alleviate of discrete interface problem of dissimilar material. Similar results have been found by Mumtaz et al. [43] functionally graded Zirconia powder within the nickel alloy material using SLM process for thermal barrier coating applications. Also, selective laser melting process was successfully used by Kang et al. [60] to fabricate the FGM of silicon matrix composite with various percentage of Al (wt.%).

2- FGMs with structural design gradient

FGMs based on structural design can be achieved by density variation (porosity) whether by control and manipulating the manufacturing parameters or during the designing stage of CAD model of the structure. Functionally graded material based on the manipulating and control the manufacturing properties (laser power, laser speed, hatch spacing) have been done by Erdal et al. [61], Li et al. [62] and Niendorf et al. [63], but uncontrollable the pore shape and size distribution in internal architecture is the main limitation of this method. Other studies [9, 13, 64-66] have focused on achieving the functionally graded structure during the designing stage of the CAD model before 3D printing of the final physical part using AM technologies instead of manipulating the manufacturing parameters. For instance, Maskery et al [9, 64] had experimentally investigated the functionally graded structures with density change gradually throughout the layers of the structures with abrupt transfer between the interfaces of the connected layers. The body centred cubic (BCC) unit cell made of Al-Si10-Mg was used to build the lattice structures and made by SLM, and BCC, BCC,$_z$ lattice structures made of Polyamide PA 2200 and manufactured by SLS respectively. Similarly, Grunsven et al. [65] studied the mechanical characteristics of functionally graded lattice structures made of Ti6Al4V and fabricate by EBM process, the density was separately changed in each layer in sequence. The porous size variation of functionally graded scaffolds in step-wise manner for tissue engineering applications was empirically investigated by Leong et al. [66].

It is clear that these research studies [9, 64-66] manufactured the functionally graded lattice structures with density change at every layer separately and did not provide smooth density gradient through the continuously variable of the solid strut thickness throughout the lattice structure layers. Recently, Choy et al. [13] studied the compressive characteristics and property of energy absorption of cubic and honeycomb lattice made of Ti6Al4V and manufactured by SLM process. In their study, designing and manufacturing of functionally graded lattice structures with smooth density change was achieved, but it was limited to experimental work.

It is found that limited attention has been paid in investigating the manufacturing the functionally graded lattice structure with linearly and continuously density change in lattice solid strut diameter throughout the structure layers using additive manufacturing technologies, [67-69] which is one of the main aim of this study.

This study aim to design and manufacture functionally graded lattice structures with linearly and continuously density change. In addition, it will provide a new approach of density change profile that by constant increasing rate of the density throughout the structural layers of the components.

2.5. Heat treatment of Al – alloys– SLM parts

Heat treatment or post – manufacture heat treatment is a combination of operations applied to the metals and metallic - alloys in the solid state in order to obtain desired properties and or microstructures for specific applications. Basically, it includes arising the temperature of metallic component in specific heating rate, maintain the temperature for the period of time and cool down at specific cooling rate. There are different heat treatment techniques can be employed to Al – alloys such as annealing, hardening, solution heat treatment, precipitation hardening etc., which are mainly depend on the required purpose of heat treatment like improve the mechanical properties, modify the microstructure, and reduce the residual stresses. American Society for Testing and Materials (ASTM) has in details established the standard practice for heat treatment of Al - alloys made of casting and wrought under the code B917/B917M – 12 and B918/B918M – 17a respectively[70, 71].

Recently, using metallic additive manufacturing technologies, in particular selective laser melting (SLM), to produce various metallic materials has attracted attention a large number of academic and industries sectors due to its distinct properties. The ability to produce complex geometry, fully dense part, enhance the design flexibility and reduce the wastage material are the main features of the SLM technology. In addition, the nature of SLM process, high heating and cooling rate (1×10^5 K/s)[15], results in fine microstructure component and improving the mechanical properties compared to the conventional processes are expected.

Although SLM has many advantages compared to traditional manufacturing methods, limited surface quality, little residual porosity, residual stresses, low ductility are the major drawbacks encountered in the process[25, 72-74]. Many researchers have studied various methods and strategies in order to improve the properties of SLM-parts such as different scan strategy, laser re-melting strategy, manipulating the processing parameters and heat treatment techniques.

An investigation and study the effect of heat treatment on SLM - parts have been conducted by many researchers for different purposes. For example, effect of the heat treatment on the hardness of 17-4PH fabricated by SLM technology has been investigated [75]. Masood et al.[75]studied the effect of the heat treatment process on two different samples fabricated with different scan strategies using SLM and compared with heat-treated wrought samples. The results showed that the hardness was improved in heat-treated SLM sample compared to heat-treated wrought sample. For SLM - Ti–6Al–4V parts, the influence of heat treatment on microstructure has been studied by Yadroitsev et al. [76]for medical applications. They concluded that heat treatment above β-transus temperature let to re-nucleation of the phases, eventually produce the required microstructure. For same material but for other purpose, Leuders et al. [77] and Kasperovich et al. [78] have studied the fatigue and crack growth behaviour of Ti–6Al–4V subjected to post manufacturing treatment. They found that improvement of the ductility and fatigue resistance were achieved compatible to the wrought TiAl6V4.

On other hand, Yasa and Kruth [74], Shiom et al. [79] and Riemer et al. [73] investigated from the effect of heat treatment on the 316L stainless steel parts made of SLM on the microstructures and fatigue crack growth behaviour respectively.

Production of Al – based alloy parts using SLM technology has received intensive research studies because of their crucial properties like low density, wear and corrosion resistance, weldability, machinability and easy recycling. The interest of many researchers in improving the properties of Al - based alloy parts fabricated by SLM process, which find their application as engineering components in structural, automotive and aerospace industries[80], has significantly increased. The investigation of the influence of heat treatment on the SLM- Al alloys parts have been done by many researchers and engineers worldwide. Table 2.2 shows the summary of the relevant studies that have been conducted using different thermal treatment techniques to improve the properties of Al- alloys parts fabricated by SLM.

The investigation of the effect of heat treatment on the mechanical properties and microstructure of AlSi-10Mg had been extensively studied for instance Aboulkhair et al. [81]. Kimura et al. [82], Li et al. [83]. The fatigue behaviour and fracture behaviour of SLM - AlSi-10Mg parts subjected to heat treatment had been investigated by Aboulkhair

et al. [72], Brandl et al. [84]. Similarly, microstructure heterogeneities of AlSi-10Mg lattice struts and manufactured by SLM with different orientation angles studied by Delroisse et al [85]. They found that the heat treatment process improved the microstructure homogenization, but it let to minor soften due to eutectic spheroidization.

Table 2.2 summary of the relevant publish papers

No	Authors	Manufacturing process	Material	Heat treatment process
1	Kang, Coddet [86]	SLM	Al-50Si	The samples were heat treated in **air** in an electric furnace, at temperatures of **300, 350, 400, 450, 500, 550 and 600** °C with a heating rate of **20 °C/min**. The temperature was maintained **2h** and then the samples were **quenched in water**.
2	Li, Li [83]	SLM	AlSi10Mg	**T6 heat treatment process:** The specimens were solution-treated at the different temperatures of **450 °C, 500 °C and 550 °C** for **2h**, followed by **water quenching**. After the solution heat treatment, one half of the specimens were immediately subjected to **artificial aging at 180** °C for**12h**, and then all the samples were equally **water quenched** to room temperature.
3	Delroisse, Jacques [85]	SLM	AlSi10Mg	**T6 heat treatment process:** Heating to **525°** for **5h** followed by **water quenching,** and then **artificial aging** at **165°** for **7 h**).
4	Karamooz Ravari, Kadkhodaei [67]	SLM	Al-20Si	**Annealing process:** The SLM samples were annealed for **6h** at **200 , 300 ,** and **400 °C**.
5	Prashanth, Scudino [15]	SLM	Al–12Si	**Annealing process:** Heat treatment of the tensile bars was carried out under **Argon atmosphere** for **6h** at different temperatures (**200, 300, 350, 400 and 450 °C**).

6	Aboulkhair, Tuck [87]	SLM	AlSi10Mg	**T6 heat treatment process:** The samples were heat treated in the following sequence: (1) SHT at **520 C** for 1, 2, 3, and 4 hours, (2) **water quenching**; and (3) **artificial aging** at 160 C for 6, 8, 10, and 12 hours followed by **air cooling.**
7	Suryawanshi, Prashanth [88]	SLM	Al-12Si	**Annealing treatment:** SLM samples were heat treated at **300 °C** for **6h**.
8	Trevisan, Calignano [89]	SLM	AlSi10Mg	**T6 treatment process:** solution treatment at **525 °C** for **6h**, followed by **quenching** and **ageing** at **165 °C** for **7 h.**
9	Wang, Li [90]	SLM	Al-Zn-Mg-Cu	**T6 treatment process:** The samples were solution treated at **743 K** for **1h**, **water quenched**, and Then subjected to **aging at 393 K** for **24 h** followed by **air cooling**.
10	Aboulkhair, Maskery [72]	SLM	AlSi10Mg	**T6 treatment process:** The samples were solution heat treated for 1 h at 520 °C followed by water quenching to room temperature and then aged for 6 h at 160 °C.
11	Li, Wang [91]	SLM	Al-12Si	Solution heat treatment of specimens was performed in **air** at **500°C** for up to **(0.25, 0.5, 2 and 4 h**, followed by **water quenching**. (important) (NO effect after 2 hours)
12	Kimura and Nakamoto [82]	SLM	AlSi7Mg0.3	**T5 Treatment condition**, T**6 treatment condition**
13	[92]	SLM	Al-50Si	**Solution heat treatment** the sample was heated to 500 °C for 6 hours.

Improving the mechanical properties and microstructure of Al-Si material fabricated by SLM technology has been reported by many published studies. Figure 2.12 shows the phase diagram of Al-Si alloy. Kang et al. investigated the effects of heat treatments on the microstructure and residual stress of SLM- Al-50Si alloy. They performed heating in range 300- 600 C for 2 hours followed by water quenching. They found that heat at 300 C homogenises the residual stress level without and significant effect on the

microstructure. They added that sample with higher heating temp showed the average values of the residual stress decrease consistent to an increase in the grain size. Similarly, Jia et al (2017) studied the microstructure and thermal expansion behaviour of Al-50Si made by SLM. They pointed out that coefficient of thermal expansion CTE peak of Al-50Si can be change to the wide range using heat treatment process. This is due to the precipitation of Si particles from Al matrix after heat treatment compared to supersaturate Si in Al in as-build material. For Al-20Si material, Ma et al. [67] conducted study of the effect of annealing process for different conditions on the microstructures and mechanical properties of Al-20Si made of SLM. They have found that the Si particles become coarser, and the eutectic Si can be changed from fibrous to plate shape with increasing heat treatment temperature. This results in significant change in the mechanical properties of material. They concluded that the yield and ultimate strengths decline from 374 and 506 MPa to 162 and 252 MPa for the as-built SLM material and annealed sample at 673 K respectively. While, the ductility property was increased from 1.6 to 8.7%.
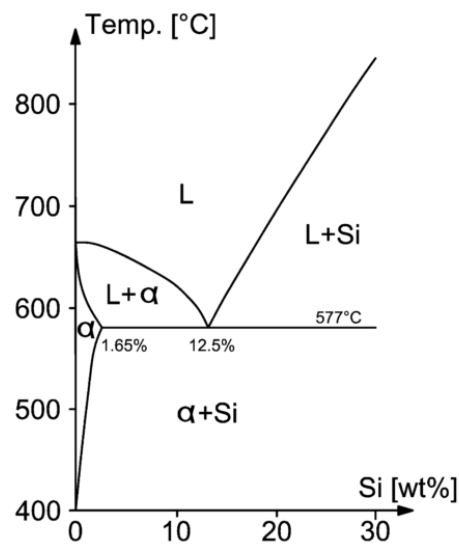
Figure 2.12 phase diagram of AL-Si alloy material [84]

The influence of various heat treatment techniques on the SLM-Al-12Si parts have been study. Li at al. (2017) study the refinement of eutectic Al-12Si alloy made by SLM using solution heat treatment process. They have mentioned that the solution heat treatment was done by heating the samples to 500 C for 0.25-4 hrs followed by water quenching. They have found that solution heated Al-12Si sample exhibited high ductility to 25% compared to as-build AL-12Si sample. They also added that the mechanical properties of the Al–12Si can be tailored through controlling the precipitation and morphology of the Si particles by changing the soaking time. Similar results found by Prashanth et al (2014)

but with different heat treatment technique. They conducted annealing process to range of temperature (200 – 450 C) for 2 hr under Argon atmosphere furnace. They claimed that that the mechanical behaviour of the Al–12Si made of SLM can be altered within a wide range of strength and ductility through proper annealing treatment. On other hand, Siddique et al. (2015) studied the effect of process parameters and post-manufacture heat treatment on the microstructure and mechanical properties of Al-12Si. Their heat treatment process was by heating the sample to 240 ∘C followed by oven cooling. They found that conducting the heat treatment beside the base plate heating can eliminated the defects of SLM- produced parts such as porosity and corresponding of improving the mechanical properties. For other properties, Prashanth et al. (2014) investigated tribological and corrosion properties of Al-12Si material fabricated by SLM process. They have found the wear and corrosion resistance were decreased in heat-treated Al-12Si sample compared to as-build sample. This is due to the growth of Si particle sizes and the loss of the connectivity between Si particles.

It is worth noting that limited attention has been paid to the investigation the effect of various heat treatment techniques on the mechanical properties of the Al − Si alloy material or structures manufactured by SLM technology in general, and energy absorption capability in practical. Recently, Maskery et al. [93] studied the effect of the heat treatment process on the compressive deformation modes and energy absorption of double gyroid lattice structure made of Al-Si10-Mg and fabricated by SLM technology. They have mentioned that application of heat treatment process improved the deformation behaviour of lattice structure by getting rid of the brittle fracture and early strain failure. Same results found in pervious study for same authors[9], which was the investigation of mechanical properties and energy absorption of functionally graded (in stepwise manner) lattice structure made from Al-Si10-Mg and fabricated by SLM technology. Further studies on influence of the different heat treatment processes on energy absorption capability and compressive properties of more advanced structures made of Al -Si alloy, in specific AL-12 Si, like functionally graded lattice structures with continues and linear density gradient are needed due to their numerous potential applications.

2.6. Research and development in lattice structures using AM technology

Lattice structures have received an extensive attention of many researchers because of their distinctive properties of combining the lightweight and high strength. There is a number of research studies done using AM technologies to manufacture various lattice structures to investigate of their performance, optimization parameters, and mechanical properties.

Maskery et al. [9] had done experimental work to evaluate the mechanical properties of lattice structures of uniform and graded form. Body Centred Cubic (BCC) unit cell of Al-Si10-Mg was used to build the lattice structures and made by selective laser melting. Also, they conducted heat treatment for cellular structures to improve the deformation behaviour and the capability of energy absorption. The results of this study show that as-built structures exhibited highly brittle failure under compressive load, while collapse behaviour and capacity of energy absorption improved significantly in heat-treated lattice structures. In addition, they observed that the same amount of energy was absorbed before entering the densification regime in both uniform and graded lattice structures. Finally, they concluded that Gibson-Ashby equations and coefficients are the basis of design processes and can be used to estimate the mechanical performance of designed lattice structures.

Smith et el. [68] have carried out the finite element modelling for body-centred-cubic (BCC) lattice structure made by SLM to predict the compressive behaviour. Lattice structures were modelled using two different element types; beam and 3D continuum for a quasi-static compression test. They mentioned that experimental test was performed for validation of simulation analysis results. Their results have shown that compressive response of lattice structures can be precisely predict using both beam and 3D continuum element types in finite element analysis. Also, they have found that the simulation results were in good agreement with the experimental results. Moreover, the results have proven that mechanical properties can be significantly enhanced by altering the unit cell aspect ratio, which is by increasing the height and reducing its width based on build direction.

Choy et al.[13] have studied the compressive behaviour of two functionally graded components which are cubic and honeycomb lattice structures. The Ti6AL4V cellular structures in gradually and uniformly dense were successfully fabricated using SLM

technology. Their study showed that the SLM technology was able to manufacture complex design with full density successfully. Furthermore, the results of the research have shown that stress-strain curve of the compressive response of both lattice structures fluctuated with few peak points of stresses. The authors have highlighted that the oscillations of stress-strain curve due to the ductility of material and the gradual increasing in strut thickness of graded lattice structures. As a result, they concluded that improving the capability of energy absorption as well as minimizing the used material can be achieved by functionally graded components made on SLM process.

Karamooz et al. [67]had conducted numerical analysis to investigate the mechanical characterises of porous structures. In this study, beam and solid elements were used for modelling the lattice structures with variation in strut diameters in order to investigate the influence of such variation on the mechanical behaviour. Collapse stress and modulus of elasticity of the bulk material and cellular structures were obtained from compression test of samples made by fused modelling deposition experimentally. Their results showed that the using beam element in lattice structures modelling was better efficient regarding computational time, while the stress-strain curve was higher than solid elements due to an inability of beam elements to detect the impact of material concentration along the variations in pillars diameters. However, the solid elements were more precisely and lower compressive stress-strain curve than beam elements even with one cycle. Consequently, they concluded that accuracy and computational time/cost are the key factors in making the decision on which type of elements could be used in modelling the structures.

Mousanezhad et al. [94]have studied the influence of cell wall material on impact resistance and capability of energy absorption of hexagonal honeycombs. They used numerical analysis to examine the regular and gradient honeycomb structures under two types of loads; constant-velocity loading and impact loading. Their results showed that the cell wall material in uniform honeycomb has affected on the deformation behaviour that by delay the deformation under dynamic loading unit the certain crush velocity before entering the plasticity range. Also, under the impact loading, the regular structures exhibited that by increase the cell wall material hardening lead to reduce the ability of structures to achieve maximum crushing strain with increase the impact energy. On the other hand, graded honeycomb structures showed a distinct deformation behaviour due to gradually increasing in material distribution compared to the uniform one.

Maskery et al. [64] have investigated the impact resistance, capability of energy absorption and compressive properties of lattice structures made by SLS. In their investigation, two lattice structures were used BCC and BCC_Z in uniform and graded form. Polyamide PA 2200 was used as reference material to build the lattice structures. In this study, compression test was conducted to examine the mechanical behaviour of lattice structures in different directions (for determent the mechanical anisotropy) of the structures. They have found that the graded cellular structures exhibit apparent behaviour with the sequentially collapse of lattice layers until full densification. Furthermore, they mentioned that the capability of energy absorption of BCC_Z graded lattice structure was approximately 114% per unit volume higher than uniform lattice structures before full densification occurs.

Woesz et al. [95] had studied to what extent the apparent density and microarchitecture of cellular solids affect its mechanical properties. SLS technology was chosen to fabricate of Polyamide cellular structures. It is stated that five types of cellular structures Gibson – Ashby (G-A), Simple Cubic (SC), Translate Simple Cubic (tsc), Body-Centred-Cubic (bcc), and Reinforced Body Centred Cubic (rbcc) were modelled using CAD ProEngineer software, and compression tests were performed to inspect the structures. The results of the study showed that mechanical characteristics (stiffness, strength and capability of energy absorption) of the structures with constant volume fraction can be influenced by changing the internal architecture of structures. In addition, strength and stiffness has a proportional relationship and are significantly affected by varying the apparent density as well as microarchitecture of structures.

Labeas and Sunaric [96] had performed an experimental and analytical study to predict the response of metallic open cellular structures under compressive loads. They conducted linear static, buckling and non-linear analysis. Three forms of open cellular structures (bcc, bcc,z and $f_2$bcc,z) were used, and manufactured from Stainless Steel 316L by SLM technique. Their results showed that plasticity material mode and understanding the behaviour of geometrical non-linearity should be considered to study the failure process in the finite element analysis. Also, it states that unit cell size, shape and struts aspect ratio play a significant role in the mechanical behaviour of metallic open cellular structures. Lastly, bcc,z and f2bcc,z exhibit a distinct behaviour with high stiffness and buckling load compared with bcc unit cell form.

Sing et al. [97] have investigated dimensional and mechanical characteristics of lattice structures using an experimental work. They used square pyramid and truncated cube and octahedron as unit cell form to build out the cellular structures and then made by SLM process. In this study, uni-axial compression test was conducted to examine the mechanical response, while the Analysis of Variance (ANOVA) was used to find out to what extent the design and manufacturing parameters have an effect on dimensional accuracy and mechanical behaviour of porous structures. They found that manufacturing parameters (laser power, scan speed, etc.) have a considerable effect on the dimensions accuracy of structure struts, but have no influence on the compressive strength of the lattice structures. On the other hand, design parameters (unit cell form, geometrical construction and struts aspect ratio/diameter) have an essential impact on mechanical properties of lattice structures under the compressive loads.

Tancogne-Dejean et al. [69] had investigated the mechanical response under static and dynamic loads of the metallic lattice structures made by SLM process. An experimental study and numerical analysis were executed to explore the compression response and energy absorption of octet truss cellular structures. They conclude that the compression response of lattice structures with relative density higher than 30% becomes a stable. They also added that specific energy absorption increases by increasing the relative density. In addition, the geometry of struts has a significant effect on the stress-strain response of metallic lattice structures.

Hedayati and Sadighi [12] had studied the elastic and post-yield response of open cell porous structures made of SLM under compression forces. They used rhombic dodecahedron unit cell to form the lattice structure. In addition, it is stated that numerical modelling was executed to explore the properties of the porous structures in point after-yielding behaviour using ANSYS software. They have found that variation in the struts thickness in FEA has a significant effect by reducing the elastic and densification strain comparing to experimental test data. Furthermore, smoothly strain stress curve was observed between irregular struts structure of numerical analysis and experiment work in yield and densification points. Consequently, they concluded that a numerical analysis using beam elements types in modelling irregular thickness of lattice structure provides convergent results with experimental results.

Zhong and Li [98] done the simulation analysis to analyse the mechanical properties and the deformation response of lattice structures with five different unit cell using ANSYS software. These unit cells are edge structure ES, vertex structure VS, face centre structure FCS, interconnect vertex structure IVS and cross face centre structure CFCS. The finite element analysis (FEA) results indicated that lattice structure build of edge structure unit cell exhibited optimal performance compared to other lattice structures when subjected to stress, bend and twist loads. In addition, they concluded that functional and bearing efficiency data of lattice structures obtained from FEA study can be used to design various lattice structures.

Yan et al. [99] had done the investigation of the manufacturability and mechanical performance of advanced cellular lattice structures made of stainless steel and fabricated by SLM. The gyroid unit cell was used to construct the cellular lattice structures with a varied range of relative densities and designed with different orientations. They found that SEM, OM and CT scan observations of fabricated gyroid lattice structures exhibited a good agreement with the CAD models. Also, these observations revealed that the solid struts of the SLM-fabricated structures were in rough surface and their dimensions were slightly higher than the CAD models. The results of this study revealed that the gyroid lattice structures with vertical and ºsteel exhibited higher mechanical performance comparable to the normal gyroid lattice structures. They also pointed out that increase the compressive mechanical properties was tied with increase the relative density of the lattice structures.

Van-Grunsven et al. [65] had experimentally studied the ability of electron beam melting EBM technique to fabricate regular diamond lattice structure with porosity gradient from Ti6Al4V material. They reported that achieving the porosity gradient was via change the strut cross section thickness in each layer throughout the structure layers. They found that SEM and micro CT analysis revealed the ability of EBM to produce periodic lattice structure with graded porosity well, although smaller strut thickness of the fabricated lattice found thicker than the CAD model one. Mechanical performance of the fabricated lattice structure under the uni-axial compression tests clearly showed its behaviour under compression was tied along the direction of gradation.

Maskery et al. [93] studied the deformation modes and energy absorption capability of uniform double gyroid lattices with range of different unit cell sizes made of Al-Si10-Mg and fabricated by SLM process. They conducted the post-manufacture heat treatment for the fabricated lattice structures to study the effect of heat treatment on the compressive deformation modes. They have mentioned that the findings of this study divide to following key results. First, the unit cell size has a significant effect on the compressive properties of lattice structure that smaller unit cell provides high mechanical properties. Second, using heat treatment process can successfully getting rid of well-known brittle failure of Al-Si 10-Mg lattice structure. Third, the energy absorption calculation demonstrated that double gyroid lattice structure absorbed energy three times higher than BCC lattice structure under the compressive loads.

Delroisse et al. [85] investigated the microstructure heterogeneities of Al-Si10-Mg lattice structures with different struts orientations manufactured by SLM techniques as shown in Fig. 2.12. The fabricated lattice structures, inclined and normal were subjected to the heat treatment.
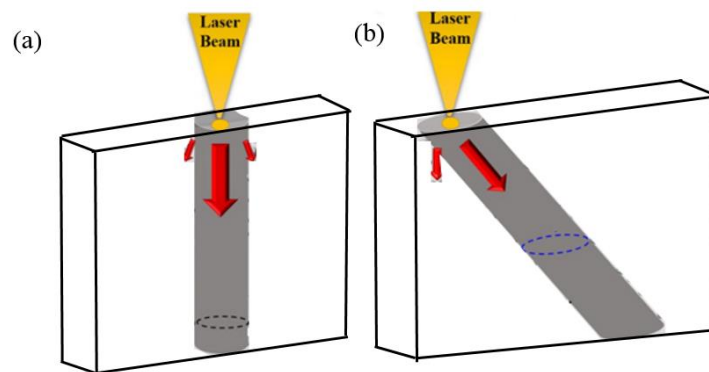
Figure 2.13 Schematic of lattice struts (a) the vertical, (b) the inclined [85]

They pointed out that the strut build direction plays an important role on the microstructure heterogeneities of the lattice structures. Lattice structures with vertical struts orientation present a fully dense homogenous microstructure with compared to included struts – lattice structures. They also added that large amount of porosity was found in bottom part compared to top part of the inclined struts. The concluded that conducting the T6 heat treatment let to improve the microstructure homogenization, but also let to increase the softening on the expense the hardness.

2.7. Summary

Functionally graded lattice structure, or material is a new class of advanced engineering material that provides promising solutions to the problems and limitations of the traditional engineering materials for a wide range of applications. There are numerous works that have been done in studying and investigation the cellular structure and functionally graded material. As has been established from literature review, many limitations were tied with traditional manufacturing techniques. Development of additive manufacturing technology has offered an answer for the most of the problems of the traditional manufacturing processes.

Literature review has shown that using additive manufacturing techniques to produce such materials and structures have been reported by many researchers recently. Although there are many studies investigating the different aspects of lattice, scaffold and cellular structure, little can be found on functionally graded profile especially with continuous and linear density gradient. Most of the studies were concerned with the formation of lattice structures from various metallic alloy like 316L stainless steel, Ti6Al4V, Al-Si10-Mg, polymer material like PLA, ABS, and polyimide. Little attention has been paid using Al-Si alloy especially Al-12Si. Investigations of mechanical properties and microstructures of SLM-Al alloy showed that various heat treatment processes could turn of the microstructure and thus mechanical properties to SLM-Al alloy to the range of required characteristics. Therefore, the response of the SLM – Al-12Si material to solution heat treatments T6 requires investigation. The effect of a heat treatment such as T6 (solution heat treatment and ageing) on the various mechanical properties and energy absorption capability of SLM-AL-12Si has not yet been fully studied.

Published studies investigating the mechanical properties of energy absorption capability of SLM- lattice structures focussed on either conducting experimental work such as compression, tensile, impact tests or the numerical simulation study. Assessment of compressive mechanical properties of SLM- lattice structures using the combing approach of experimental and finite element analysis is quite limited.

**The research gaps that have been highlighted from the literature review:**

1- The evolution of the SLM processed Al-12Si microstructure due to heat treatment (T6) requires investigation in understanding the mechanical behaviour as well as the response of SLM – Al-12Si lattice structures to the heat treatments.

2- Modelling functionally graded density lattice structures with continuous and linear gradient throughout the structural layers has not yet been studied, needs more attention.

3- Using F2CCZ unit cell in the construction of 3D periodic lattice structure, especially the new approach of functionally graded lattice structures, and its mechanical performance need to be studied.

4- Assessing the compressive mechanical properties and energy absorption capability of functionally graded lattice structure using the experimental and simulation approaches need to be developed and compared.

Chapter 3

METHODOLOGY

3.1. Overview

This chapter includes descriptions of all materials, equipment and the procedures used to conduct this research study. It provides comprehensive information begin from the unit cell selection of lattice structure and to the end of the manufacturing process. Figure 3.1 illustrates the methodology of the current study.
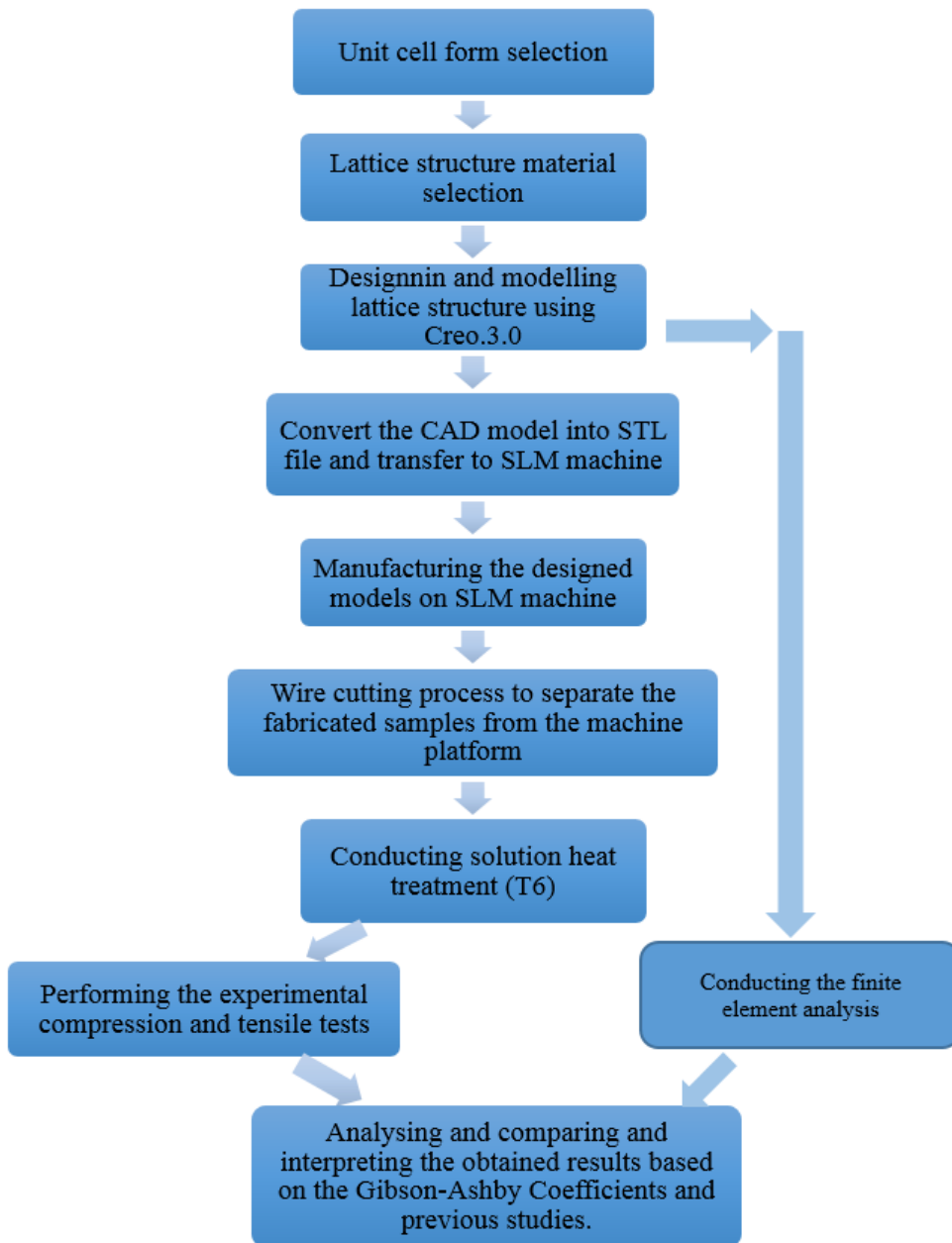
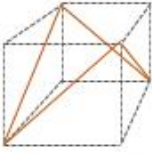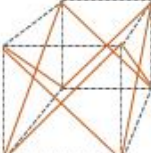*Figure 3.1 flow chart of methodology of the current study*
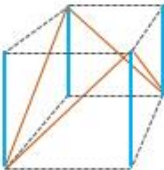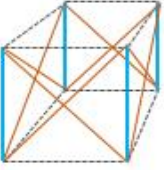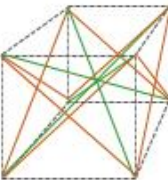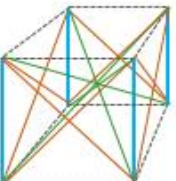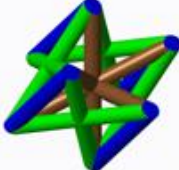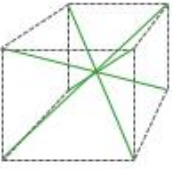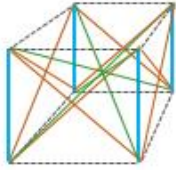
3.2. Selection of unit cell form of the lattice structure

There are many different types of unit cells of architectural form that have been used in the design and fabrication the 3D- periodic lattice structures for various fields of applications. For example, body centered cubic (BCC) and face centered cubic (FCC) unit cells are commonly used in modelling the lattice structures for AM technology [9, 64, 68]. These types of unit cells can be strengthened by combining them or by adding more struts and rods in various directions. Figure 3.2 shows different unit cells (FCC, FCC_Z, F_2CC, F_2CC_Z, BCC, BCC_Z, F_2BCC and F_2BCC_Z) (Ahmed et al. 2015) and (Rehme et al. [100]). They had investigated the compressive properties and failure modes of cellular structures built from different types of unit cells. Ahmed at el. (2015) pointed out that the F2BCCz exhibited the best performing under the compressive loads due to its higher relative density and lower porous compared to other unit cells. Also, it is pointed out that F2BCCZ unit cells took the longest time to get manufactured due to the increase of their relative density. It is clear from the Ahmed's conclusion that F2BCCz unit cell could not be preferred for energy absorption applications, although it's higher compressive properties. They added that F2CCz and F2BCC could be considered for applications that required combination of the lightweight and high strength.

Rehme et al. [100] conducted comprehensive study to investigate the mechanical properties and energy absorption of various unit cell forms that are used in AM technology- lattice structures. They concluded that F2CCz unit cell exhibited best yield strength – to- relative density compared with other unit cell forms.

However, since lightweight and high strength of the lattice structure are the key objectives of this research study, therefore, F2CCz unit cell form will be used to construct the lattice structures based on Ahmed's and Rehme's investigations in order to gain the combination of lightweight and high strength.

Unit cell name	Unit cell schematic	CAD model of Unit cell
FCC		
F2CC		
FCCz		
F2CCz		
F2BCC		
F2BCCz		
BCC		
BCCz		

——— Z rod   ——— Face-centered-rods   ——— Body-centered-rods

Figure 3.2 schematic of different unit cell forms of lattice structures

3.3. Aluminium-silicon alloy powder (Al-12Si)

Aluminium-Silicon Alloy (Al-12Si) was used in this study to manufacture the designed lattice structures on ProX DMP 200 selective laser melting machine. The particle size distributions of the AlSi-12 powder was (~ 40 µm) and supplied by 3D Systems Company. The properties of the fabricated material determined from tensile tests that were done using dog bone tensile test specimens and compared to other studies.

3.4. Design of the lattice structure

Computer-Aided Design systems (CAD software) have been widely used in designing and modelling components with variety in geometric complexity. Today, there are many different CAD systems available in the markets such as SOLIDWORKS, CATIA, PTC Creo. In this project, PTC Creo. Parametric 3.0 was chosen to model the lattice structures because it has a large number of parametric feature modelling tools that make the design process much easier and faster. In addition, it provides the designers ability to calculate the physical properties (density, volume) of designed part and a wide range of file format like STL with fast converting process. However, two different lattice structures were designed in this study which are uniform and functionally graded lattice structures, as well as dog-bone tensile test and cubical microstructures samples.

3.4.1. Uniform lattice structures

The uniform lattice structures composed of 3D periodic unit cells of F2CCz with dimensions ($5\times5\times5$ mm). Fig 3.3a illustrates the CAD model of the F2CCz unit cell with its dimensions. The F2CCz unit cell has 12 struts with cylindrical cross section, four in the vertical direction Z, and eight as double face diagonals in the X-Z and Y-Z plane (two at each face). The diameter of the cylindrical struts in the uniform lattice is (812.5µm). After that, the pattern feature was applied to replicate the completed unit cell in three directions (X, Y, Z) to build the whole uniform lattice structure in ($30\times30\times30$ mm) that means the structure will contain six-unit cell in each direction as shown in Fig. 3.3b.
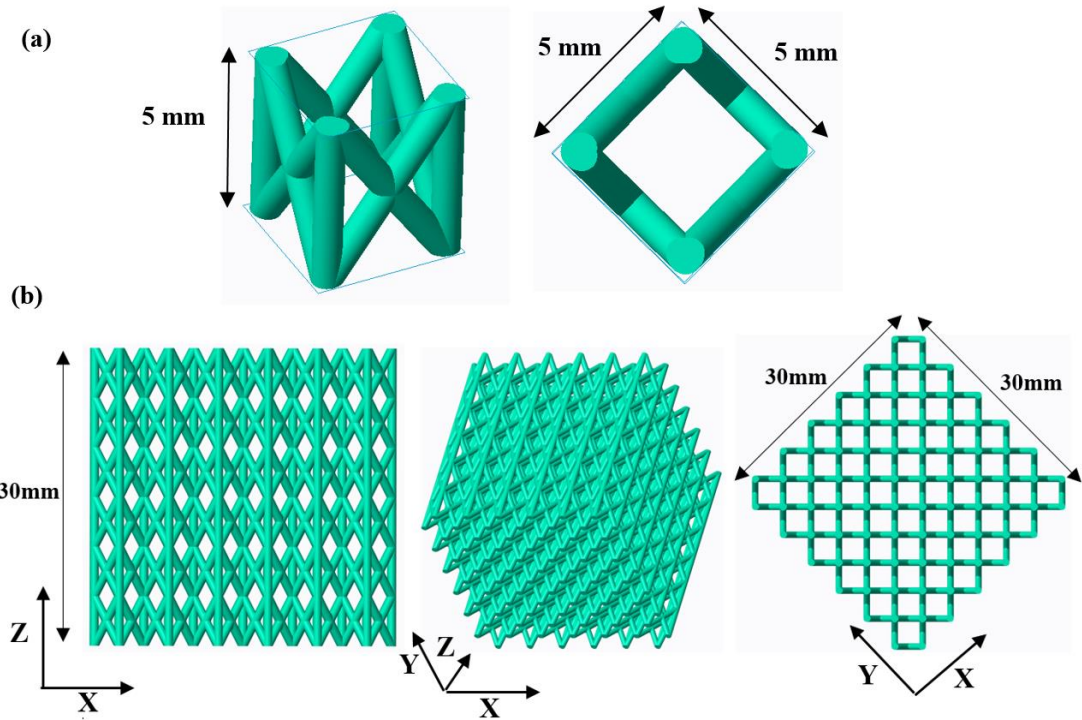
Figure 3.3 CAD model of (a) F2CCz unit cell, (b) uniform lattice structure

3.4.2. Functionally graded lattice structures

Functionally graded lattice structure is characterized by spatial gradation in solid material and porosity. Functionally graded lattice structures designed with material density increase gradually and continuously from top to bottom layers throughout the six structural layers. Technically, it is very complex architectural geometry since we attempt to compare the two different lattice structures based on the equal relative density. However, it has six layers of cells, and each layer has certain density in which the density increase continuously and linearly at 50% rate in sequence. This was achieved by designing cell struts diameters varying from 350 - 500, 500 - 545, 545 - 735, 735 - 834, 834 – 1082.5, and 1082.5 - 1270 µm for six structural layers respectively. The cell struts diameters were changed in one direction (build direction) with linear and continuous change, thus resulting in smooth density change at the boundaries of the lattice structure layers. Figure 3.4 shows the CAD model of the graded lattice structure with its dimensions.
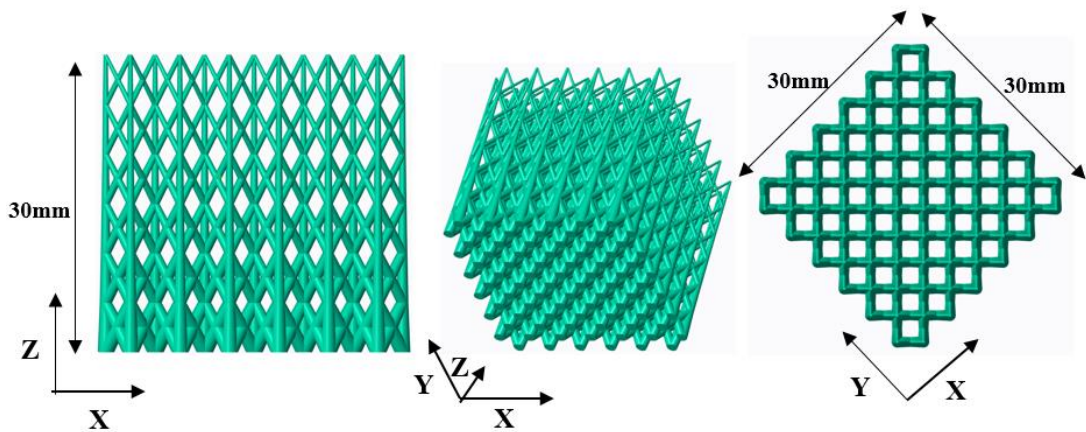
Figure 3.4 CAD model of graded lattice structures

3.5. Design of tensile test and microstructure specimens

The four dog-bone tensile test specimens have been designed according to ASTM standard under the code E8/E8M − 16a 2016, in which total length, gauge length and width at centre are 80.96, 25.4 and 5.72 mm respectively. The main purpose of design and manufacturing the tensile test specimens is to get on the material properties and for investigation the effect of solution heat treatment process on the mechanical properties. In addition, two microstructures specimens (1×1.5×1.5 mm) have been modelled to study the microstructure of the material before and after the conducting heat treatment process. Figure 3.5 shows the CAD models of tensile test and microstructures specimens.
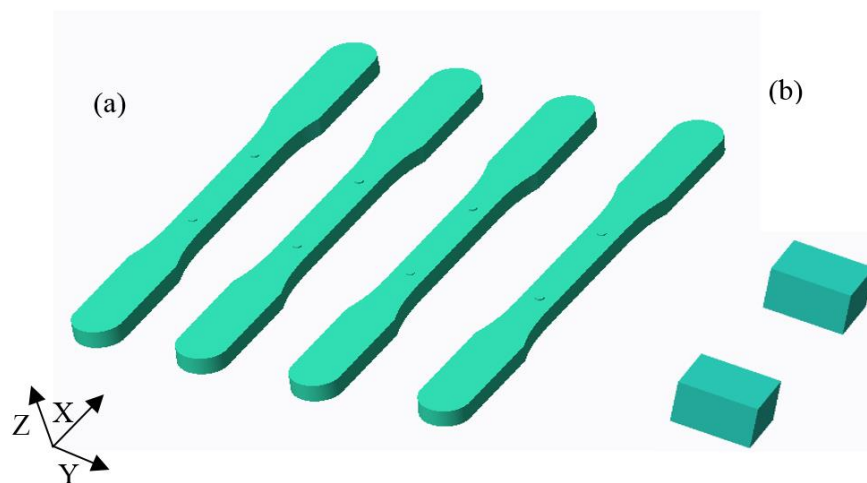
Figure 3.5 CAD models of (a) tensile test, and (b) microstructure specimens

3.6. Converting process of CAD model

The process of converting the final digital model to the STL file is a necessary to ensure that the CAD model has been correctly designed and there is no errors with modelling process. In addition, STL file extension is important to read CAD data by the additive manufacturing machines like ProX DMP 200 selective laser melting machine.

3.7. Manufacturing process

The 12 samples of ($30\times 30\times 30$ mm) designed lattice structures, four dog-bone tensile test specimens, and two ($1\times1.5\times1.5$ mm) cubical microstructure specimens were manufactured using SLM technology on a ProX 200 3D system machine, as shown in Fig 3.6. This SLM machine is installed on the ground level of AMDC building in Swinburne University / Hawthorn camps. It has been commonly used in manufacturing metal components from the wide range of metal alloy powders like AlSi-12, Ti6AL4V, and 17- 4 PH. However, after STL file was transferred to the SLM machine software, the process of slicing of CAD model was done with layer thickness of 40 µm, and thus contained 726 layers for one structure.

After the slicing process and arrangement process of samples on the platform had been done, the manufacturing parameters were set up as shown in table 3 .1. Fig 3.7 shows the fabricated-SLM specimens on the machine plates before the wire cut process. For clarification, all samples were fabricated in same build direction (Z-direction) to avoid the build direction effect.

Table 3.1 manufacturing parameters

SLM parameters	values
Laser type	Nd:YAG laser (1070 nm)
Laser power	285 W
Laser scan speed	2500 mm s^{-1}
Laser hatch spacing	100 µm
Powder deposition thickness	40 µm
Chamber gas	Argon

Figure 3.6 ProX 200   SLM machine
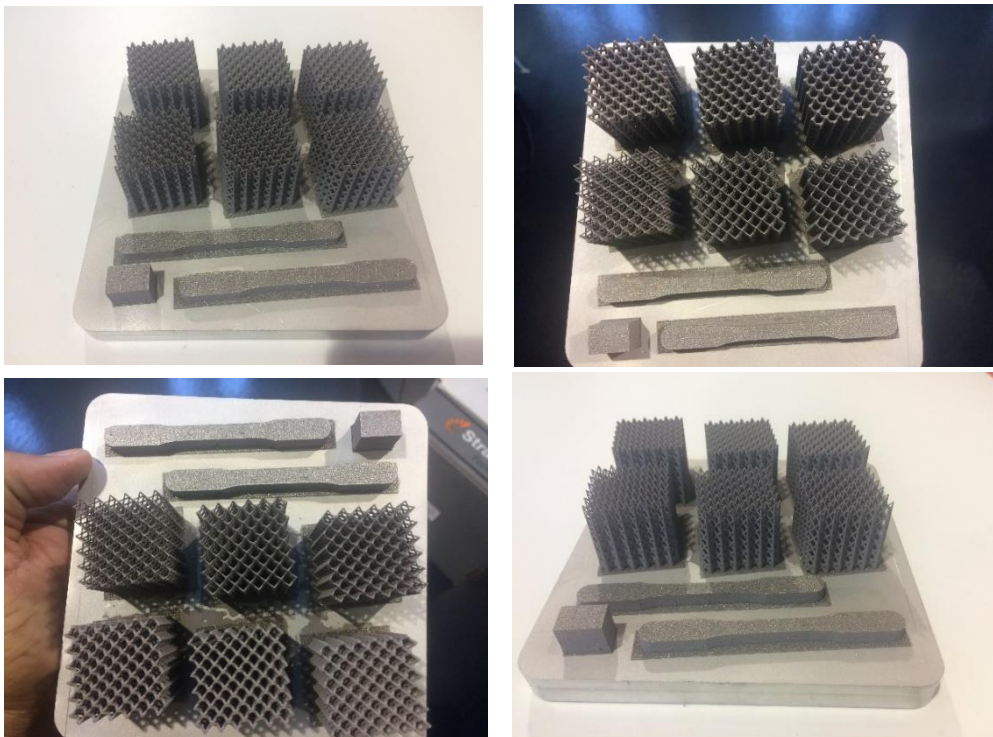
Figure 3.7 fabricated samples on the machine platform before wire cut process.

3.8. EDM wire cutting process

The EDM wire cutting process was conducted carefully to separate the completely fabricated lattice structures, tensile test and microstructure samples from the machine platform, because the lattice structures are very delicate and there should be no damage to the structures. Therefore, wire cutting process was done on FANUC robcut alpha OC at ATLAS tooling company. Fig 3.8 shows the EDM machine, and the cutting process parameters illustrate in table 3.2. Fig 3.9 demonstrates all sample after EDM cutting process.

Table 3.2 Wire cut parameters

EDM process parameters	
Dielectric fluid	Dionising water
Flushing type	Water flushing
Pulse on time	8 µs
Wire feed	8 mm/min
Tool material	brass
Tool shape	Wire (0.25 mm) diameter

Figure 3.8 FANUC ROBCUT ALPHA OC wire cutting machine
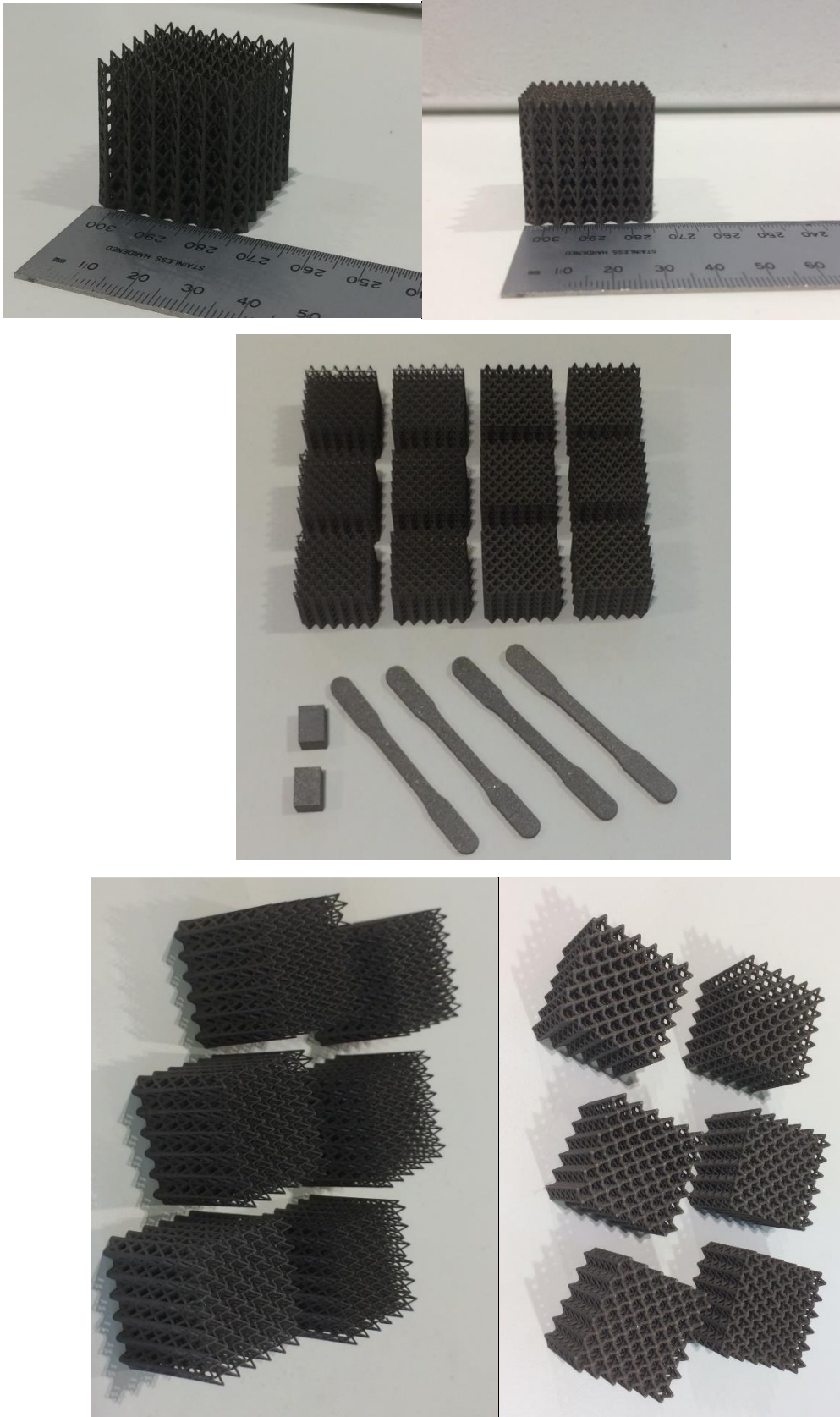
Figure 3.9 fabricated lattice structure, tensile test and microstructure specimens

Chapter 4

MECHANICAL AND ENERGY ABSORPTION CHARACTERISTICS OF THE LATTICE STRUCTURE

4.1. Overview

In this chapter, typical deformation modes of the lattice structures and Gibson and Ashby's equations are illustrated in detail. In addition, calculation of the compressive mechanical properties (young's modulus, yield strength and onset densification strain) and the energy absorption property of the lattice structures has been explained.

4.2. Deformation modes of lattice structures

There have been a large number of studies and researches conducted to investigate and describe the mechanical properties and deformation behaviour of the cellular structures. The most important research work is that performed by Gibson and Ashby [1] for studying and defining the deformation behaviour and mechanical properties of the porous solids structures. They have developed a series of equations that can explain the deformation behaviour of the cellular structures under the compressive loads as given in equations (1), (2) and (3) in current study. Basically, these three equations represent the elastic region, plateau region and densification region respectively as shown in Fig 4.1. In addition, the ISO standard has comprehensively described mechanical properties of cellular solids under the code ISO 13314:2011. In this study, it is defined as the mechanical and energy absorption characteristics based on the previous studies and ISO standards. Table 4.1 shows the meaning of the symbols in equations (1), (2) and (3).

$$\frac{E_{latt}}{E_m} = C_1 \left\{ \frac{\rho_{latt}}{\rho_m} \right\}^n \text{--------------------- (1)}$$

$$\frac{\sigma_{pl.latt}}{\sigma_{yl.m}} = C_5 \left\{ \frac{\rho_{latt}}{\rho_m} \right\}^m \text{------------------- (2)}$$

$$\varepsilon_D = 1 - \alpha \left\{ \frac{\rho_{latt}}{\rho_m} \right\} \text{------------------- (3)}$$

Where the constants C_1, C_5 and α are given in range of value $0.1 - 4.0$, $0.25 - 0.35$ and $1.4 - 2.0$ respectively. While, the n and m are constant, and their values are ~ 2 and $\sim 3/2$.

It is clear from Fig 4.1 (a) and (b) that the structural deformation of the cellular structure under the compressive loads exhibits three ideal regimes. The first regime is a linear elastic region, which is characterized by the elastic modulus of lattice structure as expressed in equation (1). The buckling and the bending failure in lattice structure struts under the compressive loads is the main cause of deformation in this region. The second region of the stress-strain curve is the plateau regime, which mainly depended on the material properties that the lattice structure is made from. Fig 4.1 (a) compressive stress – strain curve for ductile material shows a long, smooth plateau region, this is due to the formation of plastic hinges in contact points (nodes) of lattice structure struts under the compressive loads. For the brittle material, Fig 4.1 (b) shows a long fluctuation as second region of the stress – strain curve. This can occur due to the fracture and flake formation in lattice structure struts. The long plateau stress region and its tied energy absorption are considered an essential region that has made the cellular structures more desirable for energy absorption applications (Ashby at al. [18], Winter at el. [101] and Maskery et al. [9]. The third regime is densification region, when continued compressive loads will lead to full compaction of the structure due to contact of the cell struts with the next cell struts causing a considerable rise in lattice structure stiffness. This is expressed by equation (3) of Gibson and Ashby[1]. The value of onset densification ε_D as the densification region starts, is considered a practical limit to use lattice structure for energy absorption applications. After this limit of strain, lattice structure will continuously absorb the energy, but at the expense of transmitting stress throughout the lattice structure. This may lead to damage (in case of goods, packaging) or harm (in case of personal protective equipment).
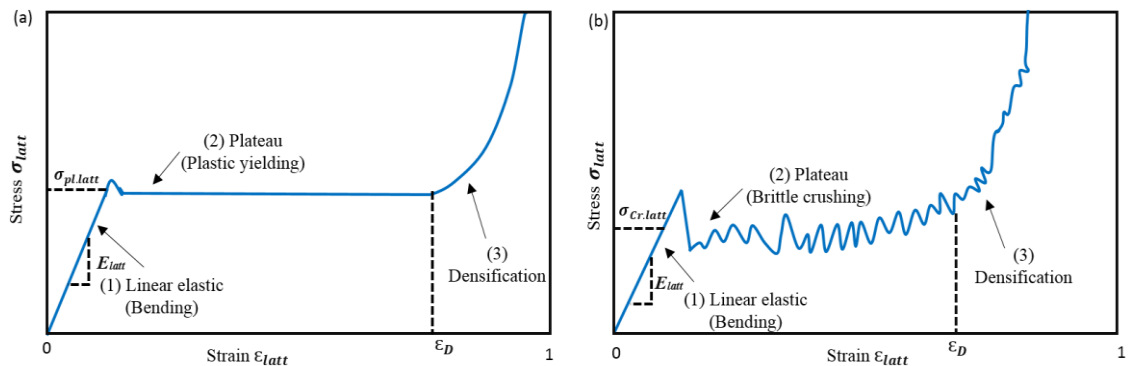
Figure 4.1 typical schematic of compressive stress – strain curves of lattice structures
(a) ductile material, (b) brittle material. [1]

It is apparent from the above details that the relative density of lattice structures is the most important variables and the key factor in determining the mechanical properties and deformation behaviour of the lattice structures. Besides, architectural cell form, an aspect ratio of the unit cell, distribution of the material and its properties that the structures are made from, also influence on the mechanical behaviour of the lattice structures. Next section, it provides how the relative density of lattice structures has been calculated in current study.

Table 4.1 notations used in description of the mechanical properties of lattice structure

No	Symbolization	Characteristics
1	E_{latt}	Young's modulus of lattice structure
2	E_m	Young's modulus of parent material
3	E^*	Relative young's modulus of lattice, which is $\frac{E_{latt}}{E_m}$
4	ρ_{latt}	Density of lattice structure
5	ρ_m	Density of parent material
6	ρ^*	Relative density of lattice structures, which is $\frac{\rho_{latt}}{\rho_m}$
7	$\sigma_{pl.latt}$	Plateau stress of lattice structure
8	$\sigma_{yl.m}$	Yield stress of parent material
9	ε_D	Onset densification strain of lattice structure
10	Wv	Energy absorption of lattice structure

4.3. Relative density

It is a ratio of the physical density of the lattice structure as occupied by solid struts over the theoretical density of the parent material used in lattice[1, 18]. Equation (4) represents the relative density formal.

$$\rho^* = \frac{\rho_{\text{latt}}}{\rho_m} \quad \text{----------------- (4)}$$

Where:

ρ^* : Relative density

ρ_{latt} : Structure density of lattice

ρ_m : Parent material density

3.7.1. Uniform lattice structures

In order to find the volume fraction (relative density) of the uniform lattice structures, the physical density of the structures after manufacturing process should be calculated according the following equation.

$$\rho_{\text{latt}} = \frac{M}{V} \quad \text{--------------------- (5)}$$

Where: M is the mass of manufactured lattice structure in air, which has been determined by using a digital scale (Sartorious with capacity of 250 g) installed on the ground level of Factory of future lab at AMDC building, which is (13.9020 g) as shown in Fig. 4.3. While: V is the total volume of the lattice structure that has been obtained directly by multiplying width, height and length of the structure (30*30*30 mm).

So, the density of the uniform lattice structure is

$$\rho_{\text{latt}} = \frac{13.9020}{27} = 0.514 \text{ g/cm}^3$$

Thus, relative density is calculated based on the equation (4), after the physical density of the lattice structures has been found from the equation (5), and the parent material density is (2.7g mm^{-3}).

The relative density is
$$\rho^* = \frac{0.514}{2.7} = 0.19$$
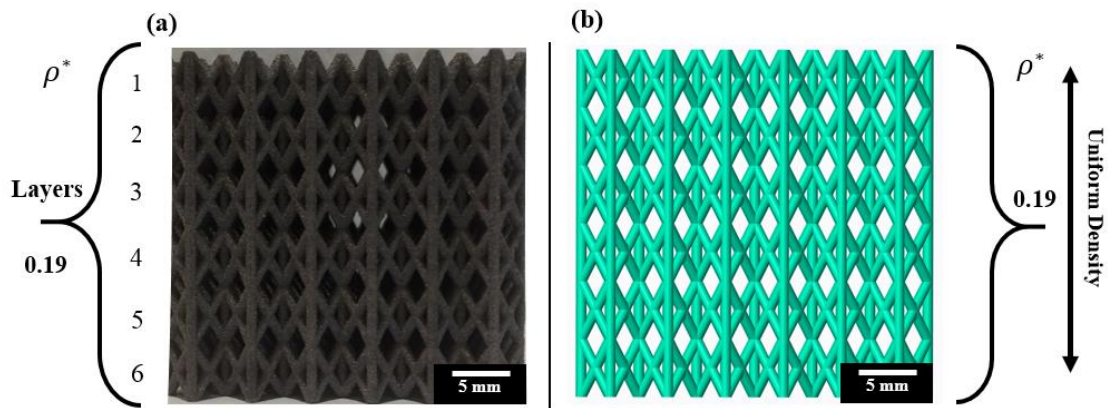
Figure 4.2(a) manufactured lattice structures, (b) CAD model of the lattice structure
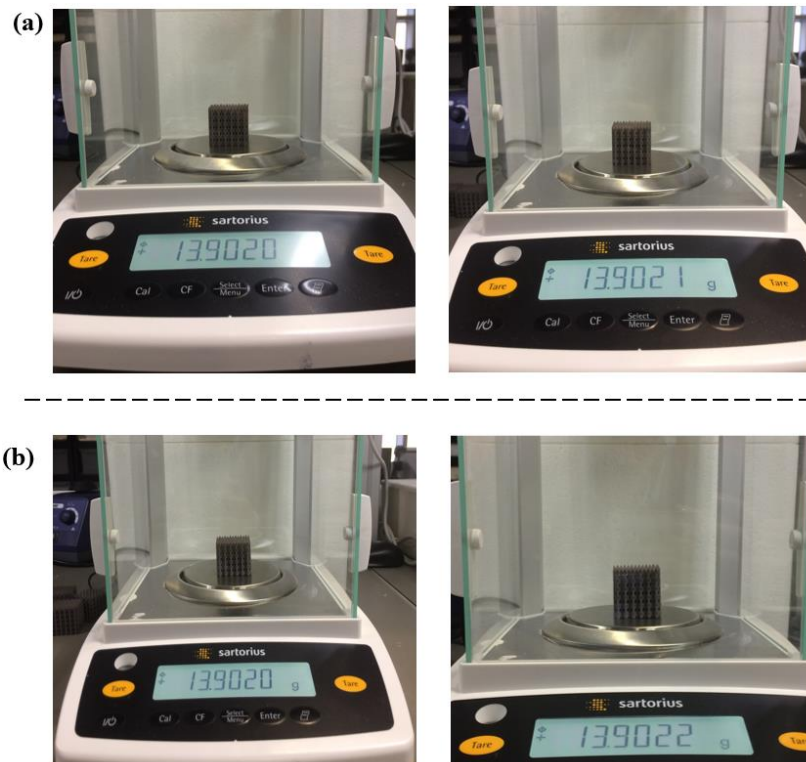
Figure 4.3manufactured lattice structure on Sartorious scale device, (a) uniform, (b) graded

3.7.2. Graded lattice structures

Basically, same concept that was used to find physical density and the relative density of uniform lattice structure applied on the functionally graded lattice structure.

Accordingly, from the equation (5), we find the physical density:

$$\rho_{\text{latt}} = \frac{13.9020}{27} = 0.514 \text{ g/cm}^3$$

Where:

      13.9020 g: is the mass in air

      27 cm³: is the total volume

Thus, **the relative density** of the functionally graded structures is based on equation (4):

$$\rho^* = \frac{0.514}{2.7} = 0.19$$

However, the relative density of each layer will be varying gradually from top to bottom as shown in Fig 4.4.
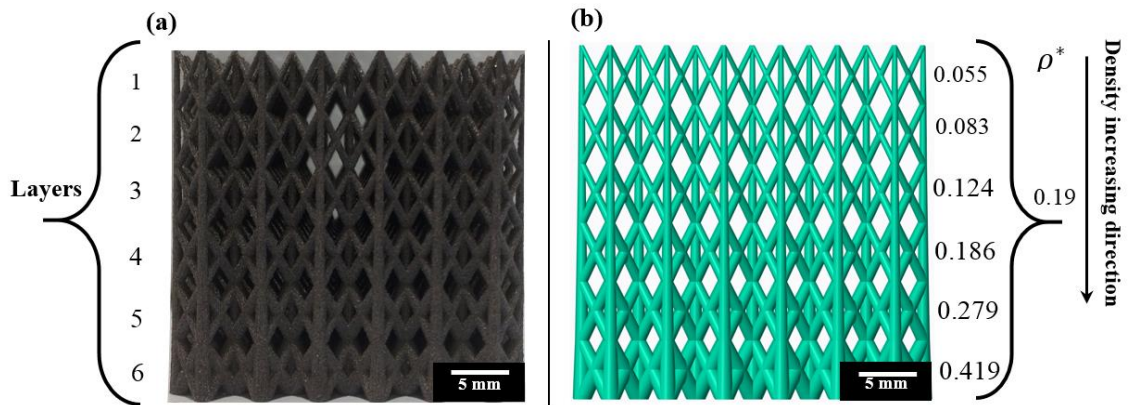
Figure 4.4(a) manufactured lattice structure, (b) CAD model of the structure

1.   Relative density of each layer in functionally graded lattice structure

To illustrate the new approach of designing functionally graded lattice structures with gradually increasing density throughout the six layers from the top to the bottom, the relative density (volume fraction) of each layer was determined to ensure that the gradient density increases at a constant rate of 50% in sequence as it signed in designing stages. Equation (6) represents the formal.

$$\rho^*{}_{lay} = \frac{\rho_{\text{lay}}}{\rho_m} \qquad \text{-------------------------- (6)}$$

In order to solve the above equation, we need to find the physical density of the each layer ρ_{lay} separately. The next equation (7) provides the formal of calculation the physical density of each layer.

$$\rho_{lay} = \frac{M_{\text{lay}}}{V_t} \qquad \text{------------------------ (7)}$$

Where M_{lay} and V_t are the mass in air of the layer and the total volume of layer (30×30×5 mm), respectively.

Thus, M $_{lay}$ can be determine by using equation (8).

$$\rho_m = \frac{M_{lay}}{V_{lay}} \qquad \text{-------------------------- (8)}$$

Or $\qquad\qquad\qquad M_{lay} = \rho_m \times V_{lay}$

Where: ρ_m, M_{lay} and V_{lay} are the density of parent material, mass of the layer and the volume of solid struts in layer that can be calculated directly from CAD model on Creo Parametric software, respectively.

Where:

- $\rho^*{}_{lay}$: Relative density of layer
- ρ_{lay} : Density of the one layer
- ρ_m : Density of parent material
- M_{lay} : Mass of layer
- V_{lay} : Volume of solid struts in layer (CAD model)
- V_t : Total volume of the layer (30×30×5 mm)
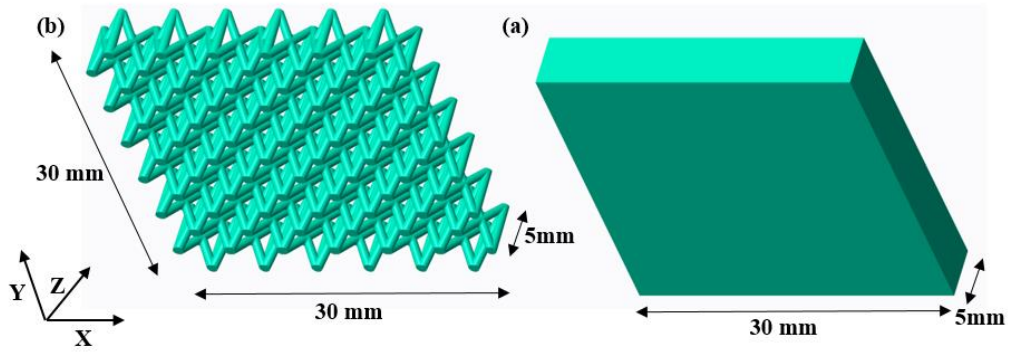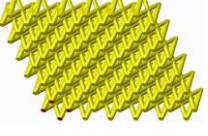
Figure 4.5(A) volume of the solid struts in layer, (B) total volume of whole layer

Table 4.2 relative densities of the six layers of the graded lattice structure

No	V_{lay}	$M_{lay} = \rho_m \times V_{lay}$	$\rho_{lay} = \dfrac{M_{lay}}{V_t}$	$\rho^*_{lay} = \dfrac{\rho_{lay}}{\rho_m}$	layer
	cm^3	gram	g/cm^3		
Layer one	0.2481085	0.669893	0.148865	0.055	
Layer two	0.37216275	1.004839	0.223298	0.083	
Layer three	0.558244125	1.507259	0.334946	0.124	
Layer four	0.837366188	2.260889	0.50242	0.186	
Layer five	1.256049281	3.391333	0.75363	0.279	
Layer six	1.884073922	5.087	1.130444	0.419	

Where: ρ_m: 2.7 g/cm^3 V_t : 4.5 cm^3

4.4. Compressive mechanical properties

4.4.1. Young's modulus (E_{latt})

It can be defined as a ratio between stress over the strain at the elastic region in which the material is deformed under stress that is linearly proportional to strain, and usually before the yield point or when material starting deform permanently. Fig 4.6 shows compressive stress strain curve of a cellular lattice structure.

4.4.2. Plateau stress

It is an average value of stresses that should be taken at (20% - 30%) or (20% - 40%) of strain during the compressive loading test according to (ISO code 13314: 2011). While, Olurin et al. [102] state that plateau stress is supposed to be taken as averages compressive stress at (5% -30%) of compressive strain as shown in Fig 4.6.

4.4.3. Onset densification strain (end of the plateau region)

Many different ways can be considered in determining the value of the onset densification strain. As an example, ISO standard under the code (13314: 2011), has determined that onset densification strain ε_D could be taken as a point on compressive stress strain curve at 1.3 times of plateau stress. Whereas, Olurin et al. [102] claim that onset densification strain shall be taken as point that equal to the twice value of determined plateau stress as shown in Fig 4.6.
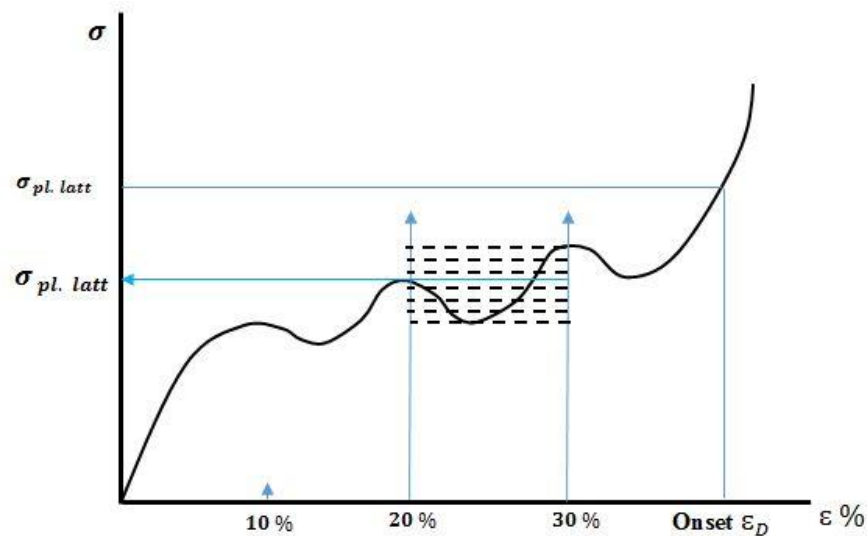
Figure 4.6 plateau stress, plateau end stress and onset densification strain on typical compressive stress strain curve of cellular structure.

4.5. Energy absorption characteristic

It is one of the important properties of lattice structures or foam structures that has made them more attractive in packaging and personal protection applications. There has been a large number of researches conducted in defining and investigation the energy absorption property of lattice structures. Generally, the lattice structures absorb energy during the deformation under compression loads, which can be expressed as the area under the curve of stress-strain (Gibson and Ashby[1] and ISO standard [103]. Fig 4.7 illustrates the area under the curves that determine the energy absorption capability of the lattice structure.

In order to calculate the area under the curve, the equation (9) is used to find the energy absorption property.

$$Wv = \int_0^\varepsilon \sigma(\varepsilon)d\varepsilon \quad \text{-------------------- (9)}$$
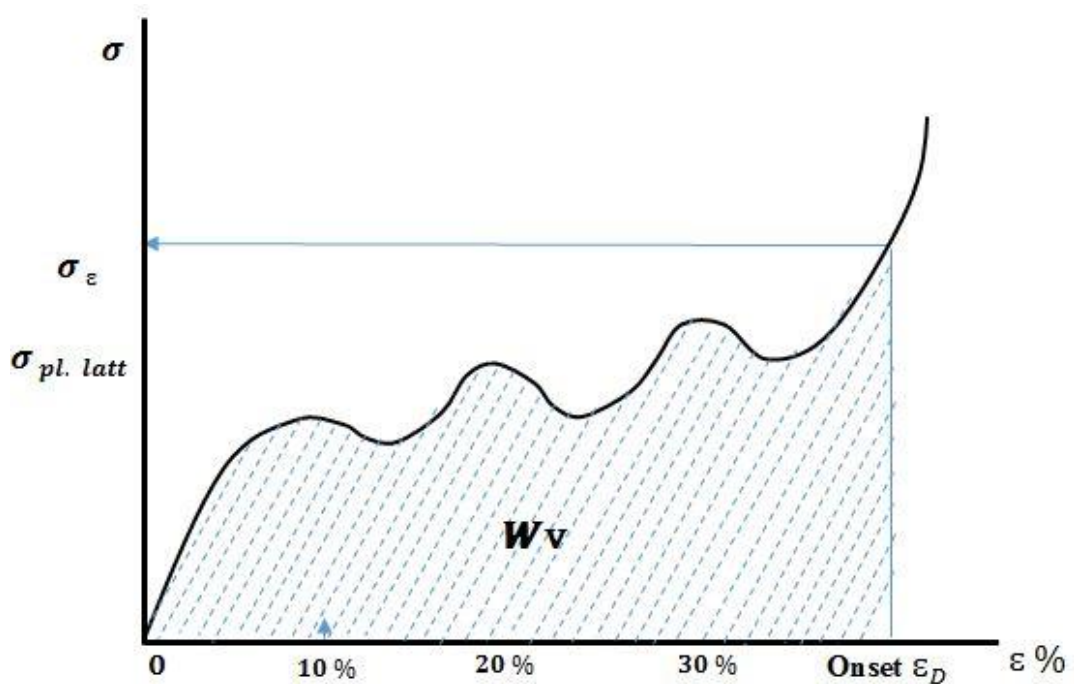
Figure 4.7 typical compressive stress strain curve of cellular structure.

Chapter 5

METHODOLOGY AND FINITE ELEMENT ANALYSIS

5.1. Overview

This chapter provides comprehensive information related to the experiment work and finite element analysis FEA that have been executed after the samples were manufactured for getting the main objectives of this study. The experimental measurements will be illustrated and experimental tests, as well as numerical analysis models.

5.2. Experimental measurements

5.2.1. The dimensions and the relative density

The diameters and thickness of the fabricated solid struts of the lattice structures were measured using optical microscope (OM) (OLYMPUS U-TV1X-2) and Digital Vernier Caliper with tolerance 0.001 mm to compare the fabricated and CAD models of the solid struts dimensions of the lattice structures. Also, measurement processes provide clear picture about the ability of SLM technology to manufacture such micro-lattice structures.

The relative density of fabricated lattice structures is considered the most critical parameter in designing and determining the mechanical properties of the lattice structures. Therefore, it was found by dividing the calculated physical density of the manufactured lattice structure by the material density of Al-12Si (2.7 g cm^{-3}).

The calculated physical density of the fabricated lattice structures is determined by dividing the mass to the total volume of the lattice structure ($30 \times 30 \times 30$ mm). A digital scale Sartorious with capacity of 250 g with tolerance 0.0001 (figure 5.1) was used to determine the weight of the lattice structures in air as it is explained in detail in section4.3.

Figure 5.1OLYMPUS U-TV1X-2 optical microscopy

5.2.2. Surface morphology and microstructural study

An optical microscope (OM) (OLYMPUS U-TV1X-2) and scanning electron microscopy (Gemini -ZEISS), which are installed on the basement level of AMDC and ATC buildings at Swinburne university respectively, were used to investigate and study the surface morphology and fracture surfaces of the solid lattice struts before and after the deformation processes. Technically, prior to processing, air jet clean was employed for few minutes to ensure that all loose powder and any other contaminations had been removed from the solid struts of the lattice structures.

A microstructure study and investigation has been conducted on cubical samples, as-build and heat-treated of Al-12Si material, using X-ray diffraction, SEM and Optical Microscope OM (Olympus Bx61) as shown in figure 5.2.

Figure 5.2 Optical Microscope (Olympus Bx61), (lift), SEM device (Gemini -ZEISS), (right).

It is worth noting that specimen preparation process was implemented to get the samples ready to the microstructure study, which include the following steps.

1. A cubical microstructure samples (1×1.5×1.5 mm) as-build and heat-treated have been cut using electrical saw to two halves (1×1.5×0.75 mm) in order to use two samples for OM and SEM and other two samples for XRD as shown in figure 5.3.
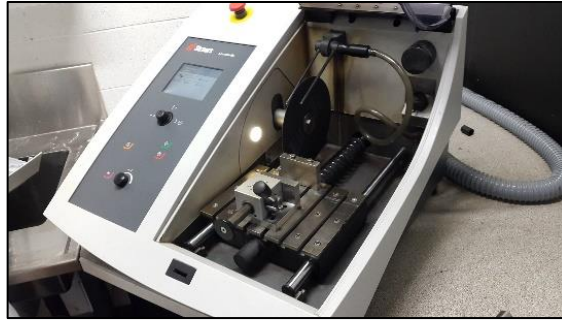
Figure 5.3 Cutting machine with 2200 RPM

2. OM and SEM samples were mounted in Bakelite using Buehler device (SIMPLIMIT 1000) as shown in figure 5.4.
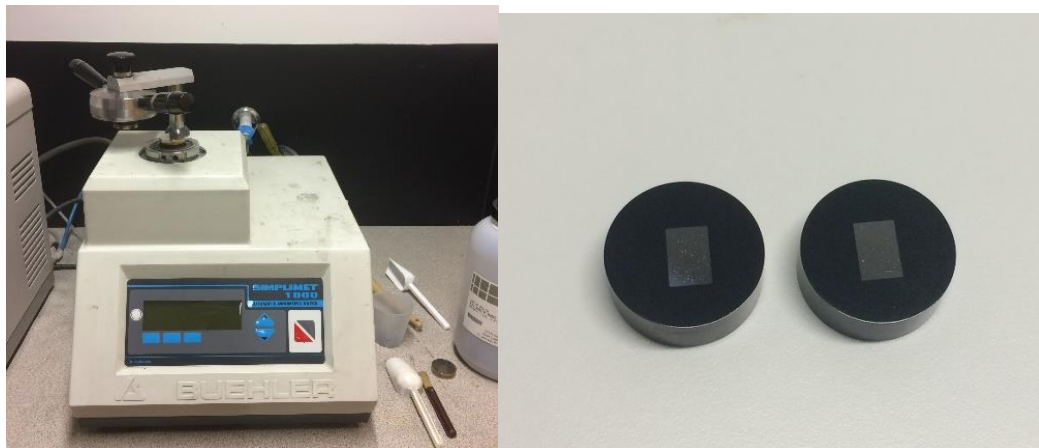
Figure 5.4 Buehler device (lift), mounted samples (right)

3. After cutting and mounting processes, the grinding processes have been carried out through three stages by using three types of grinding papers, starting from 320 grits, 500 grits, and finally 1200 grit, with water at each step. On the other hand, ethanol solution has been used to clean the samples after any activity, moreover, some other devices were used such as, dryer and ultrasonic device to achieve the cleaning processes faster (Figure 5.5).

Figure 5.5 (A) Grinding machine (B) Ultrasonic device

4. Then, polishing of the specimens have been done by using ultra polishing machine through three steps started with 6 µm, 3 µm, and eventually 1 µm. Moreover, the polishing time at each specimen took 5 – 10 minutes with continuous using of Microid Diamond Compound, ethanol solution, and ultrasonic device in order to achieve the premium smooth surface with 1µm surface finish (Figure 5.6).

Figure 5.6 (A) Polishing machine with 3 & 6 µm, (B) Polishing machine with 1µm

5.3. Heat treatment study

A half of the fabricated samples (three uniform, three functionally graded lattice structure, two tensile test and one cubical microstructure sample) were used for heat treatment study. The aim of this study is to explore the effect of a solution heat treatment (T6) process on the SLM- Al-12Si material. The T6 plan process for this experiment study is illustrated in Figure 5.7.
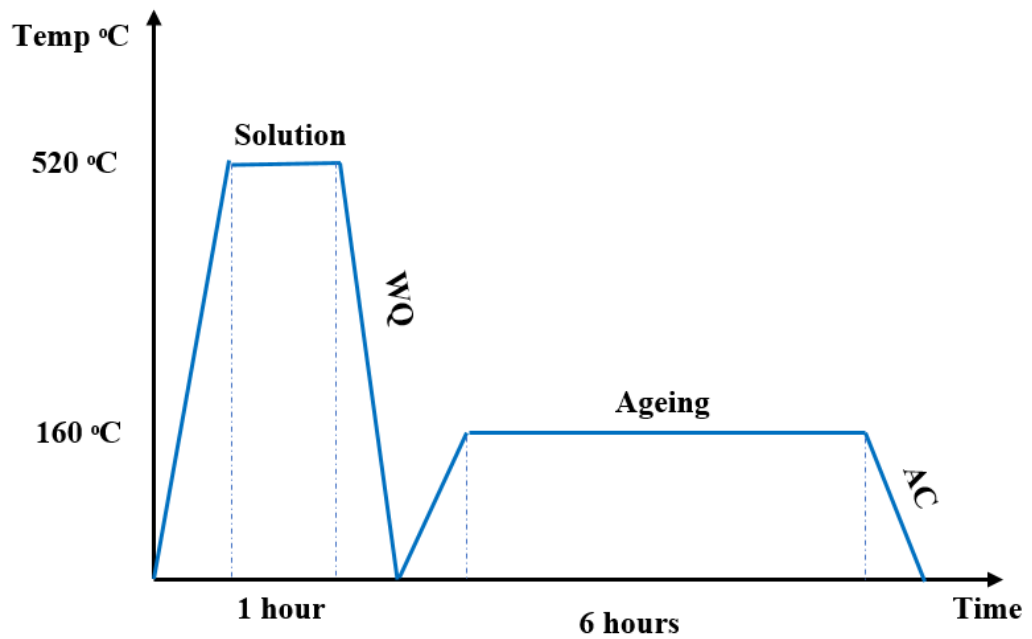
Figure 5.7 T6 solution heat treatment plan

T6 solution heat treatment included heating the samples at 520 °C with soak time of 1 hr, followed by water quenching (WA) to room temperature. Then, the sample were artificial ageing heated (AA) at 160 °C for 6 hours followed by air cooling (AC). The heat treatment was conducted in an air atmosphere using electrical furnace with load capacity 1300 °C as shown in figure 5.8.

Figure 5.8 electric furnace with air atmosphere

5.4. Experimental tests

5.4.1. Compression tests

Series of compression tests were carried out on fabricated-SLM lattice structures for both as-build and heat-treated structures. Quasi-static compression tests were conducted using MTS Criterion model 43 universal testing machine with 50 kN capacity as shown in figure 5.10. During the tests, the fabricated lattice structures were centrally located between two cross heads movement. The deformation speed was 1 mm/min downwardly, which resulting in strain rate 5.5×10^{-4} s^{-1} as shown in Fig 5.9. The compression test was conducted following the ASTM standard E9-09. The compressive strain data was collected from linear displacement that were provided by using an extensometer, while the applied loads were used to obtain the compressive stress data by dividing the collected loads to the effective area of the lattice structure. Moreover, 50 frames/ sec video camera was employed during all the compressive tests in order to capture and record all deformation stages of fabricated lattice structures.
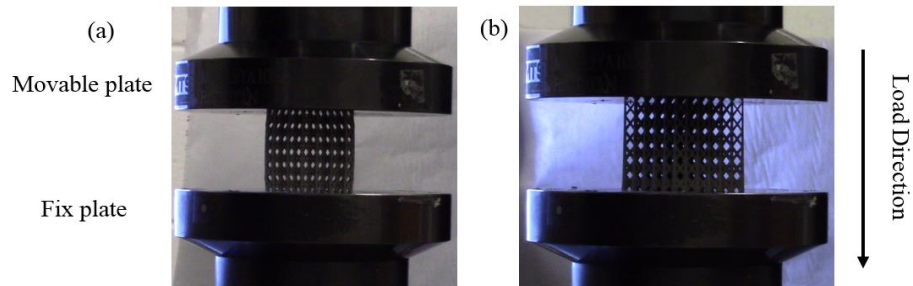
Figure 5.9 Compression test set up of lattice structures (A) uniform, (B) graded
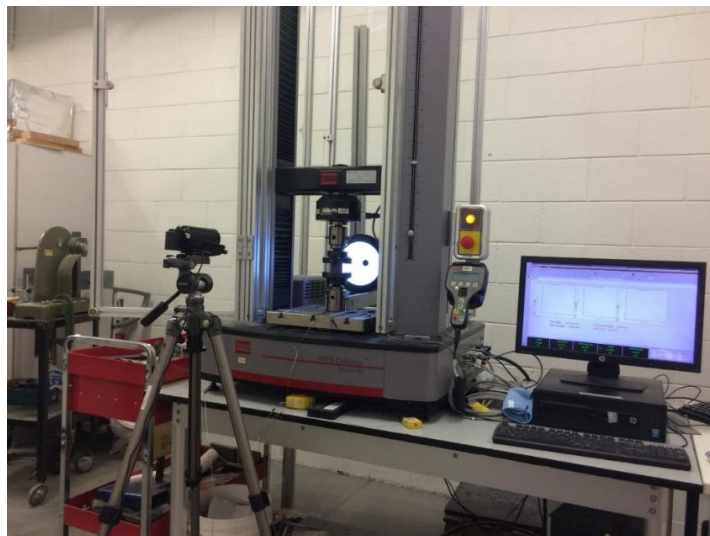
Figure 5.10 MTS Criterion model 43 mechanical testing machine

5.4.2. Tensile tests

The four of manufactured dog-bone tensile test specimens, two as-build and two heat-treated, were used to implement the tensile tests. Fig 5.11 shows the ASTM standard E8/E8M − 16a tensile test sample with SLM-build direction [104]. Un-axial tensile tests were conducted using MTS Criterion model 43 universal testing machine that has capacity of 50 kN as shown in figure 5.10. The tensile tests were carried out in accordance with the ASTM standard E8/E8M [105] . The loads speed was 1 mm/min resulting in strain rate 5.5×10^{-4} s^{-1}. A white and black spray paint was used for applying a random spatter pattern on the dog-bone tensile test samples in order to capture the displacement using an extensometer video record. The engineering strain data was collected from linear displacement dividing by original gauge length, while the applied loads were used to obtain the engineering stress data by dividing the collected loads to the initial cross section area of gauge region. After that, the fracture surfaces of the tensile test samples were imaged using SEM device.
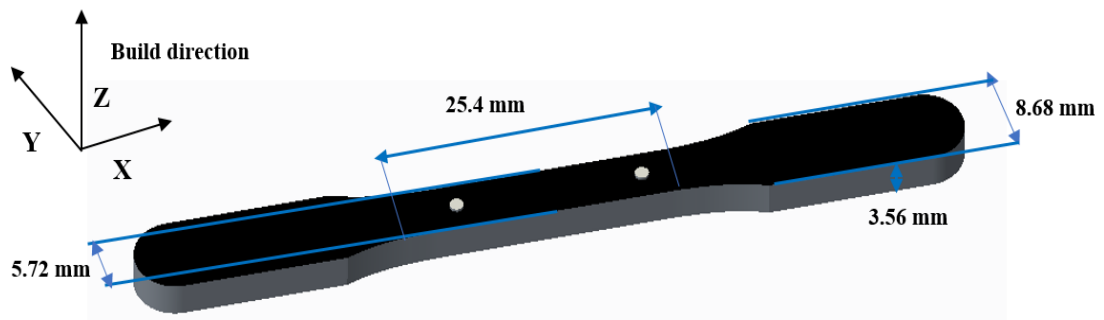
Figure 5.11 Tensile test specimen

5.5. Finite element analysis (FEA)

To simulate the deformation behaviour of the lattice structures after elastic range under compressive loadings, LS-DYNA code of ANYSYS© software was used with the connection to LS-PrePost software to display and review the results. For both lattice structures uniform and functionally graded, 3D solid elements were employed to mesh lattice models with six degrees of freedom. During all the numerical analysis, the models were assigned with constant material properties that shown in table 6.2, which is supposed to be multilinear material response under compression tests. Since the lattice structures have separated small areas (nodes) on the top and bottom of the models which may cause some errors during the applying boundary conditions, two connected plates with 1 mm thickness were modelled on top and the bottom to overcome this issue.

The boundary conditions were applied to simulate exactly what has happened in experimental test, in which the top plate was freely moved in Z direction at the constant velocity and fixed in other directions, and the bottom one was fully fixed in all degrees of freedom. In addition, the type of contact between the rigidly plates and the model was used an automatic node to surface contact, while the automatic single surface contact was used to define the interaction between the connected struts of the cells. This work is almost similar to what had been done by (Hedayate and Sadighi 2016) in terms of boundary conditions and contact types. For clarification, no boundary constraints were used to the sides of the lattice models during the all simulations. Fig 5.12 shows the setup and boundary conditions of the finite element analysis.
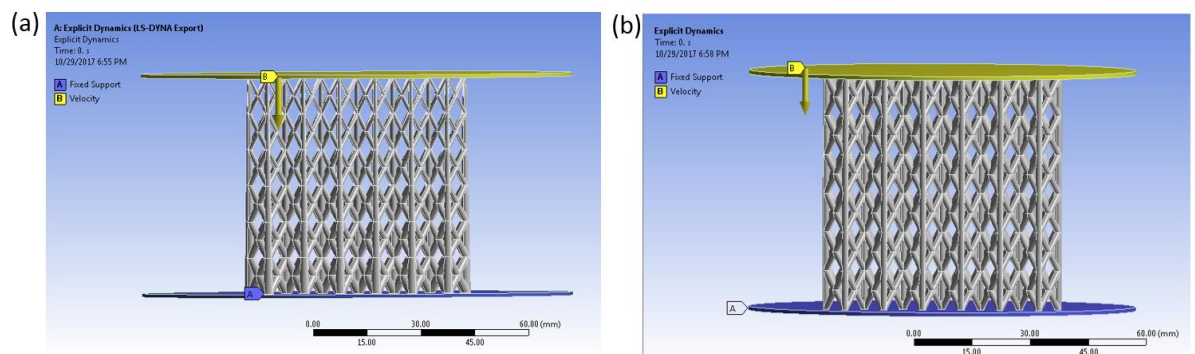
Figure 5.12 boundary conditions of FEA, (a) graded, (b) non-graded

Chapter 6
RESULTS AND DISCUSSION

6.1. Overview

This chapter will provide and discuss the obtained results from the experimental procedures and FEA models. Furthermore, it attempts for clarification and interpretation of all results and observations that had happened during the study in order to provide clear picture and compared to the previous relevant studies.

6.2. Dimensions measurement of lattice structures

Table 6.1 provides designed and measured dimensions of the both lattice structures uniform and functionally graded. It is clear from the table that the dimensions of the solid struts are not identical between designed and manufactured lattice solid struts. The measurement process exhibited that the dimensions were slightly higher in manufactured solid struts than designed struts of the lattice structures. The differences between the manufactured and designed lattice structures were expected due to the nature of the selective laser melting process that was used to fabricate the lattice structures. However, it is found to be in good agreement and it is similar to what previous studies had found. As an example, Yan et al. (2013) and Van Bael et al. (2011) have mentioned that dimensions of manufactured porous structures via SLM technology exhibits thicker and higher values than designed dimensions. Similarly, Maskery et al. (2016) had done relevant studies to investigate cellular structures made of aluminium alloy by SLM. They have found that the fabricated lattice structure of SLM dimensions agreed well with CAD model dimensions. Likewise, Qiu et al. (2015) had performed research on the effect of manufacturing properties of selective laser melting on the accuracy of cellular structure struts. They state that struts dimensions increase monotonically with variations of manufacturing parameters. However, this increase in dimensions in our study can be attributed to unmelted or partially molten particles that are bonded to struts surfaces, the differences in molten pool size, roughness of the surface, and stair-stepped effect.

Table 6.1 dimensions and relative densities of the lattice structure

design lattice	sample	struts thickness (µm)		Mass (gram)	Relative density of layers	Relative density
		design	measured	measured	measured	measured
uniform lattice	regular	812.5	853 ± 25	13.902	……	0.19
graded lattice	Full Lattice	…….	……..	13.9022		0.19
	layer one	350 - 500	380 - 538 ± 30		0.055	
	layer two	500 - 545	538 - 585 ± 45		0.083	
	layer three	545 - 735	585 - 770 ± 25		0.124	
	layer four	735 - 834	770 - 855 ± 30		0.186	
	layer five	834 - 1082	855 - 1115 ± 35		0.279	
	layer six	1082 - 1270	1115 - 1310 ± 15		0.419	

The SEM images of lattice struts in Fig 6.1a show clearly that many powder particles are attached to struts surfaces and are not fully molten. Also, it can be observed from high magnifications images that the variations in molten pool size and stair stepping effect are clear on the outer surface of struts Fig 6.1. In addition, the optical micrograph images also show the surface roughness of the lattice structure struts Fig 6.1b. These observations were also highlighted in similar research studies previously (Yan et al, 2013; Sing et al, 2016 & Qiu et al, 2015).
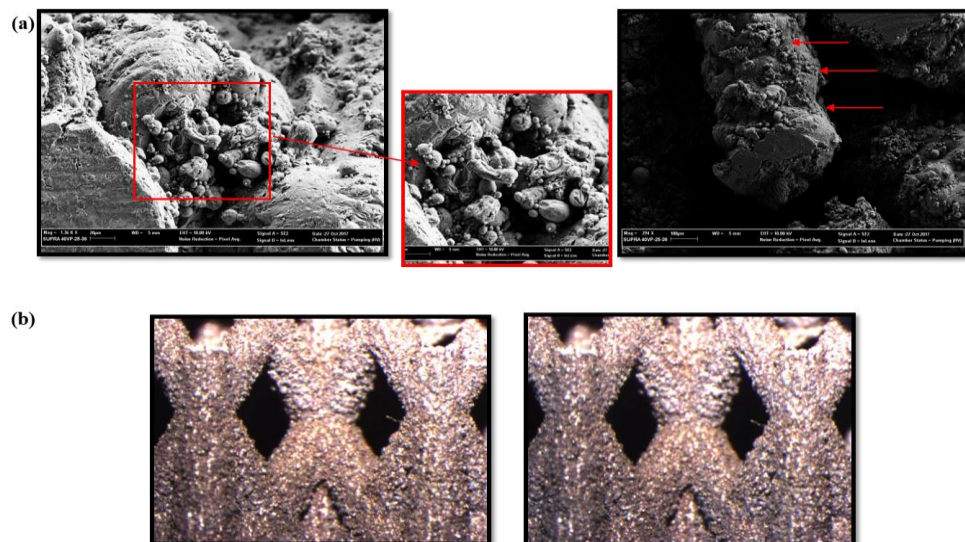
Figure 6.1 SEM and OM images of solid struts of the as-build functionally graded structure

6.3. Mechanical properties of Al-12Si material

Tensile test results of the dog – bone tensile specimens are presented as stress – strain curves for both conditions, as-build and heat-treated, in Fig 6.2a. Fig 6.2b displays the large-scale section of stress - strain curves that shows the calculation process of mechanical properties of both conditions.
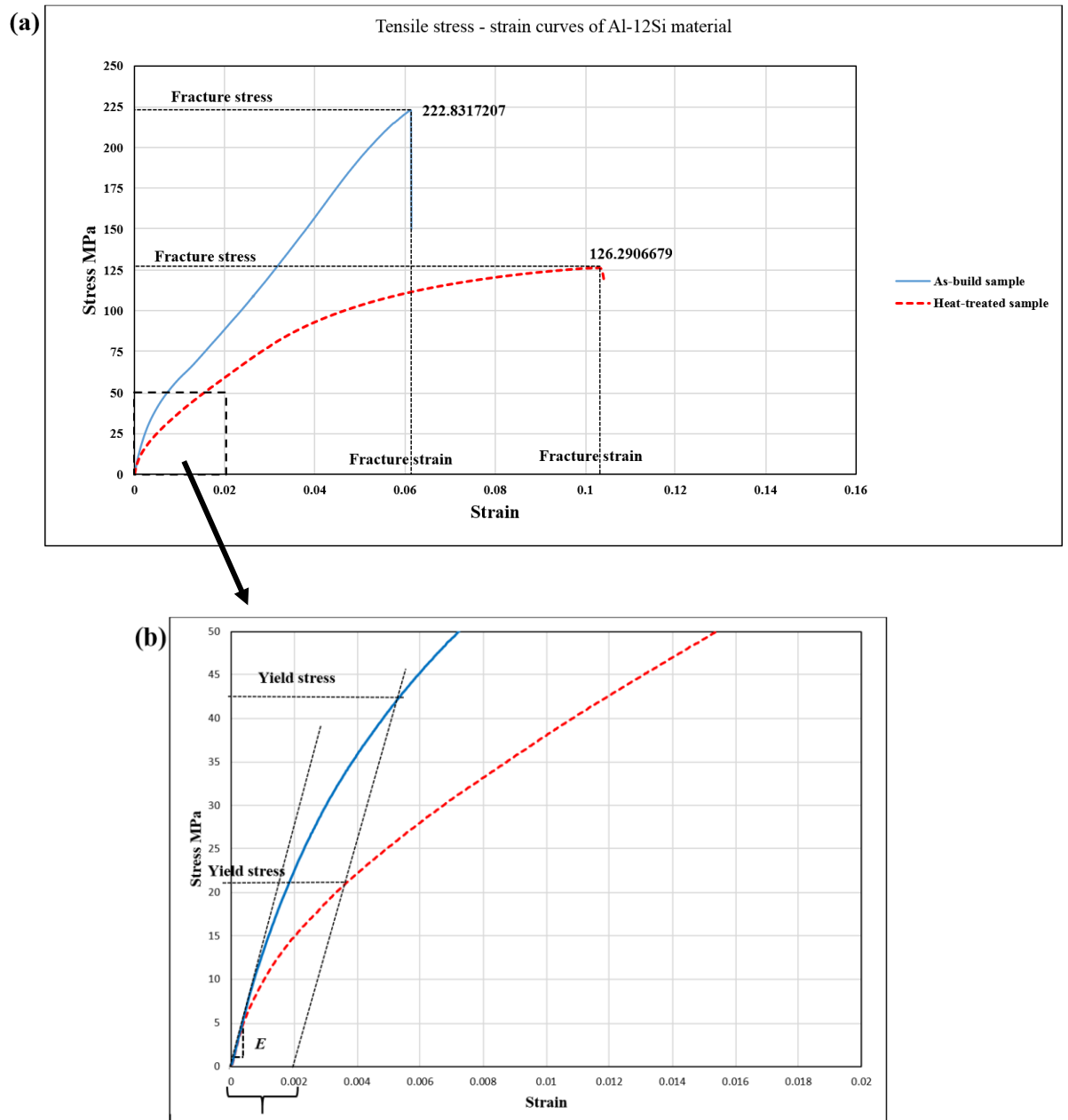
Figure 6.2 tensile stress – strain curves of as-build and heat-treated tensile samples (a), large scale of the mechanical properties up to 0.02 strain (b).

The calculation the variations in the mechanical properties of SLM – Al-12Si material in as-fabricated and after thermally treated are given in Table 6.2. It can be seen from Fig 6.2 and Table 6.2 that the as-build SLM – Al-12Si material exhibited higher elastic modulus and yield stress and tangent modulus and fracture strength than heat-treated SLM- Al-12Si material. In contrast, the fracture strain (ductility) exhibited lower level in as-build than heat-treated conditions. This is expected that in as-build SLM – part provides high yield and fracture strength due to the nature of SLM process that characterized by high heating and cooling rate 1×10^5 K/s resulting in grain refinement of the microstructure [15, 91]. The solution heat treatment has a significant effect on mechanical properties of SLM- samples that it decreases the yield and fracture strength up to approximately 50% and 43% respectively, while the ductility (fracture strain) was remarkably improved by an increase up to 68%. It is well known that there is an opposite relationship between the strength and ductility properties when the strength increases, the ductility is decreased and vice versa [15, 25, 89].

Table 6.2 mechanical tensile properties of Al-12Si material

Properties		AS-build	Heat-treated
Elastic modulus	(GPa)	12.5	8
Yield stress	(MPa)	45	22
Tangent modulus	(GPa)	3.2	1.2
Fracture stress	(MPa)	222.8	126
Fracture strain	%	0.0613	0.103

These variations arise from the influence of conducted solution heat treatment on the microstructure of SLM-Al-12Si material. The microstructures study was performed on cubical samples using OM and XRD and SEM devices after sample's preparation process as explained in section 5.2.2. The optical micrographs of as-built and heat-treated microstructure conditions are shown in Fig 6.3 and 6.4 respectively. The SEM images of the microstructures of SLM samples in as-fabricated and heat-treated conditions are presented in fig 6.6a and b. The microstructural study of SLM samples can be described in the following observations.
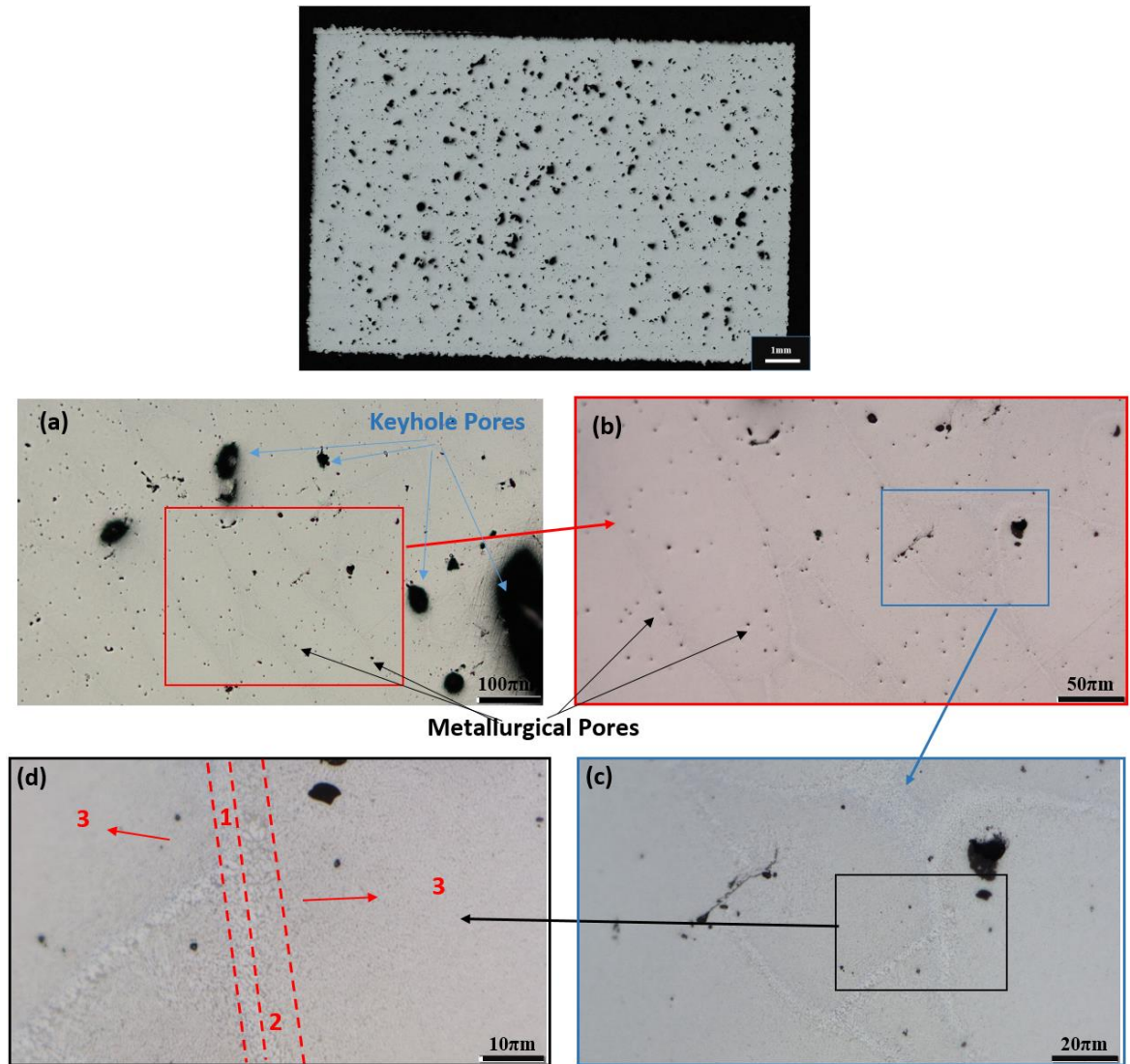
Figure 6.3 typical microstructures of the as-build sample (polished and non-etched), section is perpendicular to the longitudinal axis of the sample.

First, it has been observed from OM micrographs that there is a porosity, which is visible in both conditions of SLM – samples. The porosity in as-fabricated condition seems to be in larger size and irregular shapes than what can be seen after thermally treated conditions as shown in overview picture of samples in fig 6.3 and 6.4. Following the T6 treatment, the porosity is become in uniform distribution with small size and spherical morphology. Second, high magnification OM micrographs reveal that there are different microstructure regions in as-build condition as shown in red dashed line Fig 6.3d and c. The boundary of hatch overlaps (laser tracks) marked by region 1 between to red dashed lines, followed by heat affected zone marked by region 2 between two red dashed lines and core hatch zone marked by region 3.

This observation indicates that these microstructure regions have various thermal histories [15, 87]. It is stated that the microstructure of SLM-parts have mainly been influenced by different heat generated by laser scan overlaps and creation layers sequentially according to Thijs et al. [106]. This resulted in a significant change in microstructure of SLM-Al-12Si material, where the microstructure become coarser in hatch overlaps and heat affected zone due to re-melted two times and partial thermally treatment by laser scan overlaps, while the microstructure is become finer in core hatch zone (core track) due to single laser scan line [15, 87-89] as shown in fig 6.3d and c. However, the microstructure of SLM-as-build sample was found to be finer than SLM heat-treaded microstructure. Similar results have been previously reported by Prashanth et al. [15], Li et al. [87] and Birol [107].
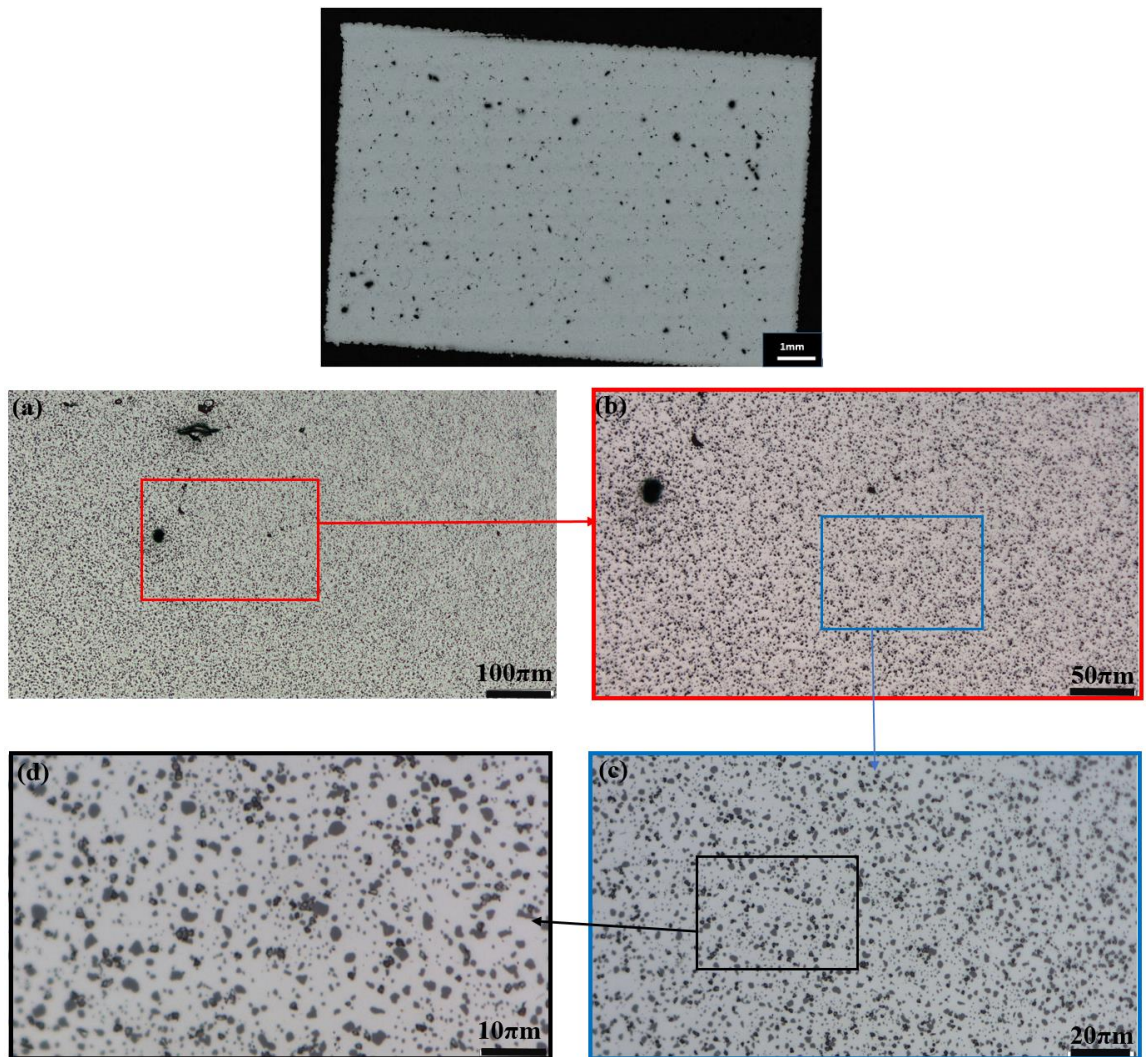
Figure 6.4 typical microstructures of the T6 sample (polished and non-etched), section is perpendicular to the longitudinal axis of the sample.

In contrast to the as-build microstructure, microstructure study showed that the SLM - heat − treated microstructure was different than as build SLM- microstructure in which the variation in microstructure regions (laser track, heat affected zone and core hatch) was completely disappeared. The high magnification OM images in Fig 6.4c and d reveal that heat-treated microstructure was homogeneously and become coarser and there is no different in microstructure regions. It has been observed and according to the phase diagram of Al-12Si (Fig 2.12) that the microstructure of Al-12Si consists of Si particles phase and α-Al matrix phase. In current study, such kind of microstructure has been observed with dark grey (white) is Si phase contrast and light grey is Al phase contrast. It can be seen that crystalline size of Si and Al particles increase significantly after the solution heat treatment as shown in Fig 6.4c and d. This indicates that solution heat treatment let to grow the Si particles size after rejecting out the Al-matrix. The size and morphology of Si particles were clearly visible as shown in Fig 6.4c and d. Fig 6.3c and d illustrate clearly the well-known as-fabricated SLM microstructure, which is characterized by cellular Al-rich boundaries supersaturated and surrounding by fine Si particles [15, 87-89]. XRD analysis arise the evidence of increase the Si and Al particles as can be seen in Fig 6.5a and b. XRD patterns analysis demonstrate that the two diffraction peak phases of Al and Si has been identified. It has been observed that there was no phase change, but the peak intensities of both Al and Si elements were remarkably modified. Fig 6.5 a is the XRD diffraction of heat − treated condition, while Fig 6.5 b is the as-build condition, clearly show the increasing the peak intensities which corroborating the increase of Al and Si particles size as shown in Fig 6.3 and 6.4.
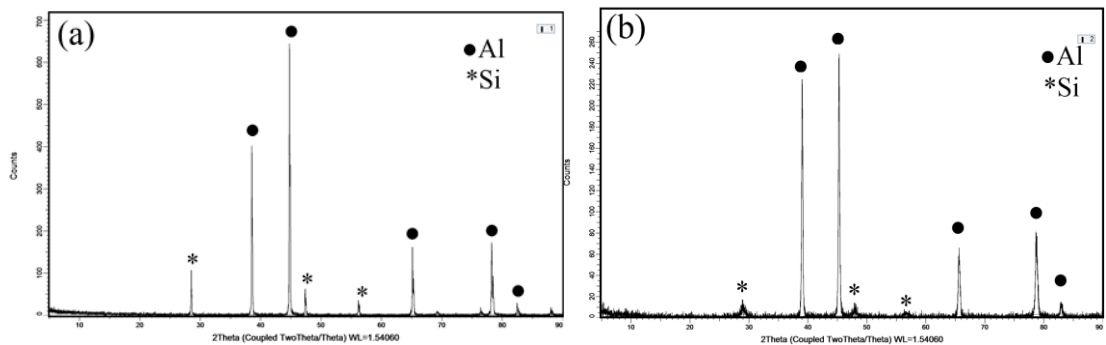
Figure 6.5 XRD diffraction patterns of Al-12Si material (a) heat-treated, (b) as-build conditions.
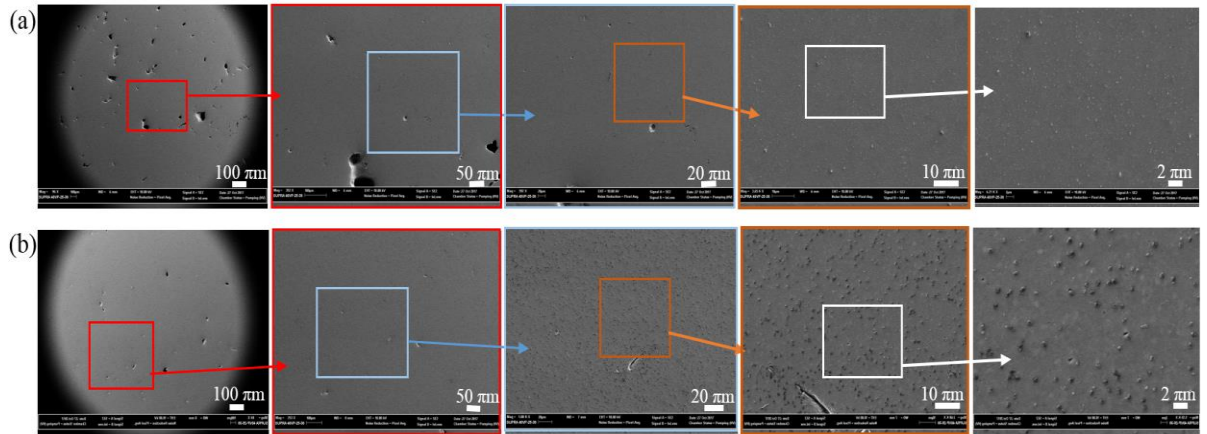
Figure 6.6 SEM images of SLM-microstructure, (a) as-build and (b) heat-treated conditions.

6.4. Deformation modes of the lattice structures

6.4.1. Deformation of as-build uniform lattice structure

Fig 6.8 demonstrates the stress strain curves obtained from the average of experimental compressive tests of three SLM samples for each uniform lattice structures and functionally graded lattice structures and for both conditions, as-fabricated and heat-solution-treated. Also, Fig 6.7 provides video frames images that show deformation stages of as-build uniform lattice under the compressive loadings. From Fig 6.8, stress strain curve of as-build uniform lattice exhibited different deformation regions, commencing with a high elastic region followed by long fluctuated plateau region to onset densification region before fully crushing of the structure. It can be observed that an elastic stage is relatively linearly proportional between compressive stresses and strains. This region shows the highest stress value that the as-build uniform lattice structure can support at around 7% compressive strain before the major collapse occurred in the structure. Fig 6.7 video frames illustrate the significant deformation of the structure at around 10% strain, by which the structure lost approximately 93% of its strength. In this stage, solid struts of structure cells start bending, and after a short time, some struts fail due to shearing and breaking band at 45° angle to the applied load direction as shown by red arrows and red circles in Fig 6.7 (c) and (d). This leads to significant decrease in strength of the lattice structures as shown in Fig 6.8.

After the elastic section, the continued compressive forces lead to develop a plastic collapse region. Based on observations in Fig 6.7, the deformation and fracture behaviours are repeated, and the structure is continuously weakened. During the collapse, some cells work against the applied load, which leads to rise in stress until the densification strain is reached at strain of 59%. The fracture has mostly occurred at the contact point (nodes) between the solid struts of cells in X, Y or Z directions, and at the middle of some solid struts after the bending. It is worth mentioned that the SLM-Al-12Si material exhibited very high brittleness. Similar deformation behaviour has been reported by the previous studies (Yan et al, 2013; Maskery et al, 2016; Qiu et al 2015; Choy et al, 2017 and Campanelli et al, 2014). It is noted that the as-build uniform lattice structures are structurally sound just before the first collapse, which the structures have supported up to the maximum compressive stress at around 7% compressive strain as shown in Fig 6.7e,f,g and h.

(a) 0%   **(b)** 5%   **(c)** 7%   **(d)** 13%

(e) 22%   **(f)** 45%   **(g)** 58%   **(h)** 70%
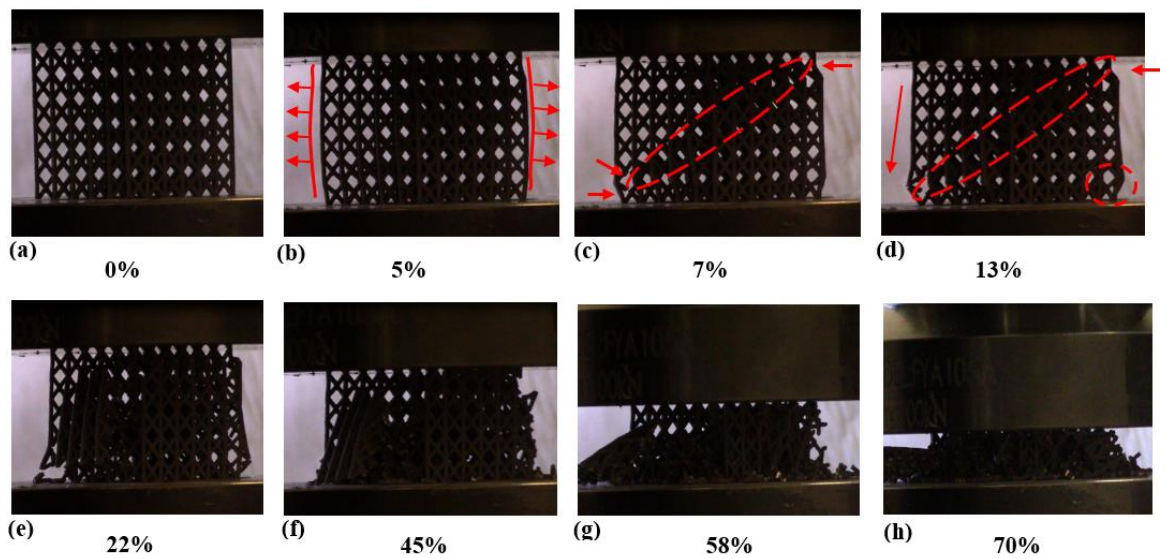
Figure 6.7 (a), (b), (c), (d), (e), (f), (g), and (h) deformation stages of as-build uniform lattice structure from recorded video camera
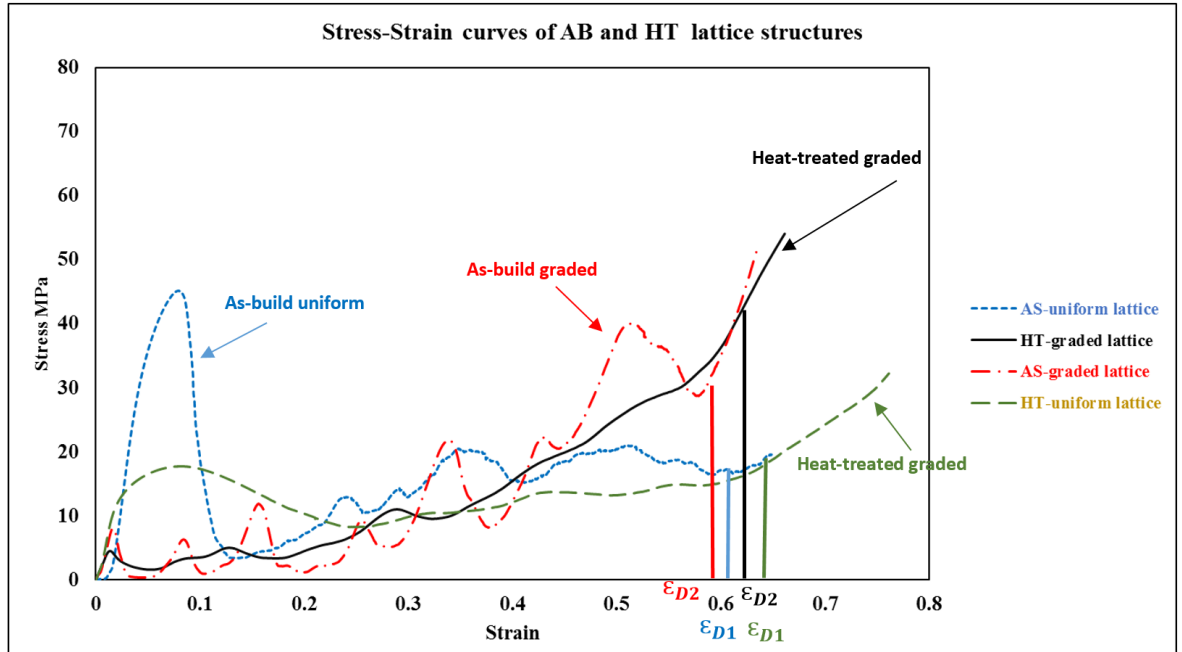
Figure 6.8 compressive stress strain curves of as-build and heat-treated conditions
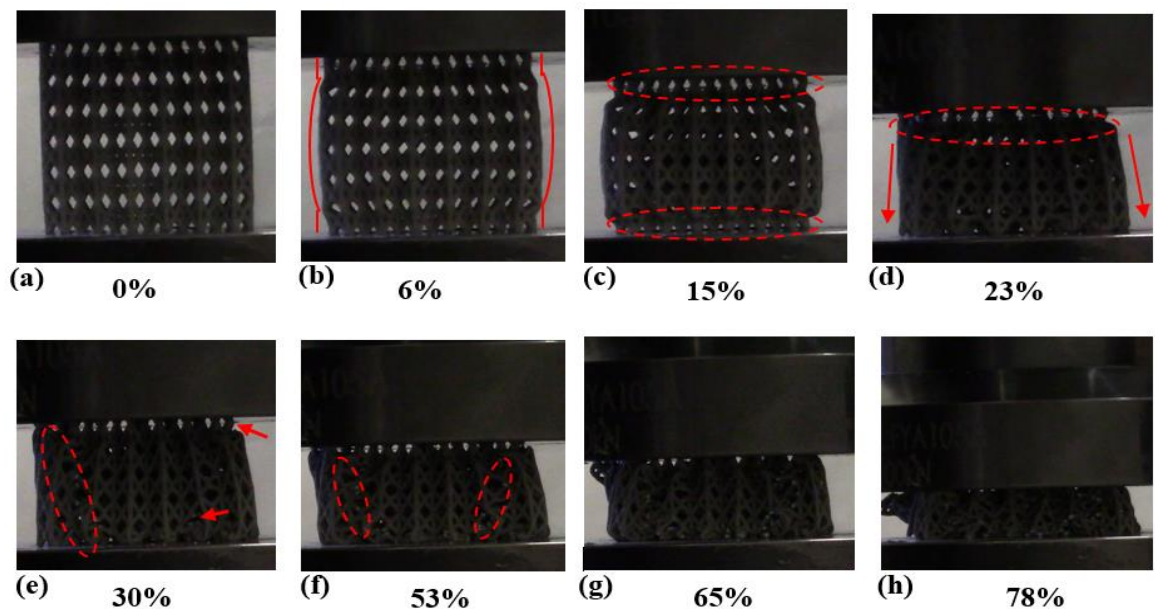
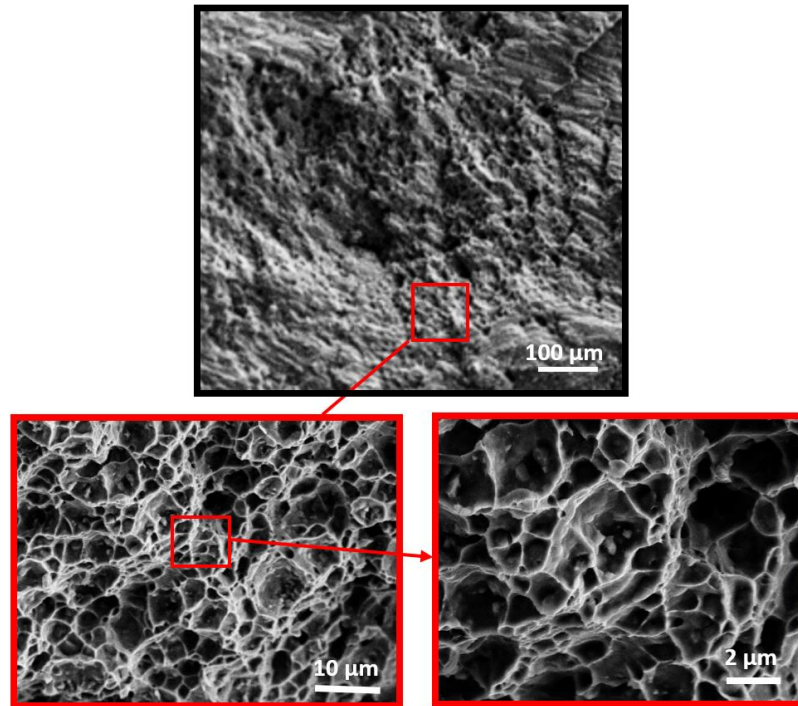### 6.4.2. Deformation of heat-treated uniform lattice mode

Three samples of the SLM- uniform lattice structures were solution heat treated to study the effect of such heat treatment on the deformation behaviour of the SLM-Al-12Si uniform lattice structures as explained in section 5.3. The data of compression tests of heat-treated uniform lattice structures are presented as stress - strain curve in Fig 6.8, which is as an average of three tested samples. Deformation behaviour of heat-treated uniform structures were found to be different than as-build one. It is clear from fig 6.8 that the stress strain curve seems to be more ideal and very close to ideal collapse behaviour of cellular solid structure that described by Gibson and Ashby[1]. The stress – strain curve includes linear elastic region, followed by long and smooth plateau stress region and then to the densification region. The effect of heat treatment clearly transfers the brittle collapse behaviour and low strain failure of as-build uniform structure to long plateau region and high strain failure in heat-treated uniform structure. This difference can be attributed to the difference in the microstructure and resistance to fracture of the solid struts between heat-treated and as-built uniform lattice structures as shown in Fig 6.10.

It is obvious from the stress strain curve that there is slightly decrease in compressive strength of the structure after 20% strain level. This is due to the deformation mechanism of heat-treated uniform lattice structure that exhibited under the compressive loads.

Fig 6.9 illustrates the deformation stages and failure mechanism. It has been observed that the friction between the structure and the plate surfaces of compression machine plays significant role in weakening of the structure. Fig 6.9b and c clearly demonstrate that friction resulted in a constraint the collapse process and thus let to central buckling of structure. After that, the continued compressive loads caused in drive the cells of layers toward the bottom of the structure (layer six) as shown in Fig6.9d and e. Then, various shear and break failures were developed in different directions around 35% strain level. Similar deformation mechanism of lattice structure subjected to post-manufacture heat treatment had been reported by Maskery at el. [93].

Figure 6.9 (a), (b), (c), (d), (e), (f), (g), and (h) deformation stages of as-build uniform lattice structure from recorded video camera
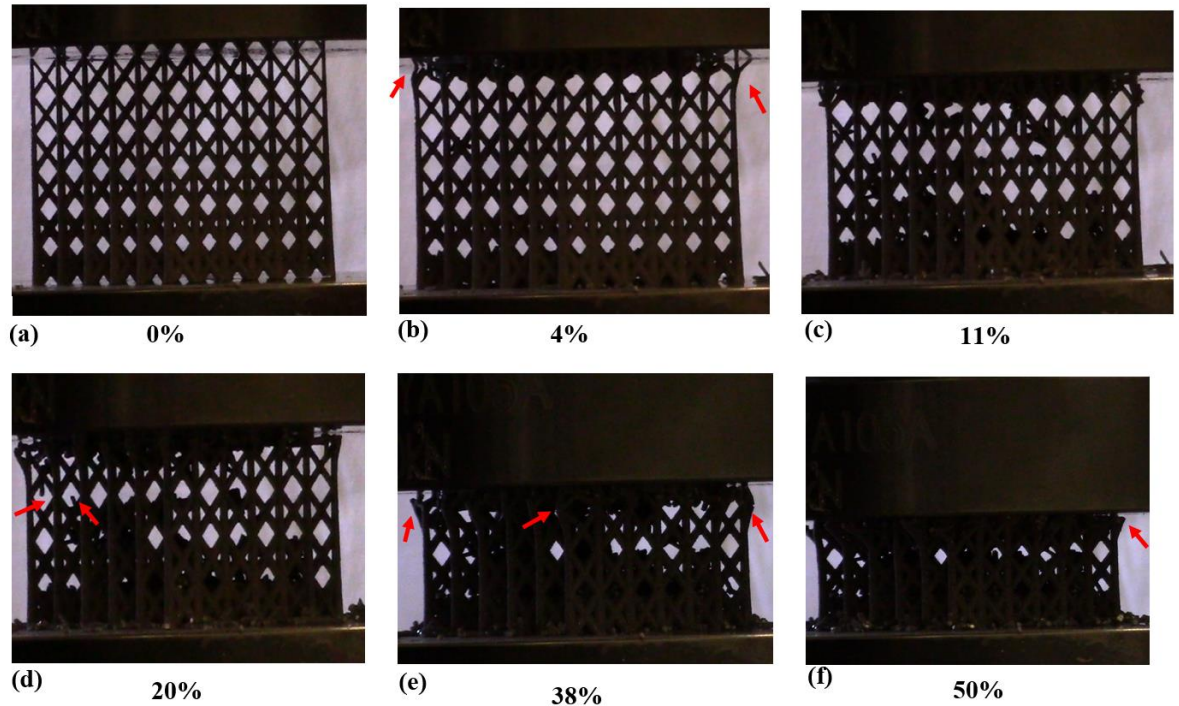
Figure 6.10 SEM images of strut fracture surface of heat-treated uniform lattice structure.

6.4.3. Deformation of as-build functionally graded lattice structures

Fig 6.8 shows the stress - strain curve of the compression tests of as-build functionally graded lattice structures as an average of three SLM samples that has been tested. In addition, Fig 6.11 shows frames of video camera that was used during the deformation of lattice structures under the compressive loads. It is clear from the stress strain curve that the deformation behaviour of the as-fabricated graded lattice structures is completely different from the collapse behaviour of uniform lattice structures. A gradually dense lattice structures exhibited a distinctive deformation behaviour as the 45° shear band failure found in uniform lattice is completely absent. This results in increased strength of graded lattice structure. It can be observed from the video frames in Fig 6.11 that the graded lattice structure deformed sequentially starting with lower density layer at the top of the structure. Gradually, increasing compressive load results in layer-by-layer collapse process. From the stress-strain curve of as-build graded cellular structures, it can be seen that in the failure process of each layer, there are a linear elastic followed by plateau zone to the densification region. These are ideal regimes of cellular structure deformation that described by Gibson and Ashby [1]. From the empirical observations, the deformation mechanism of lattice solid struts changes gradually from a bending and plastic collapse

(flake) in lower density layer at top to fracture that mostly occurred in nodes as shown in red arrows in Fig 6.11. Such observations have been mentioned by Maskery et al. (2016); Van Grunven et al. (2014) and Choy et al. (2017). Fig 6.8 and 6.11 clearly demonstrate that the compressive stress increase in a sequence, which is associated with a gradual increase of struts thickness throughout the six structural layers. This is an opposite to what had happened in collapse behaviour of uniformly dense lattice structures.

Figure 6.11 Images from video camera of as-build functionally graded lattice structure under compressive loading, (a), before the applied loads. While, (b), (c), (d), (e) and (f) are the collapse stages of structural layers respectively.

6.4.4. Deformation of heat-treated functionally graded lattice structures

Following the solution heat treatment T6 (section 5.3), functionally graded lattice structure showed a unique deformation response under the compressive loads. Fig 6.8 elucidates clearly the significant different in the stress strain curve compared to as-build graded lattice structure as well as uniform lattice structures. It can be seen that stress strain curve rises continuously with increasing the compressive loads. This behaviour was tied with collapse of the structural layers in sequence. The collapse process was found to be similar in as-build graded lattice structure in which started with lower density layer at the top to higher density layers sequentially.

Fig 6.12 presents the frames of recorded video of the collapse stages under the compression tests of heat-treated functionally graded lattice structure. From Fig 6.12, it is clear that the structures deformed in layer-by-layer sequentially. Despite the structural collapse were found similar in as-build and heat-treated graded lattice structures, the mechanism failure was a quite different. This is a clear in stress strain curves trace, in which featured by sharp decrease in compressive strength after each layer collapse that make the curve with large fluctuation until the densifications in as-build condition. Such observations were eliminated in heat-treated graded structures where the Al-12Si material exhibited high ductility, thus altered the brittle collapse to more ductile behaviour under the compressive loads. The effect of heat treatment improved the deformation behaviour that by reduce the compressive strength and increase the fracture strain to be 61%.

(a)   10%   **(b)**   19%   **(c)**   26%

(d)   46%   **(e)**   58%   **(f)**   75%
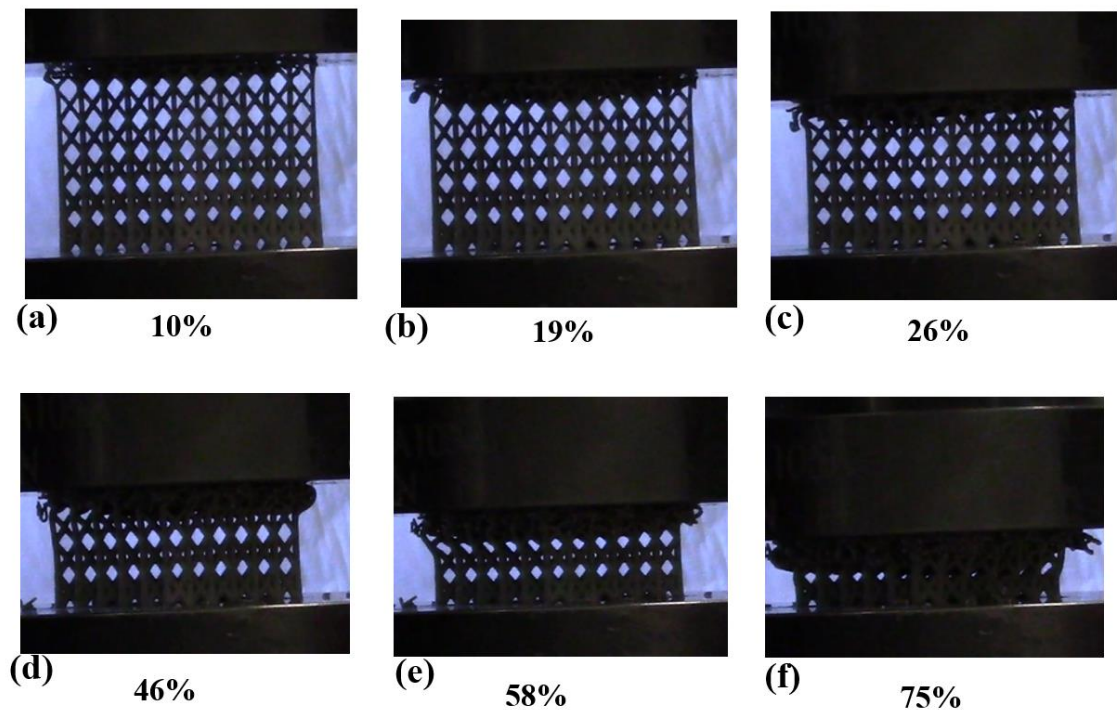
Figure 6.12 Images from video camera of heat-treated gradual density lattice structure under compressive loading, (1), and (8) are before the applied loads and after fully crushing. While, (2), (3), (4), (5) and (6) are the collapse of six layers respectively.

6.5. Compressive mechanical characteristics and Gibson and Ashby coefficients of the lattice structures

The mechanical properties of the uniform and functionally graded lattice structures under the both conditions, as-fabricated and heat-treated, have been extracted from the compressive stress-strain curves. These properties are necessary to find out the Gibson and Ashby coefficients C1, C5 and α theoretically as given in the equations (1), (2) and (3) in chapter four. These are provided in Table 6.3 in which E_{latt}, $\sigma_{pl.latt}$ and *onset* ε_D are elastic modulus, plateau strength and onset densification strain of lattice structures respectively. For clarification, the elastic modulus has been determined from the slope at 1% compressive strain related to linear elastic region curve according to Olurin et al. [100]. The plateau strength is calculated as mean value of effective stresses for the range 20 – 40% of effective strains (ISO standard 13314:2011). In addition, onset densification strain is taken as the effective compressive strain for effective stress which corresponds to the curve trace and based on the experimental observations (ISO standard 13314:2011, section 7.4).

Table 6.3 mechanical properties of uniform and gradual density lattice structures

Mechanical properties	AS-build lattice structures (F2CCz)		HT-lattice structures (F2CCz)	
	Uniform	Graded	Uniform	Graded
E_{latt} (GPa)	1.277	0.674	0.844	0.418
$E^* = \frac{E_{latt}}{E_m}$	0.1021	0.0539	0.1055	0.0523
$\sigma_{pl.latt}$ (MPa)	14.483	9.166	9.839	9.549
$\sigma^* = \frac{\sigma_{pl.latt}}{\sigma_{yl.m}}$	0.322	0.204	0.448	0.435
Onset ε_D (based on observations)	0.59	0.585	0.625	0.61

In Table 6.3, E* and σ* are the relative modulus of elasticity and relative plateau strength of the porous lattice structures respectively. These are determined from E_{latt}, and $\sigma_{pl.latt}$ normalised with E_m and σ_{yl} of parent material given in Table 6.2. From the given equations of Gibson and Ashby (1), (2) and (3) in chapter four, the pre-factors C1, C5 and α have been theoretically calculated using determined E* and σ* properties.

Table 6.4 illustrates the three Gibson and Ashby coefficients for both conditions as-build and heat-treated uniform and functionally graded lattice structures.

Table 6.4 determined coefficients values of Gibson and Ashby [1] equations.

Coefficients	Given range of Gibson-Ashby coefficients	AS-build lattice structures (F2CCz)		HT-lattice structures (F2CCz)		F2BCC (previous study)	
		Uniform	Graded	Uniform	Graded	Uniform	Graded
$C1$	$0.1 - 4.0$	2.83	1.494	2.923	1.45	1.4 ± 0.003	1.05 ± 0.002
$C5$	$0.25 - 0.35$	3.887	2.46	5.4	5.25	0.23 ± 0.006	0.64 ± 0.006
α	$1.4 - 2.0$	2.16	2.19	1.98	2.06	1.82 ± 0.008	2.84 ± 0.03

A typical stress-strain curve of the deformation process of the lattice structure consists of three regions as mentioned previously. The first region is a linear elastic region which has been expressed by equation (1) of Gibson and Ashby [1]. Using determined values of E^* and ρ^*, we can estimate the $C1$ coefficient, which should be in the given range of $0.1 - 4.0$. From Table 6.4, the calculated values of $C1$ for as-build condition are $2.83 - 1.49$, and for heat-treated condition are $2.92 - 1.45$ of the uniform and functionally graded lattice structures respectively. These values are found to be in the given range of Gibson and Ashby [1]. Despite these found values are well agree with previous reported $C1$ values $1.4 +0.003 - 1.05 +0.002$ by Dheyaa et al. 2017 for F2BCC lattice structures made of Al-12Si and fabricated by same technology, but these values are considered relatively higher than those found by other researchers. For example, Maskery at al. (2016) have found that C1 values are 0.166 for metallic cubic lattice structures made by SLM and 0.44 for polymer lattice structures made by SLS at which the relative densities were 0.22 and 0.19 respectively. Similarly, Yan et al. (2015) have reported that C1 values are 0.17 and 0.19 for the two cellular structures made of Ti6Al4V with close relative density values.
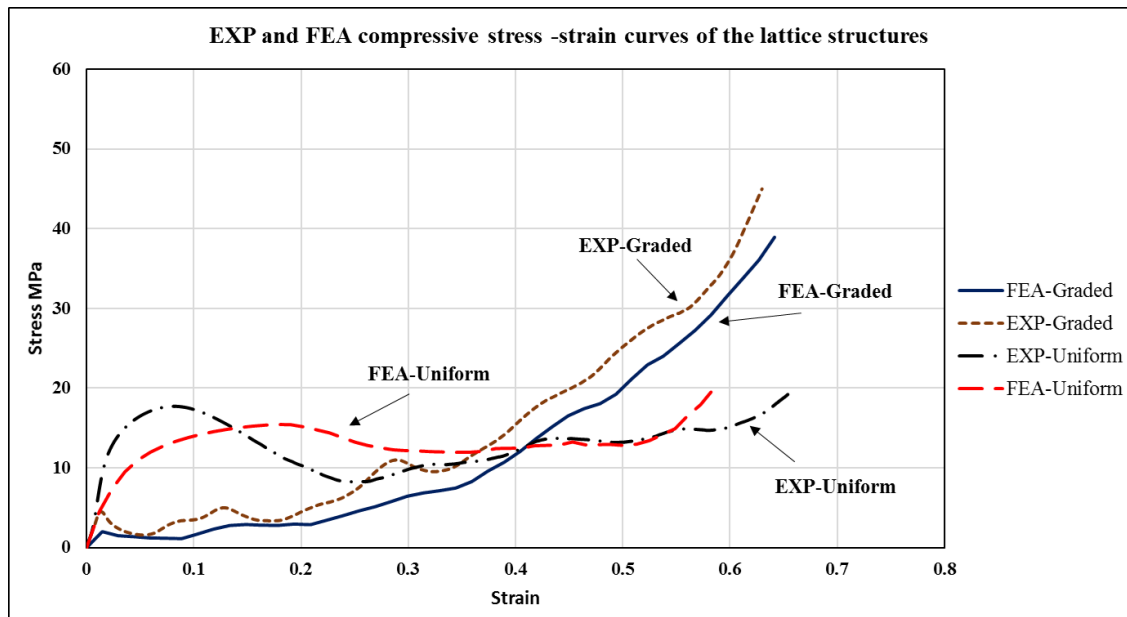
The second region of stress-strain curve is the plastic plateau regime, and is represented by equation (2) of Gibson and Ashby [1], which is used to estimate the coefficient $C5$, which has the values in the range of 0.25 to 0.35 [1]. The determined values of the both conditions, as-build are $3.88 - 2.46$ and heat-treated $5.4 - 5.25$ for uniform and functionally graded lattice structures respectively.

It is worth mentioned that calculated values of *C5* for both conditions were found in out of the given Gibson and Ashby range [1]. However, the resulting values of *C5* are higher than what Gibson and Ashby predicted for their work on metallic solid structures and expressed by equation (2). These findings must take to the considerations the fact that there is a difference between the one architectural design to another, and also on the types of material used (Maskery et al, 2016). Their study for BCCZ lattice structures made of Polyamide PA (2200) by SLS process, C5 was found to be 0.285, while for BCC lattice structure, C5 was 0.202. This indicates that coefficient C5 may vary from design to design even with identical relative density values. Similar results of C5 values has been found in previous studies. For instance, Dheyaa et al. (2017) have found that C5 value is 0.64 +0.0066 for F2BCC lattice structure made of SLM-aluminium alloy with 0.185 relative density. In addition, Yan et al. have reported for two type of lattice structures made of 316L stainless steel and Ti–6Al–4V fabricated by SLM process that *C5* values were found to be 1.29 and 1.39 respectively. This indicates that coefficient C5 may vary from design to design even with identical relative density.
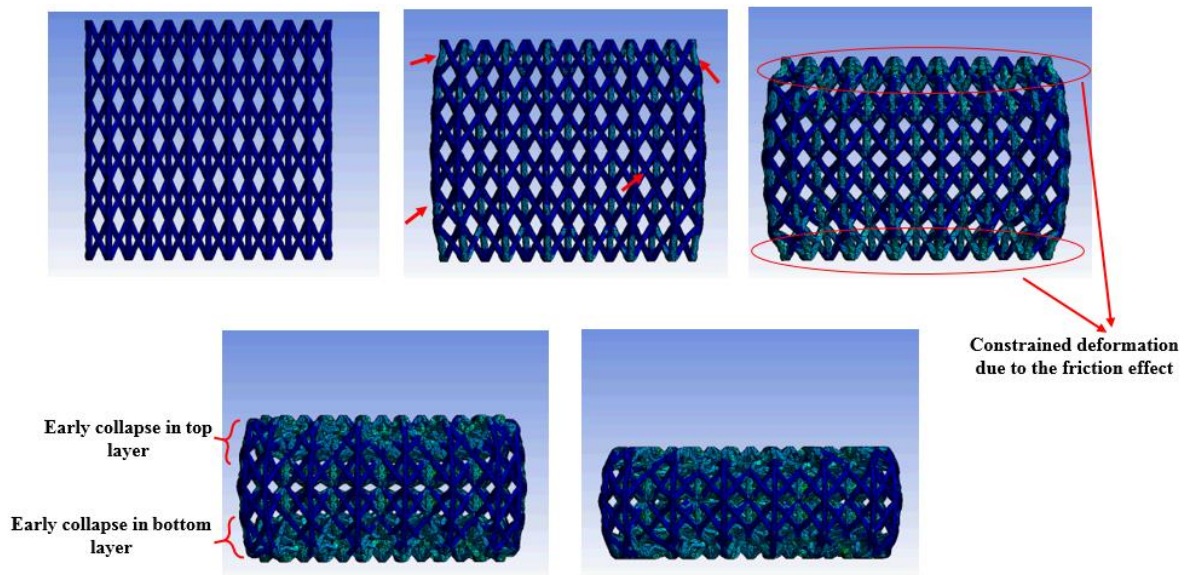
The third region of stress-strain curve is densification region, in which the equation (3) is used to determine the value of α. As it can be seen from Table 6.4, the resulting values of uniform and graded lattice structures at as-build and heat-treated conditions are 2.16 − 2.19 and 1.98 − 2.06 respectively. It is obvious that the perfector α of equation (3) is a critical parameter that is mainly affected by the value of densification strain ε_D. For as-build lattice structures, the onset densification strain happened at a lower strain level than the heat-treated lattice structure. This is due to the effect of conducted solution heat treatment. It has been observed that values of α in heat-treated lattices structures are close to the given range of Gibson and Ashby [1], while in as-build condition are higher than given range. These observations are found to agree with some findings in two studies for Maskery and his colleagues (Maskery et al. 2016 and Maskery et al. 2017), in which the determined α values were 2.47 and 2.44 for lattice structures made by SLM and SLS respectively. Thus, the rise in resulting α values may be due to the variations in deformation behaviour of the uniform and graded structures (Maskery et al. 2016). It has been explained in detail in deformation of lattice structures section.
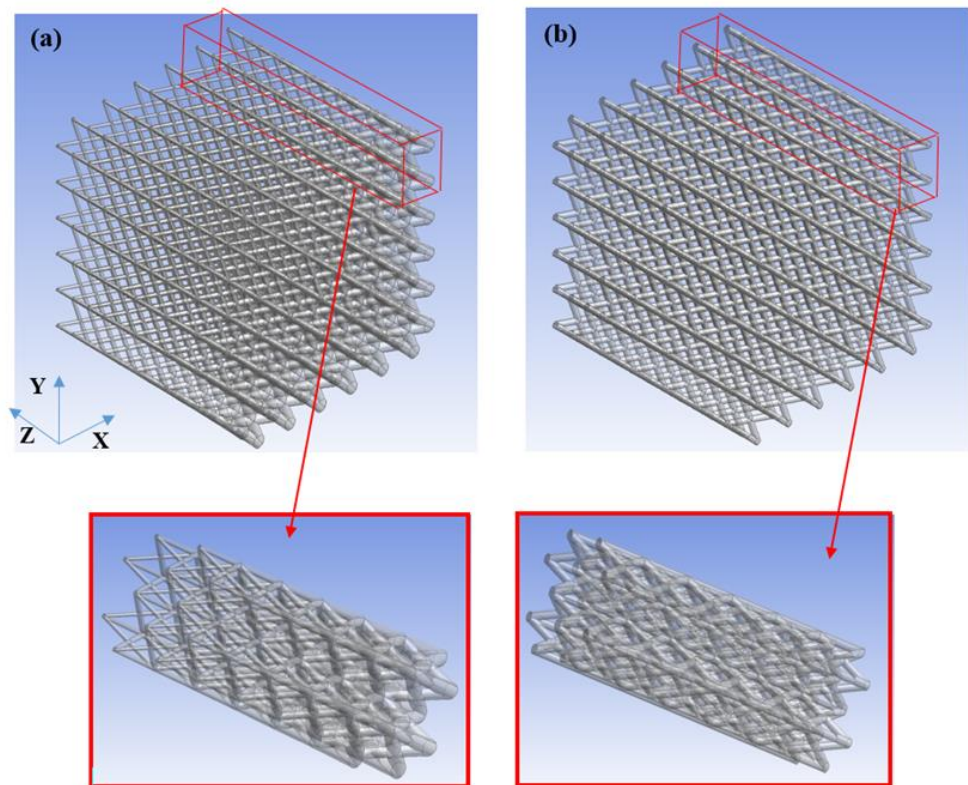
6.6. Numerical Simulation of lattice models

Figure 6.13 shows stress – stress plots of FE uniform and graded models and compared to experimental results of heat-treaded uniform and graded lattice structures. The FEA stress stain curves are similar and very close to the experimental stress strain curves. It can be seen that the curves include the steep rise of elastic region followed by long and smooth plateau stress region to the onset densification region. These results have been obtained after conducting the convergence study of the influence of element size. The effect of element size, that was used to mesh the FE models, has been studied using range of different sizes started from the default size (3.25mm) to 0.35 mm. The study resulted that the element size 0.35 mm can capture the deformation and provide more accurate results. Unfortunately, the running simulation for whole structure using 0.35 mm element size could not be conducted due to facing some of the constraints. Computational time required, limited of element number (education version of LS-DYNA provide 220.000 element number only) and capability of available computers are the main constraints that we had faced during the finite element analysis. Although running numerical analysis for whole model using 0.35 mm element size could not performed, but using default element size can be done to have clear picture about the deformation behaviour and compared to experimental observations regardless to the accuracy of the results. Figure 6.14 illustrates the deformation stages of FE uniform models, it can be seen that collapse process of FE model is similar to the experimental deformation in figure 6.9.

Figure 6.13 stress – strain curves of FEA models and experimental lattice structures

Constrained deformation
due to the friction effect

Early collapse in top
layer

Early collapse in bottom
layer

Figure 6.14 deformation stages of FEA uniform model using default mesh element

size

Figure 6.15 FEA models of lattice structures, (a) graded, (b) uniform

However, to overcome these issues, and by considering the symmetrical geometry of the designed lattice structure, a quarter of the structure contains (4 × 4 towers) was considered to conduct the numerical analysis as can be seen in Fig 6.15.

It is found that the deformation behaviour of the FE uniform model is comparable to the experimental behaviour of uniform lattice structures. Fig 6.16 illustrates the collapse process of six layers of FE uniform model under compressive loading in which the cells were deformed in corresponding manner and homogenous. The deformation process starts with buckling and bending in vertical solid struts of the cells, Fig 6.16 b, c, d and e clearly demonstrate the stress concentration. After around 20% strain, the effect of friction can be seen in Fig 6.16 e, d and f, which caused in weaken of the structure and thus decrease the compressive strength as shown in stress strain curve at 25% - 45% strain level Fig 6.14. Then, contact of the cell struts with the next cell struts under the compressive loads resulted in onset densification followed by full densification at around 56% strain. Despite the similarity in stress strain curves between FEA model and experimental results that include three ideal regions, there is different in plateau stress level and beginning of onset densification strain level. This is due to the absence of formation of the cracking and shearing that has been observed in experimental after 25% strain level.
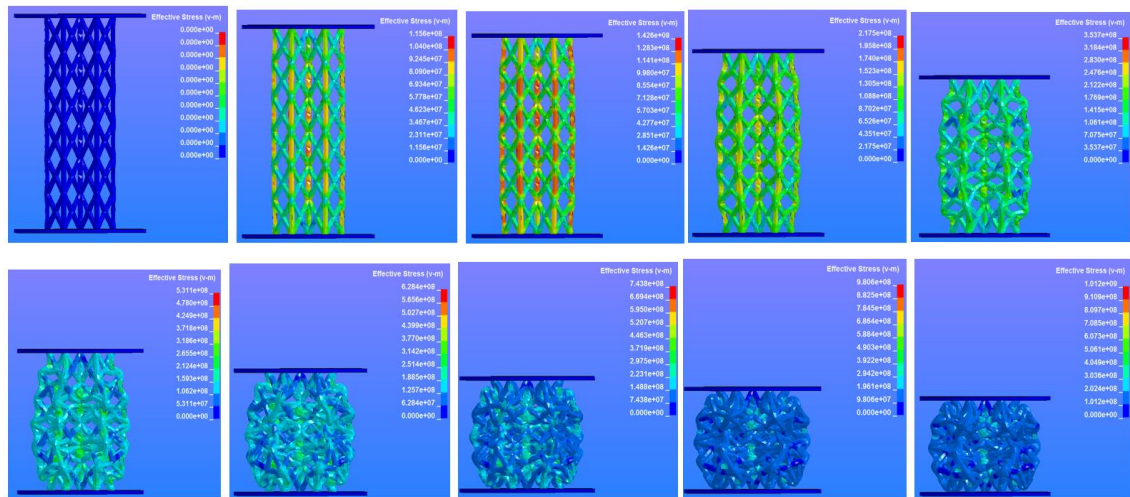
Figure 6.16 deformation stages of FE uniform model

Compared to the FEA uniform model, the FEA results of the functionally graded model exhibited close agreement with the empirical results of the functionally graded lattice structure as shown in Fig 6.14.

Fig 6.17 elucidates the pictures of collapse behaviour for FE functionally graded model. In this case, the deformation process commenced with lower density cells at the top of the towers, and then, in sequence, the collapse of cell-after-cell continues. This is like what had occurred in experimental deformation behaviour of the gradual dense structure as shown in Fig 6.12. The difference between the experiment and numerical studies is only some fluctuations (decrease and increase) at approximate 10 – 15% and 25 – 35% compressive strain. This can be attributed to the mechanism of failure process that by formation some fracture and flake in few solid struts in experimental one.
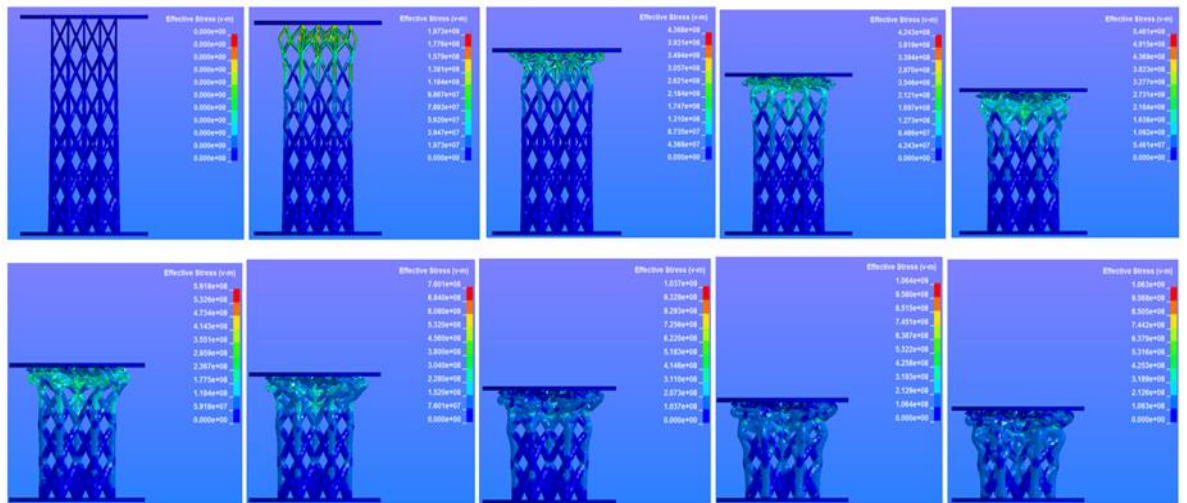
Figure 6.17 deformation stages of FE functionally graded model

6.7. Energy absorption capability

The energy absorption of lattice structures is a key objective of current research. The energy absorption capability for both uniform and functionally graded lattice structures in as-build and heat-treated conditions has been determined as the area under the compressive stress - strain curves using the numerical integration, which is represented by equation (9) in chapter four. The total cumulative values of calculated energy per unit volume up to 50% compressive strain and up to onset densification strain of uniformly and gradually dense lattice structures are shown in Table 6.5.

Table 6.5 Determined values of energy absorption properties

Lattice structures types		Energy absorption *Wv* (MJ/m^3)		
		Onset Densification strain ε_D	Up to 50% strain	Up to ε_D
AS-build lattice structures (F2CCZ)	Uniform	0.59	7.953	9.659
	Graded	0.585	4.890	7.883
HT-lattice structures (F2CCZ)	Uniform	0.625	6.119	8.033
	Graded	0.61	4.574	8.335
F2BCC (previous study)	Uniform	0.66	-------	2.6 ± 0.2
	Graded	0.465	-------	3.2 ± 0.1

The energy absorption behaviour of both conditions of the lattice structures can also be observed from the Fig 6.8 of experimental compressive stress-strain curves. In as-build uniform lattice structure, a larger amount of energy was absorbed as shown in table 6.5. This is because of the beginning of high compressive strength until the major collapse of the structure starts to happen in approximately 7% strain. After the peak point of compression stress, the structure enters the plateau region with a low level of plateau stress against the applied load due to the diagonal 45° shear band failure and fracture, which causes it to absorb lower energy. The oscillated plateau region continues till the onset of densification starts at around 59% strain. This gives 7.953 - 9.659 MJ/m^3 as the amount of total energy that was absorbed by the structures up to 50% and onset of densification strain respectively. Although the highest energy was absorbed in as-build uniform lattice structure, but the deformation mechanism revealed the evidence that such structure could not preferred in energy absorption application. Fig 6.8 and Fig 6.7 arise these evidence by showing the sharp decrease in its strength.

Following solution heat treatment T6 in uniform lattice structure, the ability of energy absorption completely turned to more ideal behaviour as explain in section 6.4.2. This is because of the influence of heat treatment on the change the material from brittle collapse to more ductile behaviour under the compressive loads as can be seen in fig 6.8 and fig 6.9. A 6.119 – 8.033 MJ/m^3 are the amount of total energy to 50% and begin densification strain respectively.

Previous results on the effect of post – manufacture heat treatment (T6) on BCC and double gyroid lattice structures are found to be similar [9, 90]. Maskey et al. [90] found that despite the same amount of energy absorbed was found in as-build and heat-treated double gyroid lattice structures made of Al-Si10-Mg and fabricated by SLM, the deformation behaviour exhibited a significant change.

On the other hand, the energy absorption behaviour of the functionally graded lattice structures in both conditions was quite different as shown in Fig 6.8. The structure starts with a much lower level of absorbed energy than the uniform lattice structure at around 10% compressive strain. Then as the compression loads increase, the energy absorption level increases significantly with the collapse of layers sequentially. It is clear from the Fig 6.8 that the gradual increase of absorbed energy was tied with the deformation behaviour of layer by layer starting with the top layer of lower density one. Although, as-build functionally graded lattice structure exhibited a novel deformation behaviour, the graded structure absorbed a lower amount of energy compard to as-build uniform lattice structure. The values of $4.89 - 7.883$ MJ/m^3 are the total energy that was absorbed up to 50% and onset densification strain level. The existence of vertical pillar with constant thickness throughout the structural layers from the top to bottom and the material brittleness caused in rising the amount of absorbed energy.

Conducting T6 heat treatment, functionally graded lattice structure showed a unique deformation response under the compressive loads. Fig 6.8 elucidates clearly the significant difference in the stress strain curve compared to as-build graded lattice structure as well as uniform lattice structures. This distinct behaviour gives $4.574 - 8.335$ MJ/m^3 amount of absorbed energy to 50% and onset densification strain respectively. Although, heat –treated functionally graded lattice structure reached the end of plateau strength region (onset densification strain) at 61% before the uniform lattice structure reached at 63% strain, the functionally graded structure absorbed a higher amount of energy. These results are found to agree with reported values of energy absorption from the literature that support the functionally graded models [9, 13 & 64]. For example, Maskery at al. [9] have found that the values of the total energy absorption were 5.7 ± 0.2 MJ/m^3 and 6.3 ± 0.2 MJ/m^3 for non-graded and graded BCC lattice structures made by SLM technology respectively.

These values were found to be lower compared to our results as different material (Al-Si10-Mg) and unit cell form, but with same volume fraction and manufacturing process were used. Similarly, 0.64 ± 0.01 MJ/m^3 and 1.371 ± 0.09 MJ/m^3 were the values of total cumulative energy for uniform and graded BCC$_Z$ lattice structures made from polymer and fabricated by SLS process respectively (Maskery at al. 2016). Their results were also lower than what have been found in this research study due to softer material was used, but the relative density was similar. In addition, Dheyaa at al. (2017) claimed that 2.6 ± 0.2 - 3.2 ± 0.1 were the values of F2BCC lattice structures with uniform and graded density profile made of same material and very close volume frication. The current results are approximately three times higher than those found by Dheyaa et al. (2017). This is because of the presence of the vertical pillars or struts that worked to support high compressive strength.

The cumulative energy absorption per unit volume versus the compressive strain for uniform and functionally graded lattice structures under both conditions, as-build and heat-treated, are plotted as shown in Fig 6.18. The exponent values from the fitting curve equations of both form of the lattice structures have been extracted from fitting the curves by the power law method as shown in Fig 6.18. These values represent the increase rate of cumulative energy absorption of the lattice structures under the compressive loads. The results indicate that the graded structure was in higher increase rate than uniform structure except as-build uniform structure as it is explained in section 6.4.1, in which the exponent value 1.567. The exponent values were 1.535 and 1.538 for the both functionally graded lattice structures in as-build and heat-treated conditions respectively. While, 1.258 was the exponent value of heat-treated uniform lattice structure.
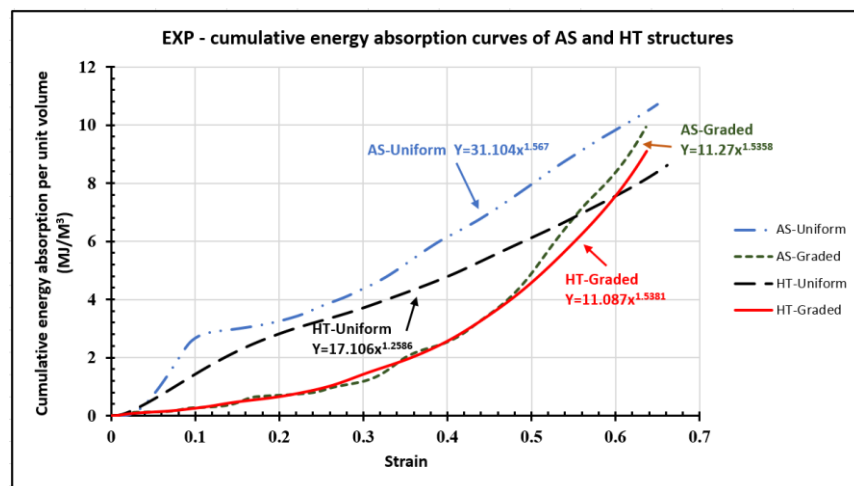
Figure 6.18 cumulative energy of as-build and heat-treated lattice structures

It can be observed from Fig 6.18 that the energy absorption behaviour of uniform lattice structure exhibited a sudden decrease in the amount of energy absorbed at approximately 10% and 20% strain in as-build and heat-treated conditions respectively. This was caused by the major collapse of as-build uniform lattice structures due to the shear band failure, and by early densification in top and bottom layers and random creaks in heat-treated uniform structure as described in detail previously. On the other hand, Fig 6.18 shows the distinctive behaviour of cumulative energy absorption for functionally graded lattice structures in both conditions due to its unique deformation behaviour under compressive loads as explained in the previous sections. Similar cumulative energy absorption behaviours were found in the previous studies from the literature. For example, Maskery at el. [9, 64] have found that the exponent values were around 2 and 3 for BCC lattice structures in the density gradient form, and manufactured by SLM from Al-Si10-Mg and by SLS with polyamide (PA 2200) respectively. Similarly, Choy at el. [13] had done a relevant study to investigate the energy absorption capability of uniform and graded honeycomb and cubic lattice structures made of Ti-6Al-4V by SLM. They have found that the exponent values of functionally graded structures in both honeycomb and cubic lattice structures were higher than the uniform structures. The increase rate values of cumulative energy absorption were 0.89 and 1.72 for uniform and graded cubic lattice structures, and 1.26 and 2.68 for uniform and graded honeycomb lattice structures respectively.
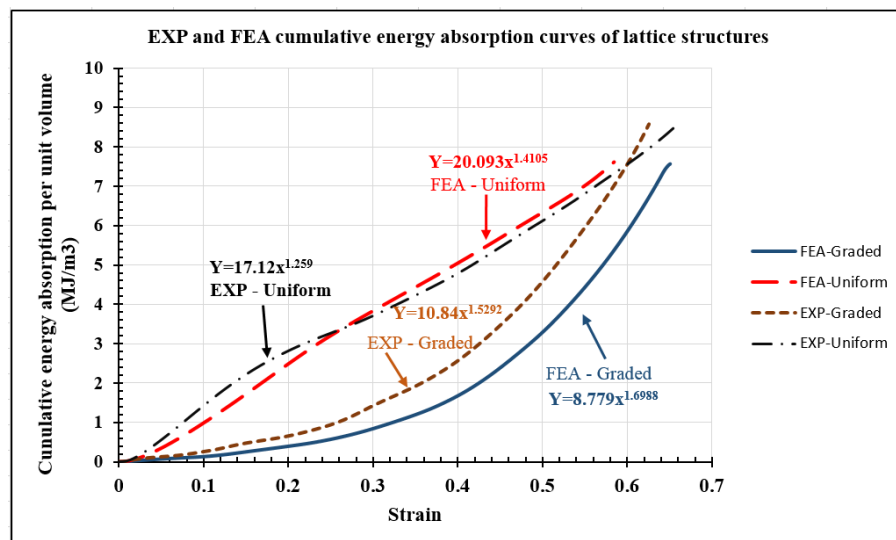

Figure 6.19 cumulative energy absorption of heat-treated and FEA models of the lattice structures

Experimental cumulative energy per unit volume of heat-treated lattice structures are compared to FEA cumulative energy per unit volume absorption as shown in Fig 6.19. From fig 6.19 it has been observed that the energy absorption behaviour well agrees between the EXP and FEA. A 1.259 – 1.52 are the exponent values of uniform and graded structure experimentally, whereas 1.41 – 1.698 are the exponent values of uniform and graded structure numerically. This is an evidence that the deformation behaviour of FEA models were found to be in close to the experimental response as it has been explained in section 6.4.

These outcomes also support the findings that the gradually dense structures or similar models of gradients would be more desirable for applications that required high energy absorption capability. Their deformation response eliminates the conventional failure behaviour by which they exhibit a sophisticated and different type of collapse behaviour

Chapter 7
CONCLUSIONS

7.1. Overview

This chapter is divided into sections. The first section illustrates briefly the work that had been done and concludes the main findings and observations in this study. The second section proposes studies that are recommended for future work expanding from this research.

7.2. Conclusion

In this research study, an experimental and numerical analysis were conducted to investigate the compressive mechanical characteristics (young's modulus, plateau strength and onset densification strain) and energy absorption capability of two types of periodic lattice structures built of the F2CCZ unit cell. The two types of investigated structures were uniformly dense and functionally graded structures, with both having the same relative density and made of Al-12Si material. The SLM technology was used to fabricate all the specimens. Before conducting the investigations, solution heat treatment was implemented on half of the fabricated Al-12Si samples to study the influence of the microstructure and the mechanical behavior. A quasi-static compression and tensile tests were performed to investigate the compressive characteristics and mechanical tensile properties of SLM-lattice structures and dog-bone tensile specimens respectively. In addition, the morphological and microstructure study was conducted using SEM, OM and XRD devices to explore the surface morphology, surface fracture and microstructure changes for as-built and heat-treated -SLM samples.

The tensile tests results showed that the as-fabricated SLM-sample exhibited significant mechanical properties. Tensile results show Young's Modulus, Yield and fracture strength about 12.5 GPa, 45 and 222.6 MPa, along with the fracture strain at approximately 6%. Microstructure study of as-fabricated SLM-sample reveal the fine microstructure of spherical Si surrounding and supersaturated in Al-matrix.

Conducting solution heat treatment T6 has a remarkable effect on the mechanical properties of Al-12Si material. The investigations show that the yield and fracture strength decreased to about 50% and 43%, while the fracture strain increased to about 68%. This provides a novel approach to turn the Al-12Si material behaviour into an extremely ductile material for special applications.

The results of the compression tests exhibited that functionally graded lattice structure exhibits distinctive characteristics in deformation under compressive loads. The collapse process of graded structures is layer by layer beginning with collapse of the lower density layer and then to higher density one in sequence. This behaviour has led to decrease some of its mechanical properties while improving some other properties when compared to the non-graded density lattice structure deformation behaviour. The experimental investigation of the as-build-lattice structure shows brittle behaviour that results in a large decrease and fluctuations in compressive strength. The elimination of brittle fracture and low strain failure of as-built lattice structures were achieved by conducting the T6 heat treatment. The deformation behaviour of the heat-treated lattice structure exhibited distinct response by providing typical stress-strain curve, which include ideal compressive regions.

Although the functionally graded lattice structure enters the onset densification strain early, it was able to absorb more higher energy under the compressive loads than the uniform lattice structure. That has been observed from the compression stress strain curve that the curve of functionally graded structures rises continuously until the densification region. The resulting values of 8.03 ± 0.03 MJ/m^3 and 8.336 ± 0.02 MJ/m^3 are the total amount of energy absorbed by functionally graded structures and non-graded structures respectively. The cumulative energy absorption per unit volume versus the lattice strain curve arise the evidence of the unique behaviour of energy absorption of functionally graded lattice structures.

In this research study, Gibson and Ashby's equations have been established for both lattice structures, the uniform and functionally graded, and under both conditions to find out the pre-factors *C1, C5* and α. For clarification, Gibson and Ashby have defined a number of equations regarding the mechanical characteristics and energy absorption under variation of applied loads and have been widely used in designing and developing the cellular structures.

The determined values of *C1* and α for uniform and functionally lattice structures were found in good agreement with the given range of the coefficients proposed by Gibson and Ashby [1], while *C5* values were relatively higher. That is due to material properties and specific deformation behaviour for which the Gibson and Ashby model does not cope with such mechanism of failure under compressive loads.

The finite element analysis results show a discrepancy with the empirical results of as-fabricated lattice structures due to the difficulty in simulating exactly the mechanism of collapse, which is a combination of 45° shear, fracture and flake formation in some struts at the same time. On the other hand, it has been observed that the deformation behaviour and FE models agreed well and close to experimental results of heat-treated lattice structures. The collapse process of FE functionally graded model started with less density layer, from the top and then layer by layer in sequence to the densification strain region with no decrease in stress strain curve track, while FE uniform model exhibited homogenous deformation with clear effect of the friction coefficient between the model and two modelled plates.

These research results will increase the potential of the gradually dense F2CCZ structures, and will help in the selection of which models of gradients would be more desirable for the application that required high energy absorption capability. Their deformation response show a departure from the conventional failure behaviour of the uniform lattice structure and exhibit sophisticated and different collapse behaviour. These results give indication that graded lattice structures would be more attractive for applications that required high impact or shock resistance.

7.3. Future work

For future work related to this field of research study, designers and researchers can investigate applying these structures for lightweight structures and energy absorption application. The followings are recommended works for future research:

1. T6 solution heat treatment with one heating temperature was used to study the effect on the microstructure and thus mechanical properties of Al-12Si material. A range of heating temperatures and soaking times should be considered to provide more comprehensive knowledge about the heat treatment effect.

2. In this study, structures with constant relative density had been examined. Structures with a series of different relative densities need to be investigated to provide comprehensive knowledge about the new approach of designing lattice structures with linear gradient density.

3. The F2CCZ unit cell was used to build the periodic lattice structures. Other unit cells with various internal architectures such as honeycomb, F2BCCZ, FCC and Gyriod with different aspect ratio can be considered.

4. Al-12Si aluminium silicon alloy was chosen to fabricate the designed lattice structures due to its distinctive properties. Other SLM materials with high ductility can be used. Also, metallic material such as stainless steel, titanium and their alloy or polymers such as APS and PLA can be considered.

5. To achieve more comprehensive understanding of mechanical properties and energy absorption capability for new approach to designing lattice structures, other mechanical testing methods could be extended such as tensile, impact and fatigue test for such structures.

6. Functionally graded lattice structures were successfully manufactured in SLM process, other AM technologies are recommended such as SLS, SLA, FDM and EBM to investigate their manufacturability for these structures.

7. LS-DYNA code of Explicit/ANSYS software was employed for conducting numerical analysis in this study. Advanced explicit software is suggested such as Explicit/ABAQUS software due to its advance tools and features and better efficiency and computation time.

8. For more accurate verification between FEA and experimental results, reverse engineering methods may need to be applied to manufactured structures in order to update the dimensions of the model before running the finite element analysis.

9. The deformation behaviour of lattice structure subjected to compressive loading in all directions (X, Y, and Z) instead of one direction should be investigated for more considerations.

REFERENCES

1.   Ashby, M.F. and L. Gibson, *Cellular solids: structure and properties*, in *Cambridge University Press*. 1997, Cambridge New York.

2.   Banhart, J., *Manufacture, characterisation and application of cellular metals and metal foams.* Progress in materials Science, 2001. **46**(6): p. 559-632.

3.   Wang, J., et al., *On the performance of truss panels with Kagome cores.* International Journal of Solids and Structures, 2003. **40**(25): p. 6981-6988.

4.   Wadley, H.N., *Multifunctional periodic cellular metals.* Philosophical Transactions of the Royal Society of London A: Mathematical, Physical and Engineering Sciences, 2006. **364**(1838): p. 31-68.

5.   Wadley, H.N., N.A. Fleck, and A.G. Evans, *Fabrication and structural performance of periodic cellular metal sandwich structures.* Composites Science and Technology, 2003. **63**(16): p. 2331-2343.

6.   Queheillalt, D.T., et al., *Synthesis of open-cell metal foams by templated directed vapor deposition.* Journal of Materials Research, 2001. **16**(4): p. 1028-1036.

7.   Zok, F.W., et al., *A protocol for characterizing the structural performance of metallic sandwich panels: application to pyramidal truss cores.* International Journal of Solids and Structures, 2004. **41**(22): p. 6249-6271.

8.   Choy, S., et al., *Functionally graded material by additive manufacturing.* 2016.

9.   Maskery, I., et al., *A mechanical property evaluation of graded density Al-Si10-Mg lattice structures manufactured by selective laser melting.* Materials Science and Engineering: A, 2016. **670**: p. 264-274.

10.   Wadley, H.N., *Cellular metals manufacturing.* Advanced Engineering Materials, 2002. **4**(10): p. 726-733.

11.   Yang, L., *Structural Design, Optimization and Application of Three-Dimensional Re-entrant Auxetic Structures*. 2011: North Carolina State University.

12.   Hedayati, R. and M. Sadighi, *A micromechanical approach to numerical modeling of yielding of open-cell porous structures under compressive loads.* Journal of Theoretical and Applied Mechanics, 2016. **54**(3): p. 769-781.

13.   Choy, S.Y., et al., *Compressive properties of functionally graded lattice structures manufactured by selective laser melting.* Materials & Design, 2017.

14.   Zargarian, A., et al., *Numerical simulation of the fatigue behavior of additive manufactured titanium porous lattice structures.* Materials Science and Engineering C, 2016. **60**: p. 339-347.

15. Prashanth, K., et al., *Microstructure and mechanical properties of Al–12Si produced by selective laser melting: Effect of heat treatment.* Materials Science and Engineering: A, 2014. **590**: p. 153-160.

16. Queheillalt, D.T. and H.N. Wadley, *Hollow pyramidal lattice truss structures.* International Journal of Materials Research, 2011. **102**(4): p. 389-400.

17. Ryan, G., A. Pandit, and D.P. Apatsidis, *Fabrication methods of porous metals for use in orthopaedic applications.* Biomaterials, 2006. **27**(13): p. 2651-2670.

18. Ashby, M.F., et al., *Metal foams: a design guide.* 2000: Elsevier.

19. Parthasarathy, J., B. Starly, and S. Raman, *A design for the additive manufacture of functionally graded porous structures with tailored mechanical properties for biomedical applications.* Journal of Manufacturing Processes, 2011. **13**(2): p. 160-170.

20. Morrish, S., et al., *Size effects in compression in Electron Beam Melted Ti6Al4V diamond structure lattices.* Materials Letters, 2017. **190**: p. 138-142.

21. Hernández-Nava, E., et al., *The effect of defects on the mechanical response of Ti-6Al-4V cubic lattice structures fabricated by electron beam melting.* Acta Materialia, 2016. **108**: p. 279-292.

22. Balla, V.K., et al., *Porous tantalum structures for bone implants: fabrication, mechanical and in vitro biological properties.* Acta biomaterialia, 2010. **6**(8): p. 3349-3359.

23. Das, M., et al., *Fabrication of Biomedical Implants using Laser Engineered Net Shaping (LENS™).* Transactions of the Indian Ceramic Society, 2013. **72**(3): p. 169-174.

24. Aboulkhair, N.T., *Additive manufacture of an aluminium alloy: processing, microstructure, and mechanical properties.* 2016, University of Nottingham.

25. Siddique, S., et al., *Influence of process-induced microstructure and imperfections on mechanical properties of AlSi12 processed by selective laser melting.* Journal of Materials Processing Technology, 2015. **221**(Supplement C): p. 205-213.

26. Bartkowiak, K., et al., *New Developments of Laser Processing Aluminium Alloys via Additive Manufacturing Technique.* Physics Procedia, 2011. **12**(Part A): p. 393-401.

27. Wessel, J.K., *The handbook of advanced materials: enabling new designs.* 2004: John Wiley & Sons.

28. Miyamoto, Y., et al., *Functionally graded materials: design, processing and applications.* Vol. 5. 2013: Springer Science & Business Media.

29. Gottron, J., K.A. Harries, and Q. Xu, *Creep behaviour of bamboo.* Construction and Building Materials, 2014. **66**: p. 79-88.

30. Mahamood, R.M. and E.T. Akinlabi, *Types of Functionally Graded Materials and Their Areas of Application*, in *Functionally Graded Materials*. 2017, Springer. p. 9-21.

31. Naebe, M. and K. Shirvanimoghaddam, *Functionally graded materials: A review of fabrication and properties.* Applied Materials Today, 2016. **5**: p. 223-245.

32. Bever, M. and P. Duwez, *Gradients in composite materials.* Materials Science and Engineering, 1972. **10**: p. 1-8.

33. Shen, M. and M. Bever, *Gradients in polymeric materials.* Journal of Materials science, 1972. **7**(7): p. 741-746.

34. Tan, T., et al., *Mechanical properties of functionally graded hierarchical bamboo structures.* Acta biomaterialia, 2011. **7**(10): p. 3796-3803.

35. Cherradi, N., A. Kawasaki, and M. Gasik, *Worldwide trends in functional gradient materials research and development.* Composites Engineering, 1994. **4**(8): p. 883-894.

36. CPM, S.A., B. Varghese, and A. Baby, *A review on functionally graded materials.* Int. J. Eng. Sci, 2014. **3**(6): p. 90-101.

37. El-Wazery, M. and A. El-Desouky, *A review on functionally graded ceramic-metal materials.* Journal of Materials and Environmental Science, 2015. **6**(5): p. 1369-1376.

38. Tejaswini, N., K.R. Babu, and D.K.S. Ram, *FUNCTIONALLY GRADED MATERIAL: ANOVERVIEW.* IJAEST, ISSN, 2015: p. 2319-1112.

39. Kieback, B., A. Neubrand, and H. Riedel, *Processing techniques for functionally graded materials.* Materials Science and Engineering: A, 2003. **362**(1): p. 81-106.

40. Sasaki, M. and T. Hirai, *Thermal fatigue resistance of CVD SiC/C functionally gradient material.* Journal of the European Ceramic Society, 1994. **14**(3): p. 257-260.

41. Kawase, M., et al., *Chemical vapor infiltration and deposition to produce a silicon carbide–carbon functionally gradient material.* Chemical Engineering Science, 1999. **54**(15): p. 3327-3334.

42. Shinohara, Y., *Chapter 11.2.4 - Functionally Graded Materials A2 - Somiya, Shigeyuki*, in *Handbook of Advanced Ceramics (Second Edition)*. 2013, Academic Press: Oxford. p. 1179-1187.

43. Mumtaz, K.A. and N. Hopkinson, *Laser melting functionally graded composition of Waspaloy® and Zirconia powders.* Journal of materials science, 2007. **42**(18): p. 7647-7656.

44. Pan, C. and X. Xu, *Microstructural characteristics in plasma sprayed functionally graded ZrO2/NiCrAl coatings.* Surface and Coatings Technology, 2003. **162**(2): p. 194-201.

45. Kim, J.H., M.C. Kim, and C.G. Park, *Evaluation of functionally graded thermal barrier coatings fabricated by detonation gun spray technique.* Surface and Coatings Technology, 2003. **168**(2): p. 275-280.

46. Watanabe, Y., et al., *Fabrication of fiber-reinforced functionally graded materials by a centrifugal in situ method from Al–Cu–Fe ternary alloy.* Composites Part A: Applied Science and Manufacturing, 2006. **37**(12): p. 2186-2193.

47. Gao, J.W. and C.Y. Wang, *Modeling the solidification of functionally graded materials by centrifugal casting.* Materials Science and Engineering: A, 2000. **292**(2): p. 207-215.

48. Prabhu, T.R., *Processing and properties evaluation of functionally continuous graded 7075 Al alloy/SiC composites.* Archives of Civil and Mechanical Engineering, 2017. **17**(1): p. 20-31.

49. Hong, C.-Q., et al., *A novel functionally graded material in the ZrB2–SiC and ZrO2 system by spark plasma sintering.* Materials Science and Engineering: A, 2008. **498**(1): p. 437-441.

50. Pellizzari, M., A. Fedrizzi, and M. Zadra, *Influence of processing parameters and particle size on the properties of hot work and high speed tool steels by Spark Plasma Sintering.* Materials & Design, 2011. **32**(4): p. 1796-1805.

51. Eriksson, M., M. Radwan, and Z. Shen, *Spark plasma sintering of WC, cemented carbide and functional graded materials.* International Journal of Refractory Metals and Hard Materials, 2013. **36**(Supplement C): p. 31-37.

52. Jin, G., et al., *Properties of multilayered mullite/Mo functionally graded materials fabricated by powder metallurgy processing.* Materials Chemistry and Physics, 2005. **89**(2): p. 238-243.

53. Chenglin, C., et al., *Hydroxyapatite–Ti functionally graded biomaterial fabricated by powder metallurgy.* Materials Science and Engineering: A, 1999. **271**(1): p. 95-100.

54. Bobbio, L.D., et al., *Additive manufacturing of a functionally graded material from Ti-6Al-4V to Invar: Experimental characterization and thermodynamic calculations.* Acta Materialia, 2017. **127**: p. 133-142.

55. Soodi, M., S. Masood, and M. Brandt, *Thermal expansion of functionally graded and wafer-layered structures produced by laser direct metal deposition.* The International Journal of Advanced Manufacturing Technology, 2013. **69**(9-12): p. 2011-2018.

56. Schneider-Maunoury, C., et al., *Functionally graded Ti6Al4V-Mo alloy manufactured with DED-CLAD® process.* Additive Manufacturing, 2017. **17**: p. 55-66.

57.	Durejko, T., et al., *Thin wall tubes with Fe 3 Al/SS316L graded structure obtained by using laser engineered net shaping technology.* Materials & Design, 2014. **63**: p. 766-774.

58.	Chung, H. and S. Das, *Functionally graded Nylon-11/silica nanocomposites produced by selective laser sintering.* Materials Science and Engineering: A, 2008. **487**(1): p. 251-257.

59.	Zhang, Y., et al., *Characterization of laser powder deposited Ti–TiC composites and functional gradient materials.* journal of materials processing technology, 2008. **206**(1): p. 438-444.

60.	Kang, N., et al., *A novel approach to in-situ produce functionally graded silicon matrix composite materials by selective laser melting.* Composite Structures, 2017. **172**(Supplement C): p. 251-258.

61.	Erdal, M., et al. *Manufacturing of functionally graded porous products by selective laser sintering.* in *Materials Science Forum.* 2010. Trans Tech Publ.

62.	Li, L., et al., *Composite Modeling and Analysis for Fabrication of FDM Prototypes with Locally Controlled Properties.* Journal of Manufacturing Processes, 2002. **4**(2): p. 129-141.

63.	Niendorf, T., et al., *Functionally graded alloys obtained by additive manufacturing.* Advanced Engineering Materials, 2014. **16**(7): p. 857-861.

64.	Maskery, I., et al., *An investigation into reinforced and functionally graded lattice structures.* Journal of Cellular Plastics, 2016. **53**(2): p. 151-165.

65.	van Grunsven, W., et al., *Fabrication and mechanical characterisation of titanium lattices with graded porosity.* Metals, 2014. **4**(3): p. 401-409.

66.	Leong, K.F., et al., *Engineering functionally graded tissue engineering scaffolds.* Journal of the Mechanical Behavior of Biomedical Materials, 2008. **1**(2): p. 140-152.

67.	Karamooz Ravari, M.R., et al., *Numerical investigation on mechanical properties of cellular lattice structures fabricated by fused deposition modeling.* International Journal of Mechanical Sciences, 2014. **88**: p. 154-161.

68.	Smith, M., Z. Guan, and W.J. Cantwell, *Finite element modelling of the compressive response of lattice structures manufactured using the selective laser melting technique.* International Journal of Mechanical Sciences, 2013. **67**: p. 28-41.

69.	Tancogne-Dejean, T., A.B. Spierings, and D. Mohr, *Additively-manufactured metallic micro-lattice materials for high specific energy absorption under static and dynamic loading.* Acta Materialia, 2016. **116**: p. 14-28.

70.	Standard, A., *Standard Practice for Heat Treatment of Aluminum-Alloy Castings from All Processes.* 2004.

71.   Standard, A., *Standard Practice for Heat Treatment of Wrought Aluminum Alloys1*. 2017.

72.   Aboulkhair, N.T., et al., *Improving the fatigue behaviour of a selectively laser melted aluminium alloy: Influence of heat treatment and surface quality.* Materials & Design, 2016. **104**: p. 174-182.

73.   Riemer, A., et al., *On the fatigue crack growth behavior in 316L stainless steel manufactured by selective laser melting.* Engineering Fracture Mechanics, 2014. **120**(Supplement C): p. 15-25.

74.   Yasa, E. and J.-P. Kruth, *Microstructural investigation of Selective Laser Melting 316L stainless steel parts exposed to laser re-melting.* Procedia Engineering, 2011. **19**: p. 389-395.

75.   Rashid, R., et al., *Effect of scan strategy on density and metallurgical properties of 17-4PH parts printed by Selective Laser Melting (SLM).* Journal of Materials Processing Technology, 2017. **249**(Supplement C): p. 502-511.

76.   Yadroitsev, I., P. Krakhmalev, and I. Yadroitsava, *Selective laser melting of Ti6Al4V alloy for biomedical applications: Temperature monitoring and microstructural evolution.* Journal of Alloys and Compounds, 2014. **583**(Supplement C): p. 404-409.

77.   Leuders, S., et al., *On the mechanical behaviour of titanium alloy TiAl6V4 manufactured by selective laser melting: Fatigue resistance and crack growth performance.* International Journal of Fatigue, 2013. **48**(Supplement C): p. 300-307.

78.   Kasperovich, G. and J. Hausmann, *Improvement of fatigue resistance and ductility of TiAl6V4 processed by selective laser melting.* Journal of Materials Processing Technology, 2015. **220**(Supplement C): p. 202-214.

79.   Shiomi, M., et al., *Residual Stress within Metallic Model Made by Selective Laser Melting Process.* CIRP Annals, 2004. **53**(1): p. 195-198.

80.   Prashanth, K., et al., *Tribological and corrosion properties of Al–12Si produced by selective laser melting.* Journal of Materials Research, 2014. **29**(17): p. 2044-2054.

81.   Aboulkhair, N.T., et al., *The microstructure and mechanical properties of selectively laser melted AlSi10Mg: The effect of a conventional T6-like heat treatment.* Materials Science and Engineering: A, 2016. **667**(Supplement C): p. 139-146.

82.   Kimura, T. and T. Nakamoto, *Microstructures and mechanical properties of A356 (AlSi7Mg0.3) aluminum alloy fabricated by selective laser melting.* Materials & Design, 2016. **89**: p. 1294-1301.

83.   Li, W., et al., *Effect of heat treatment on AlSi10Mg alloy fabricated by selective laser melting: Microstructure evolution, mechanical properties and fracture mechanism.* Materials Science and Engineering: A, 2016. **663**: p. 116-125.

84.   Brandl, E., et al., *Additive manufactured AlSi10Mg samples using Selective Laser Melting (SLM): Microstructure, high cycle fatigue, and fracture behavior.* Materials & Design, 2012. **34**: p. 159-169.

85.   Delroisse, P., et al., *Effect of strut orientation on the microstructure heterogeneities in AlSi10Mg lattices processed by selective laser melting.* Scripta Materialia, 2017. **141**: p. 32-35.

86.   Kang, N., et al., *Characterization of the microstructure of a selective laser melting processed Al-50Si alloy: Effect of heat treatments.* Materials Characterization, 2017. **130**: p. 243-249.

87.   Aboulkhair, N.T., et al., *On the precipitation hardening of selective laser melted AlSi10Mg.* Metallurgical and Materials Transactions A, 2015. **46**(8): p. 3337-3341.

88.   Suryawanshi, J., et al., *Simultaneous enhancements of strength and toughness in an Al-12Si alloy synthesized using selective laser melting.* Acta Materialia, 2016. **115**: p. 285-294.

89.   Trevisan, F., et al., *On the Selective Laser Melting (SLM) of the AlSi10Mg Alloy: Process, Microstructure, and Mechanical Properties.* Materials, 2017. **10**(1): p. 76.

90.   Wang, P., et al., *Selective laser melting of Al-Zn-Mg-Cu: Heat treatment, microstructure and mechanical properties.* Journal of Alloys and Compounds, 2017. **707**: p. 287-290.

91.   Li, X.P., et al., *A selective laser melting and solution heat treatment refined Al–12Si alloy with a controllable ultrafine eutectic microstructure and 25% tensile ductility.* Acta Materialia, 2015. **95**: p. 74-82.

92.   Jia, Y.D., et al., *Microstructure and thermal expansion behavior of Al-50Si synthesized by selective laser melting.* Journal of Alloys and Compounds, 2017. **699**: p. 548-553.

93.   Maskery, I., et al., *Compressive failure modes and energy absorption in additively manufactured double gyroid lattices.* Additive Manufacturing, 2017. **16**(Supplement C): p. 24-29.

94.   Mousanezhad, D., et al., *Impact resistance and energy absorption of regular and functionally graded hexagonal honeycombs with cell wall material strain hardening.* International Journal of Mechanical Sciences, 2014. **89**: p. 413-422.

95.   Woesz, A., J. Stampfl, and P. Fratzl, *Cellular solids beyond the apparent density–an experimental assessment of mechanical properties.* Advanced Engineering Materials, 2004. **6**(3): p. 134-138.

96. Labeas, G. and M. Sunaric, *Investigation on the static response and failure process of metallic open lattice cellular structures.* Strain, 2010. **46**(2): p. 195-204.

97. Sing, S.L., et al., *Characterization of Titanium Lattice Structures Fabricated by Selective Laser Melting Using an Adapted Compressive Test Method.* Experimental Mechanics, 2016. **56**(5): p. 735-748.

98. Zhong, L. and X. Li, *Simulation Analysis of Lightweight Cylindrical Lattice Materials with Different Unit Cells.* Journal of Coastal Research, 2015. **73**(sp1): p. 155-159.

99. Yan, C., et al., *Advanced lightweight 316L stainless steel cellular lattice structures fabricated via selective laser melting.* Materials & Design, 2014. **55**: p. 533-541.

100. Rehme, O. and C. Emmelmann. *Rapid manufacturing of lattice structures with selective laser melting.* in *Proceedings of SPIE.* 2006.

101. Winter, R., et al., *Plate-impact loading of cellular structures formed by selective laser melting.* Modelling and Simulation in Materials Science and Engineering, 2014. **22**(2): p. 025021.

102. Olurin, O., N. Fleck, and M. Ashby, *Deformation and fracture of aluminium foams.* Materials Science and Engineering: A, 2000. **291**(1): p. 136-146.

103. ISO, *Mechanical testing of metals —Ductility testing —Compression test for porous and cellular metals (13314).* 2011: Swinburne library.

104. ASTM, *Standard Test Method for Tensile Properties of Plastics-D 638 - 02a.* 2015, IHS: Swinburne University of Technology

105. ASTM, *Standard Test Methods for Tension Testing of Metallic Materials-E8/E8M − 16a.* 2015, IHS: Swinburne University of Technology/5934593001.

106. Thijs, L., et al., *Fine-structured aluminium products with controllable texture by selective laser melting of pre-alloyed AlSi10Mg powder.* Acta Materialia, 2013. **61**(5): p. 1809-1819.

107. Birol, Y., *Microstructural evolution during annealing of a rapidly solidified Al–12Si alloy.* Journal of Alloys and Compounds, 2007. **439**(1): p. 81-86.

108. Masood S. H, 2016, ' Lectures 1,2,3,4,5' *ADM80006 Additive manufacturing and tooling*, Learning material on blackboard, Faculty of Science, Engineering & Technology/ Swinburne University of Technology,

Appendix A
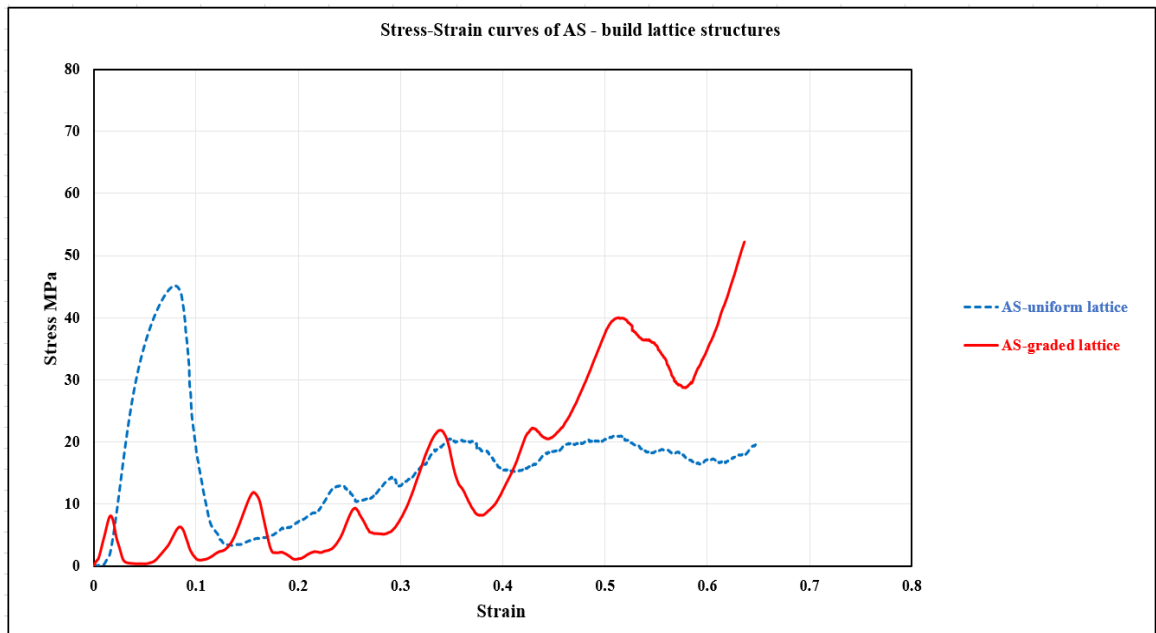
Figure 1 compressive stress strain curves of as-build graded and uniform structures
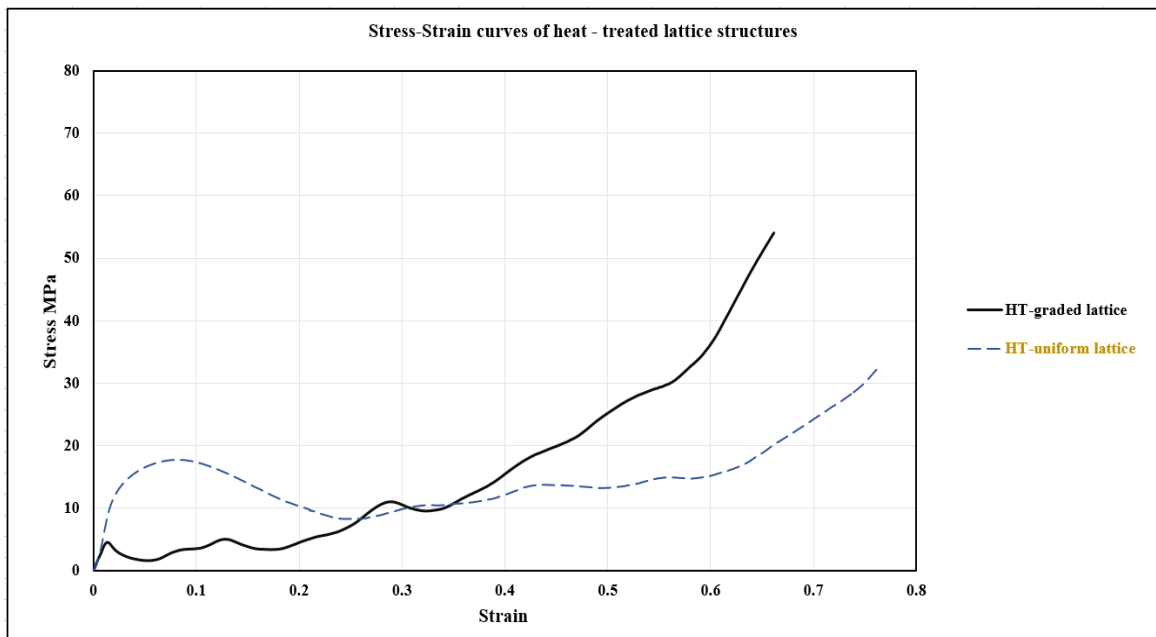
Figure 2 compressive stress strain curves of heat-treated graded and uniform structures
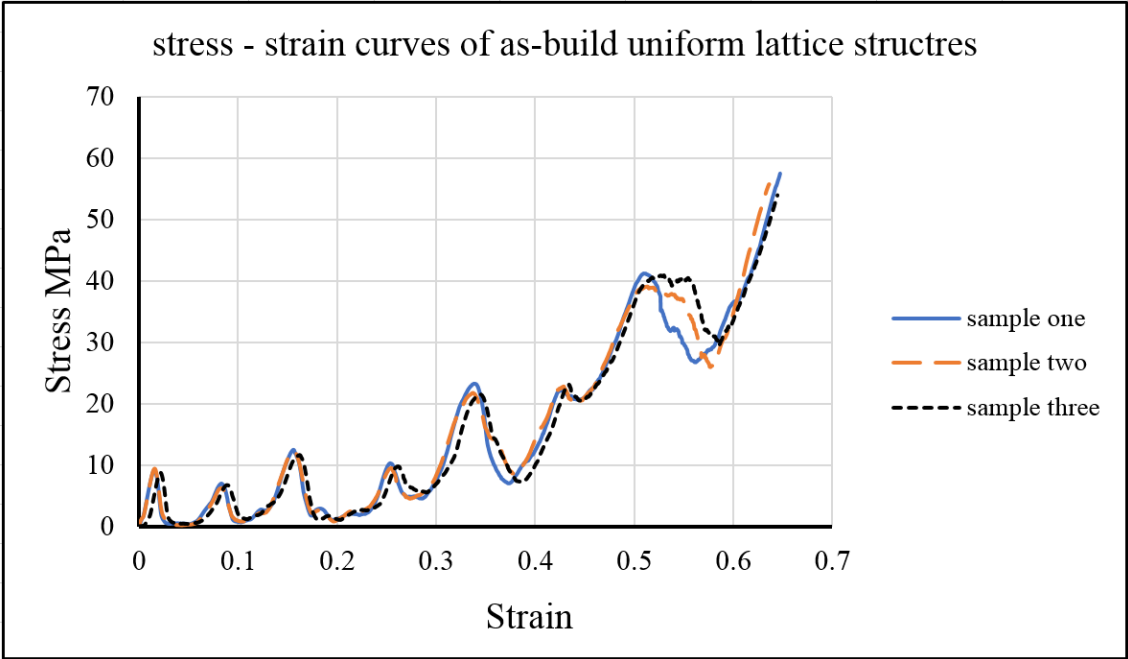
Figure 3 compressive stress strain curves of as-build graded lattice structures
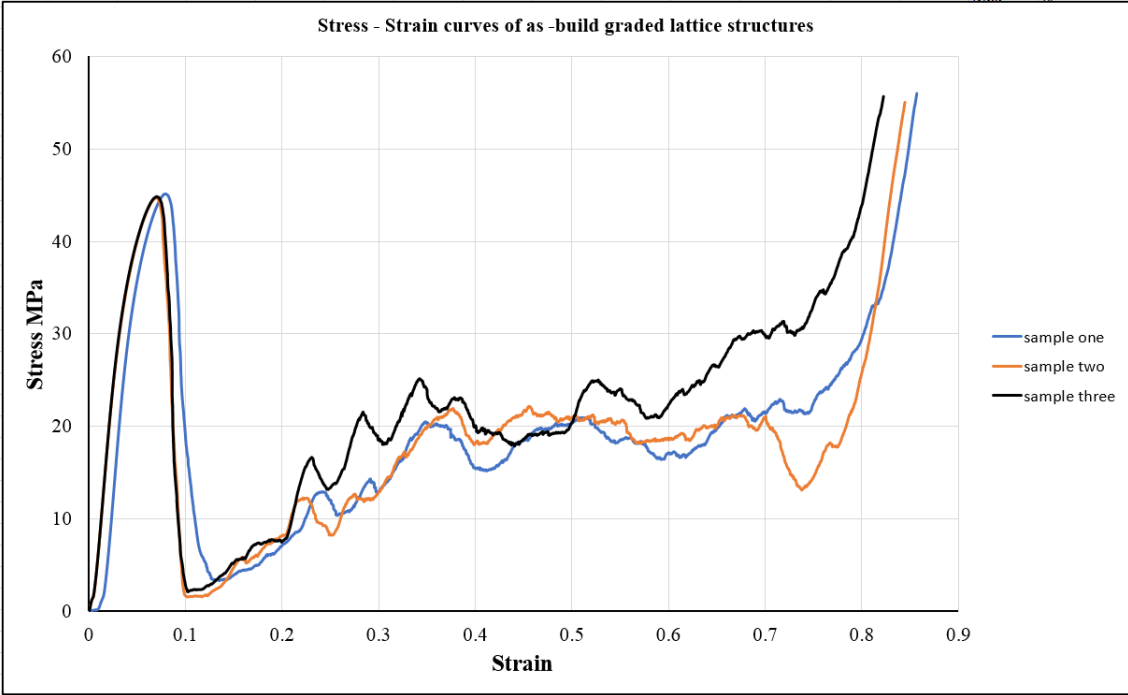
Figure 4 compressive stress strain curves of as-build uniform lattice structures
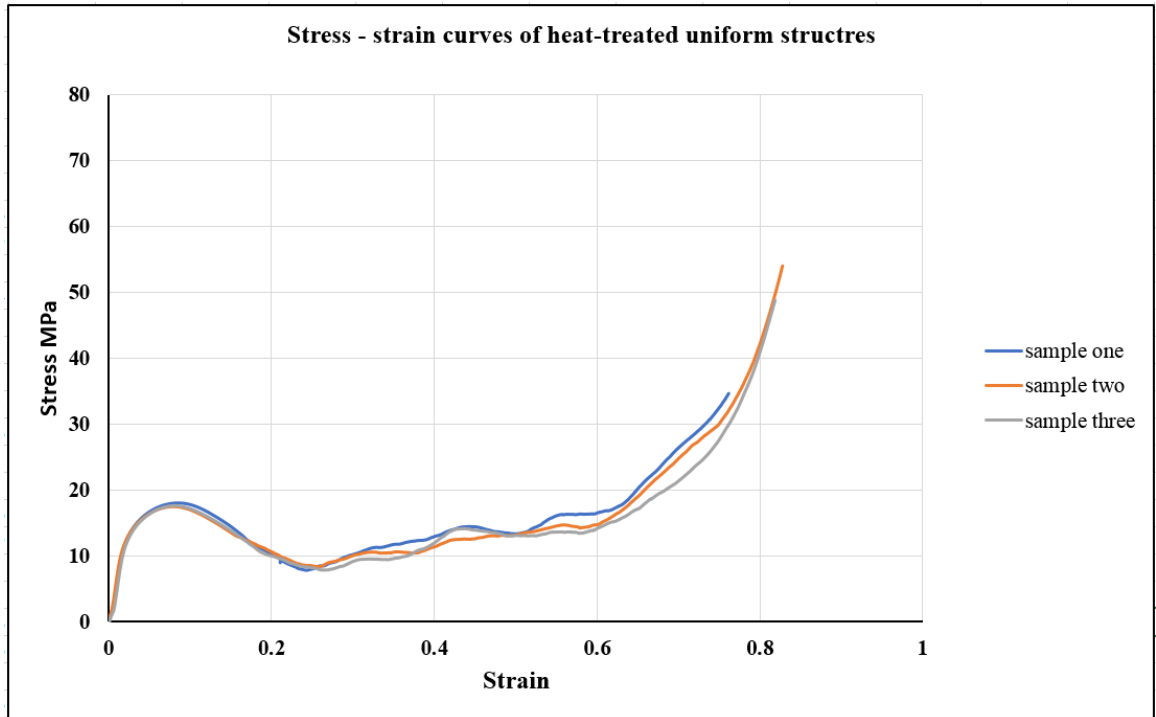
Figure 5 compressive stress strain curves of heat-treated uniform lattice structures
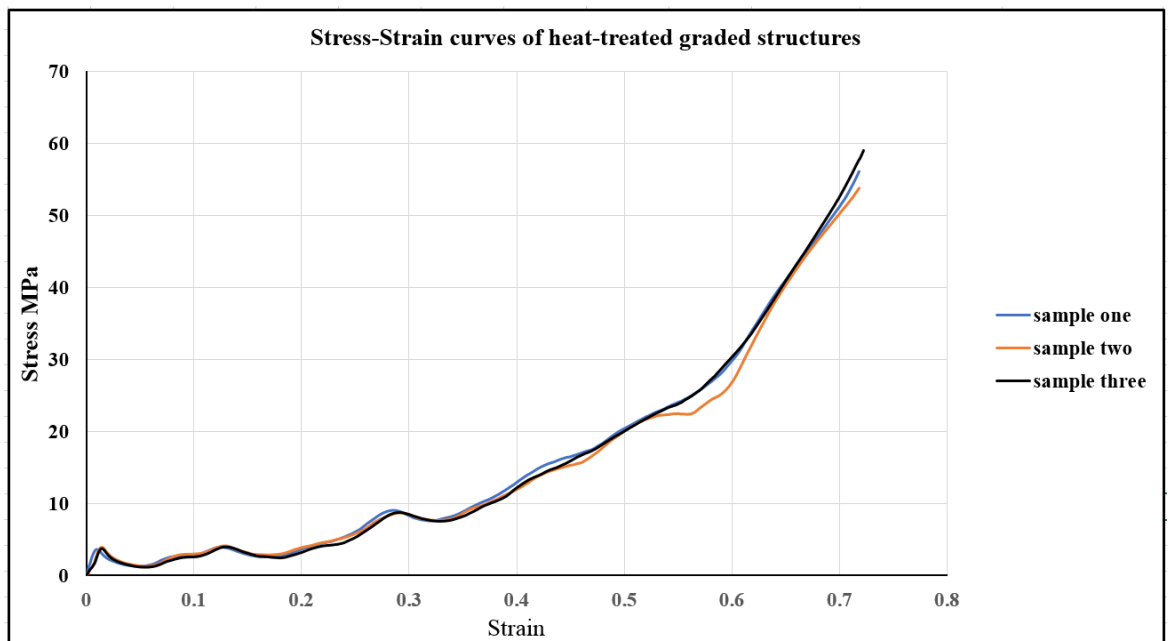
Figure 6 compressive stress strain curves of heat - treated graded lattice structures

Appendix B
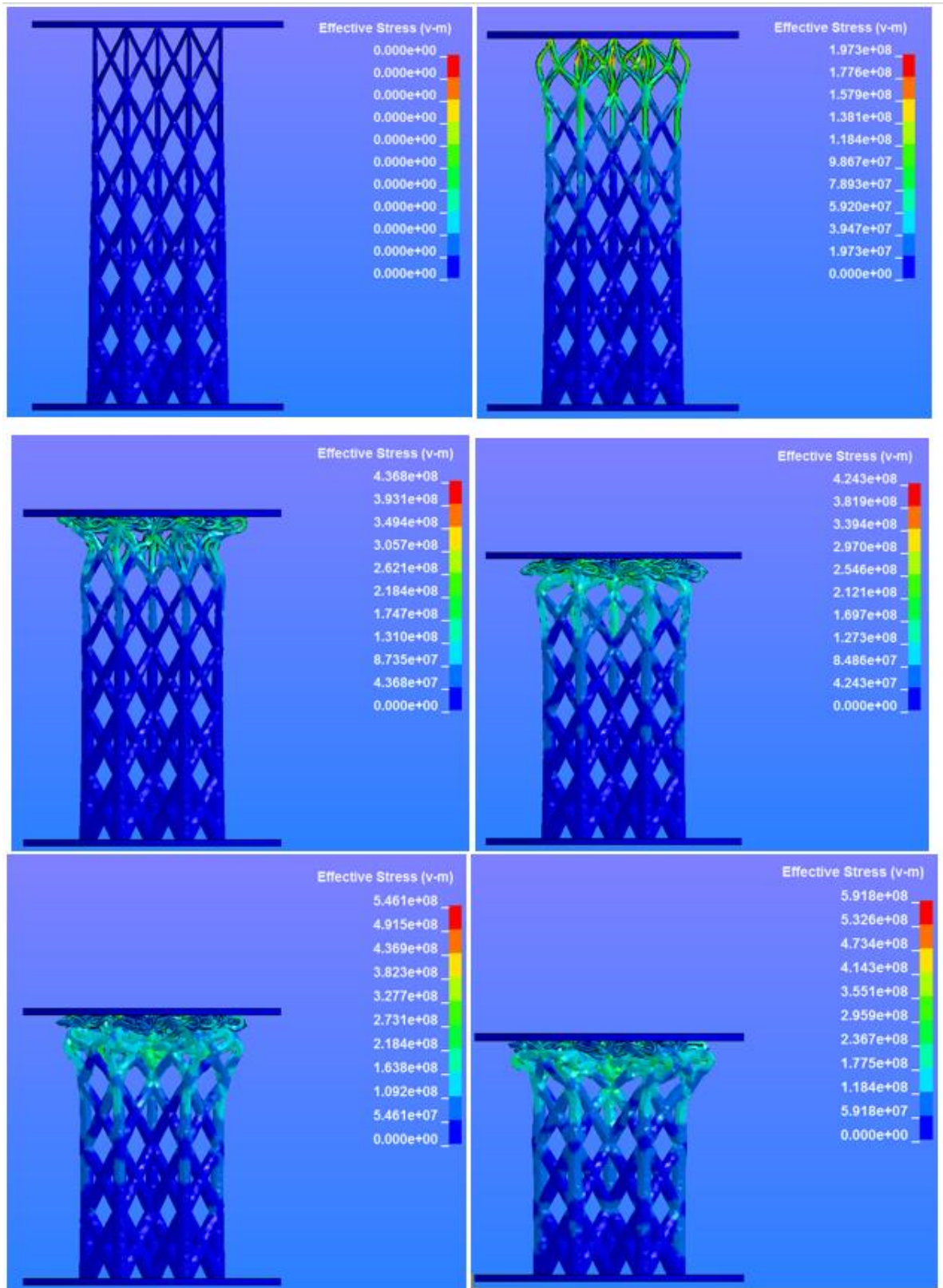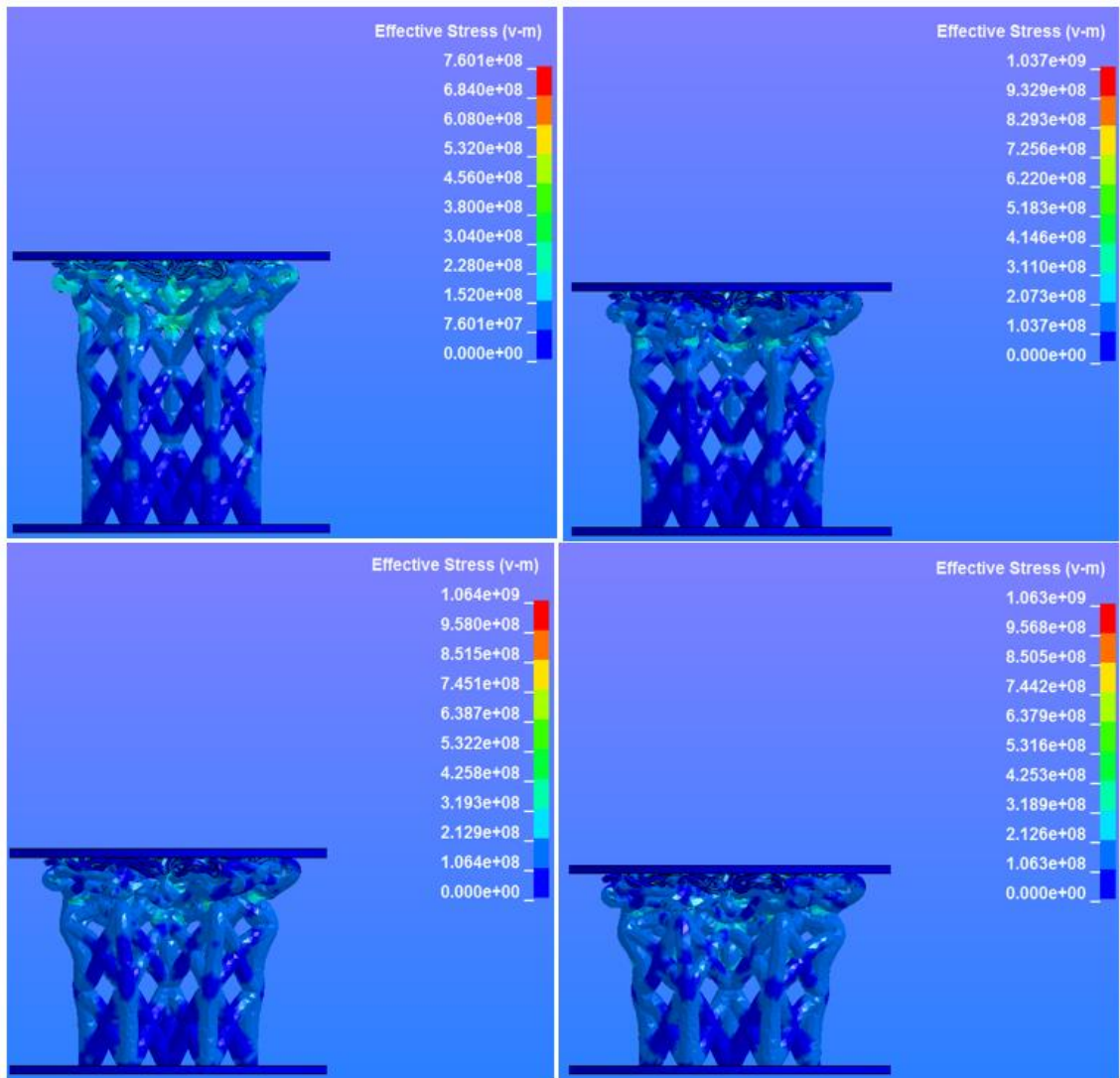
Figure 1 deformation stages of FE functionally graded model under the compressive loads
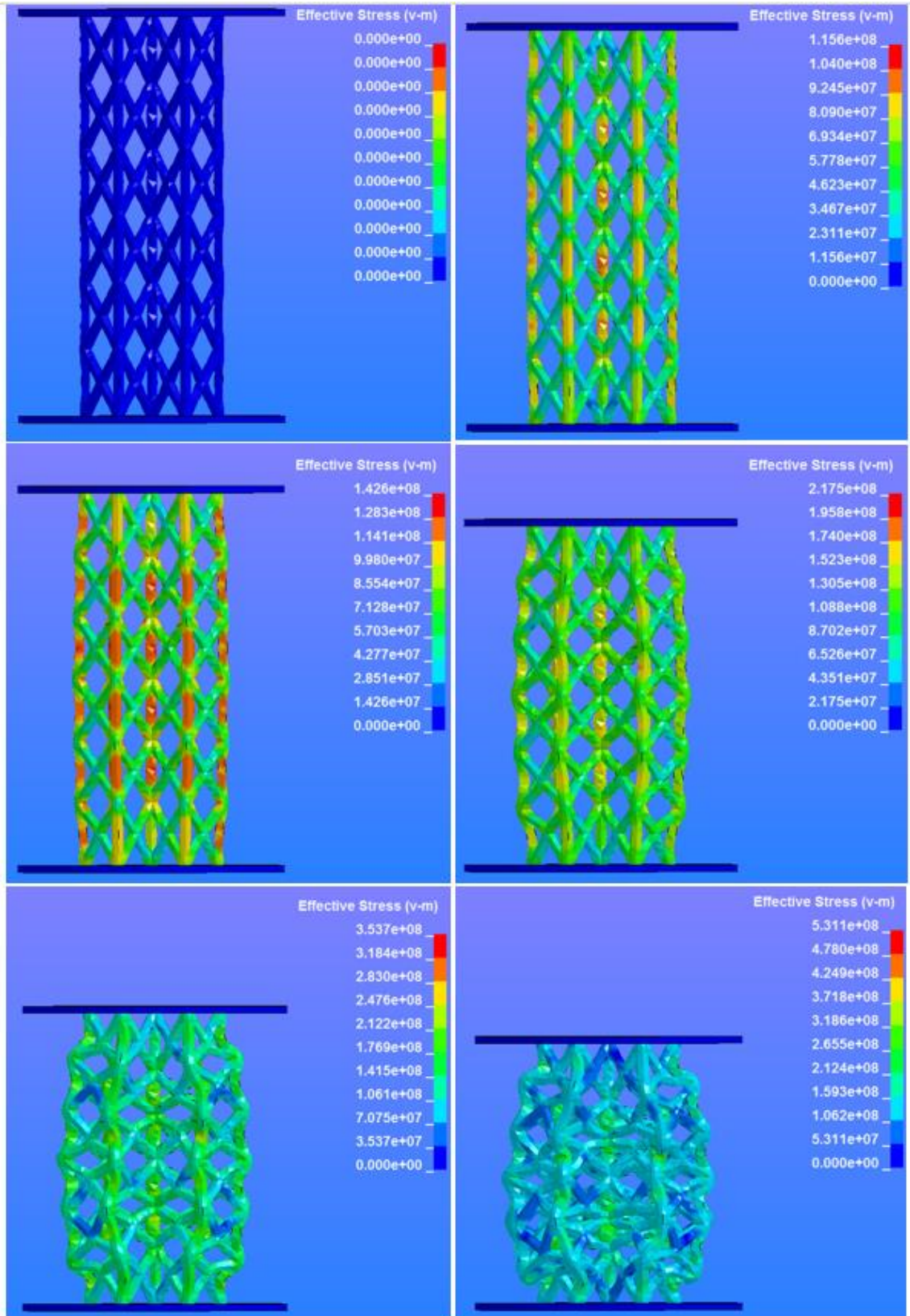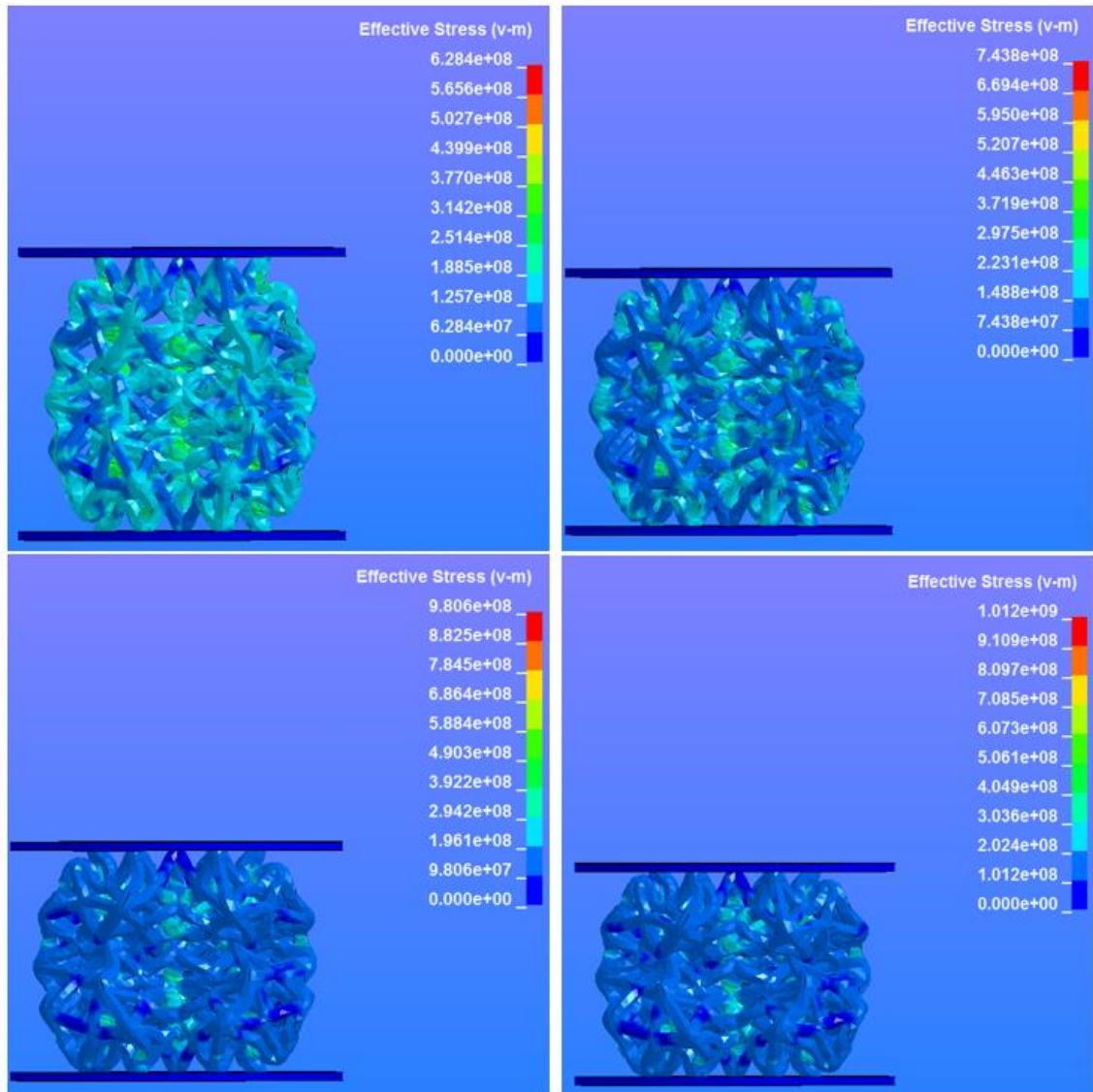
Figure 2 deformation stages of FE uniform model under the compressive loads

Appendix C
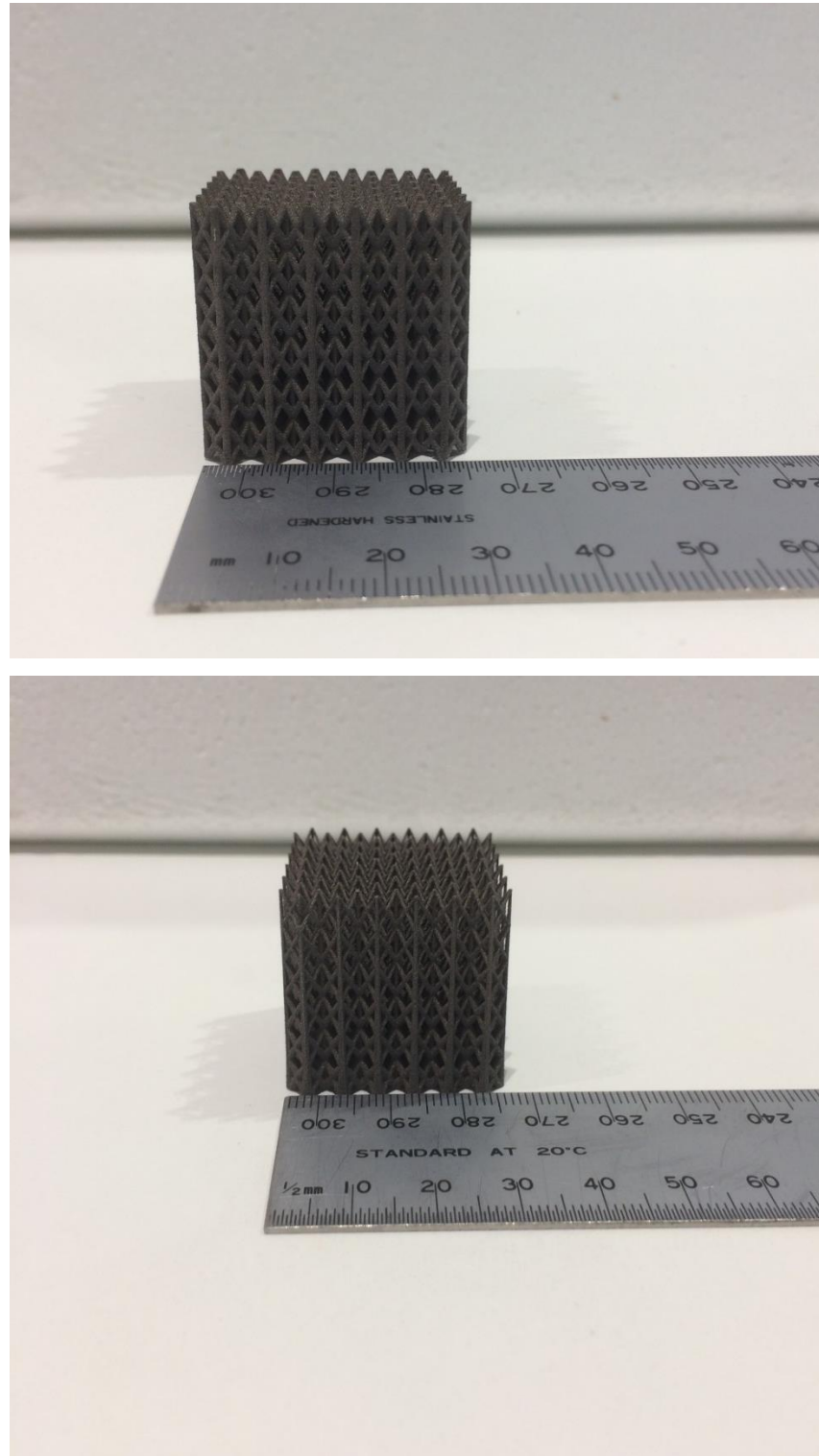
Figure 1 fabricated lattice structures with scale ruler,(top) uniform and (bottom) graded
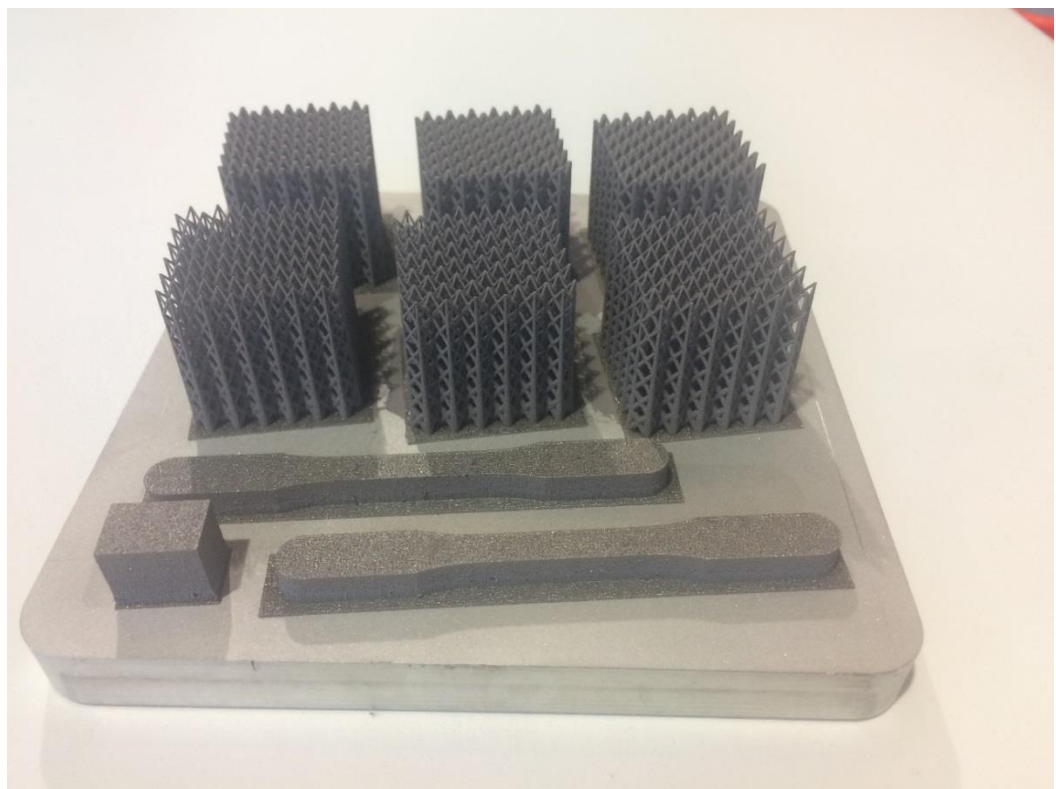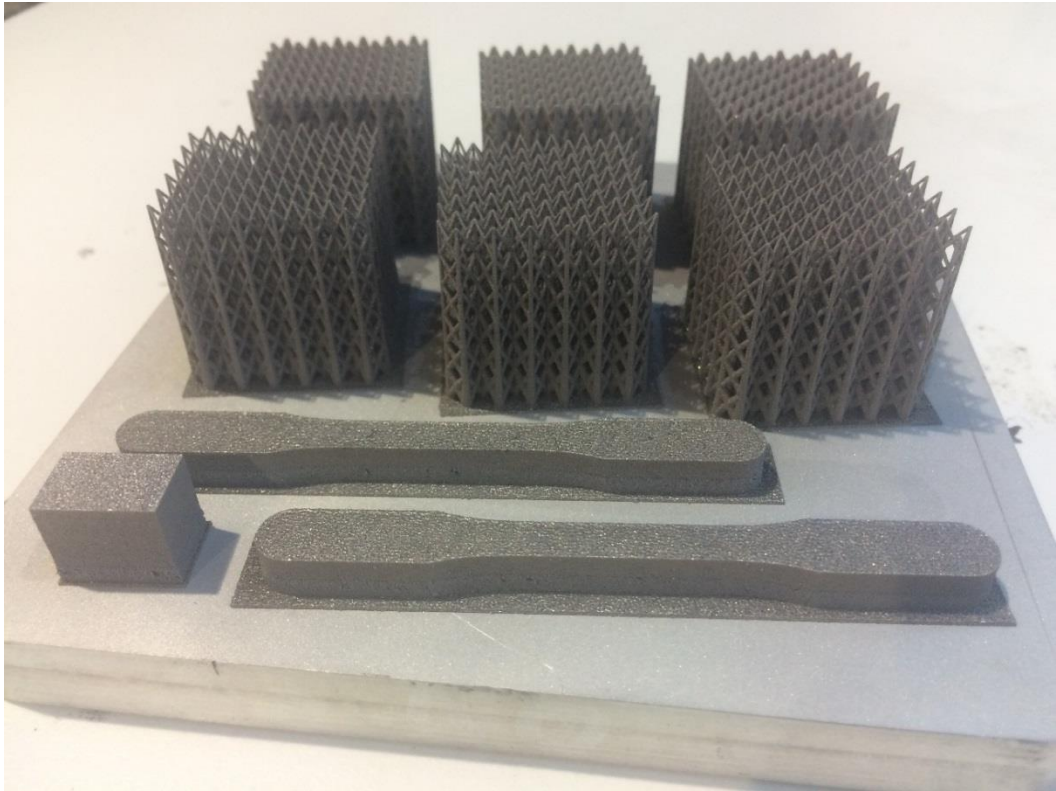
Figure 2 fabricated – SLM samples, lattice structures, dog bone tensile test and cubical microstructure on machine substrate.

Figure 3 fracture morphology of the top layer (lowest density) of graded lattice structures after compression tests, (Top) as-build , and (bottom) heat-treated conditions.
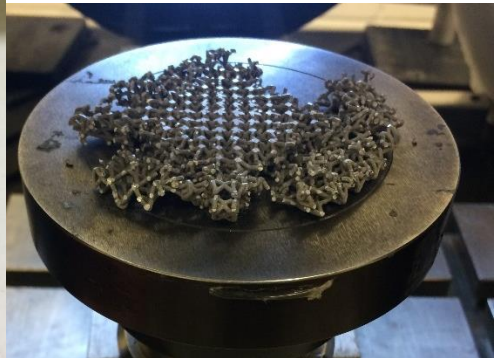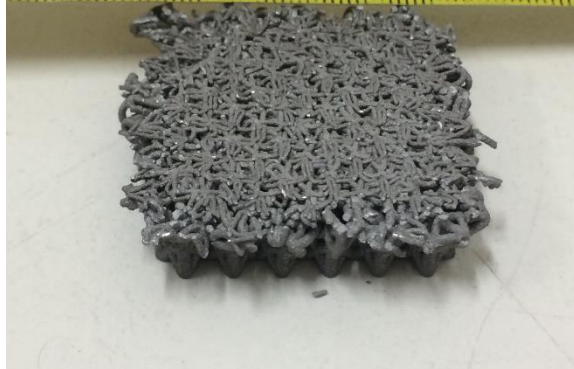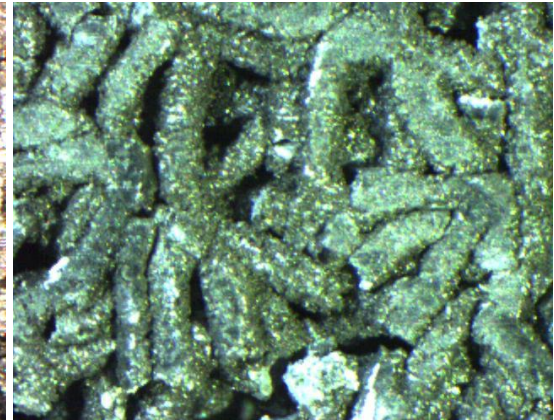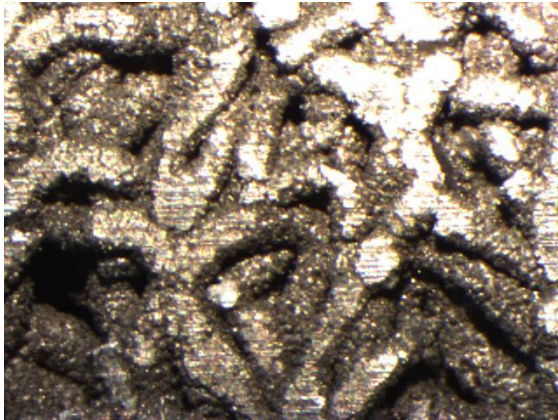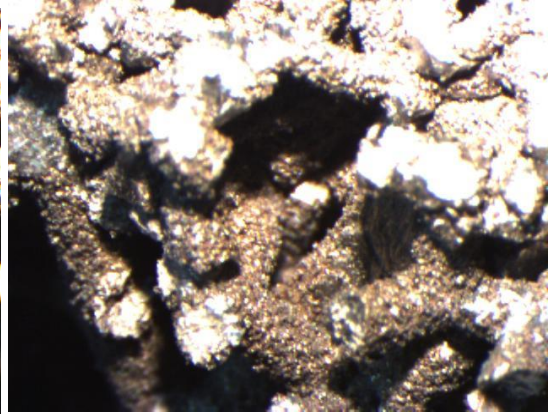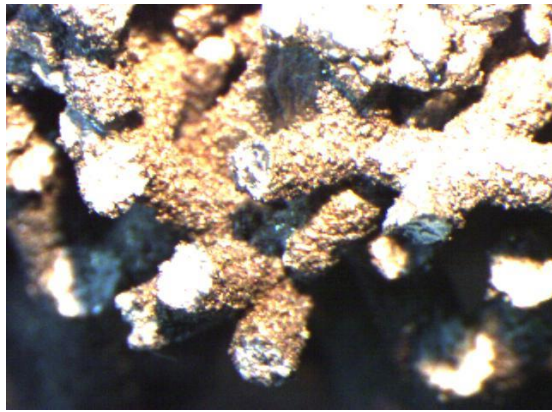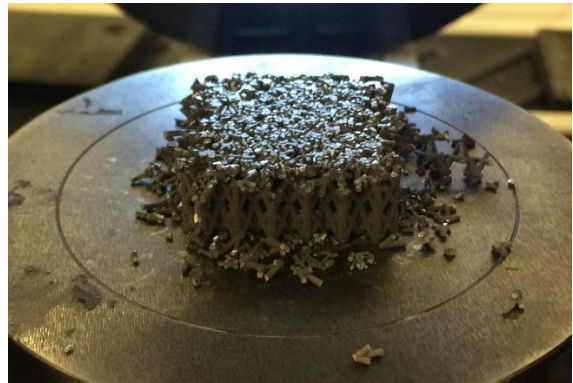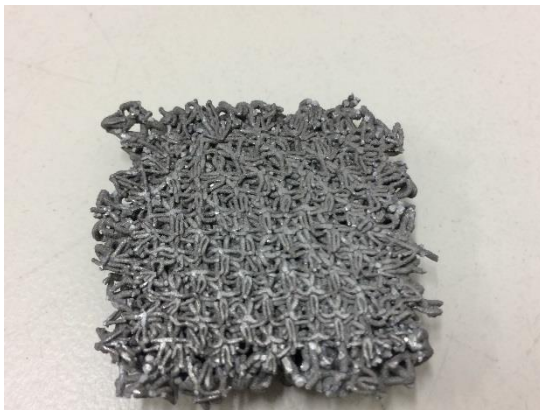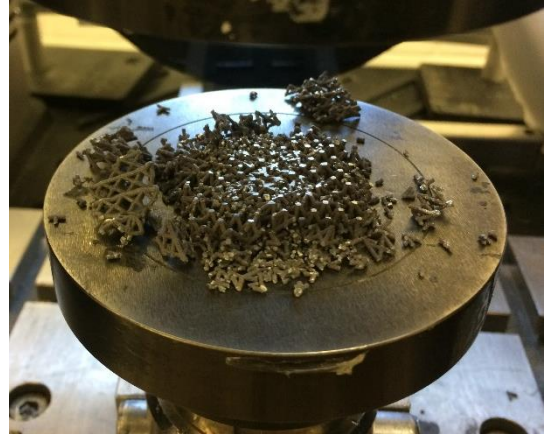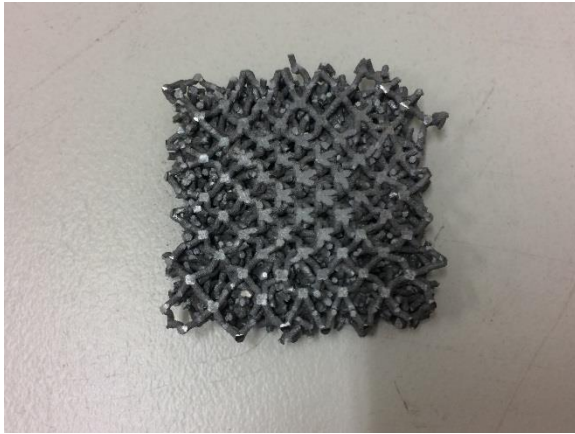
Figure 4 lattice structures in as-build and heat-treated conditions after compressiion tests, (Top) uniform, and (bottom) functionlly graded.

Appendix D
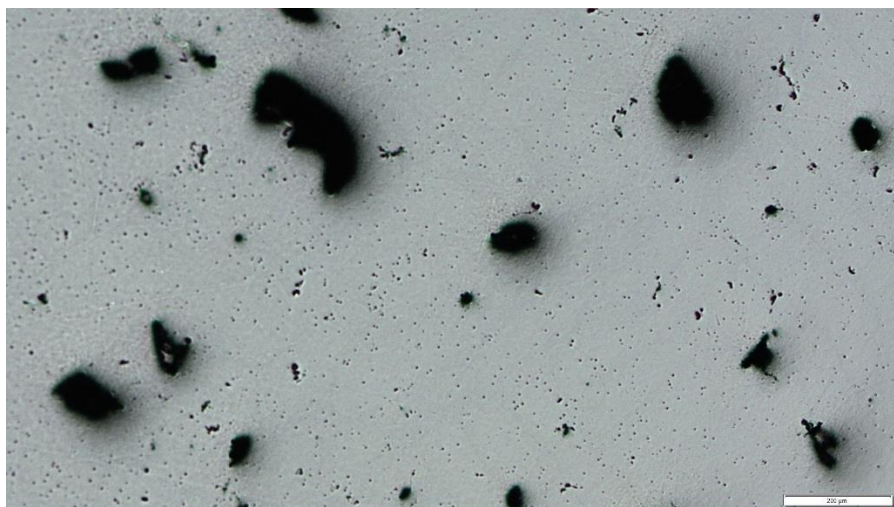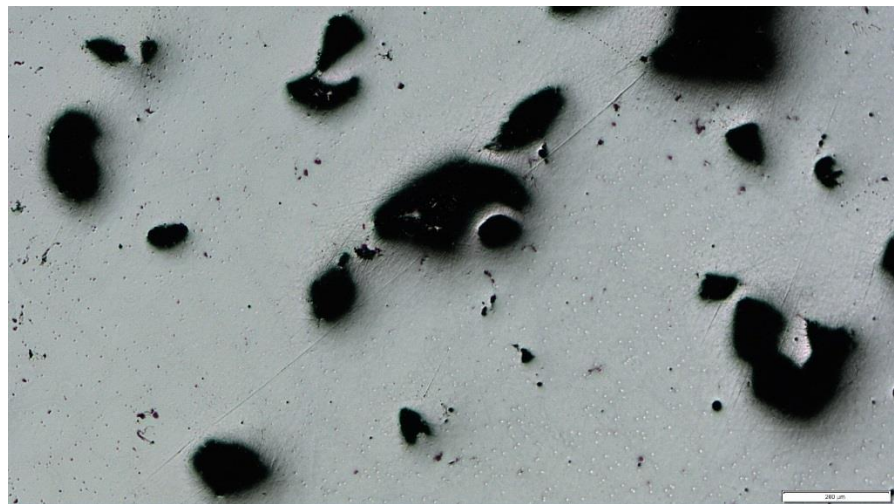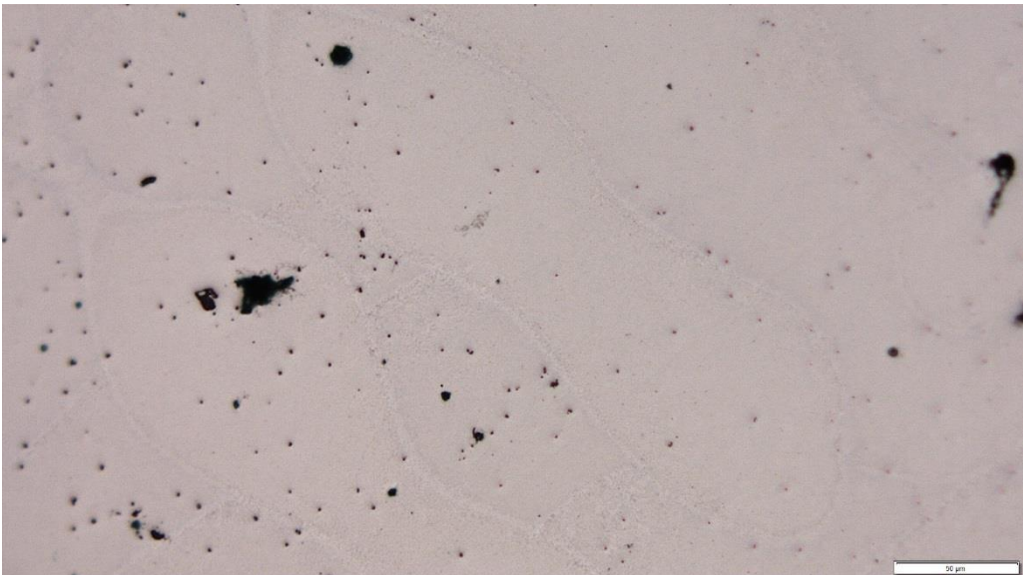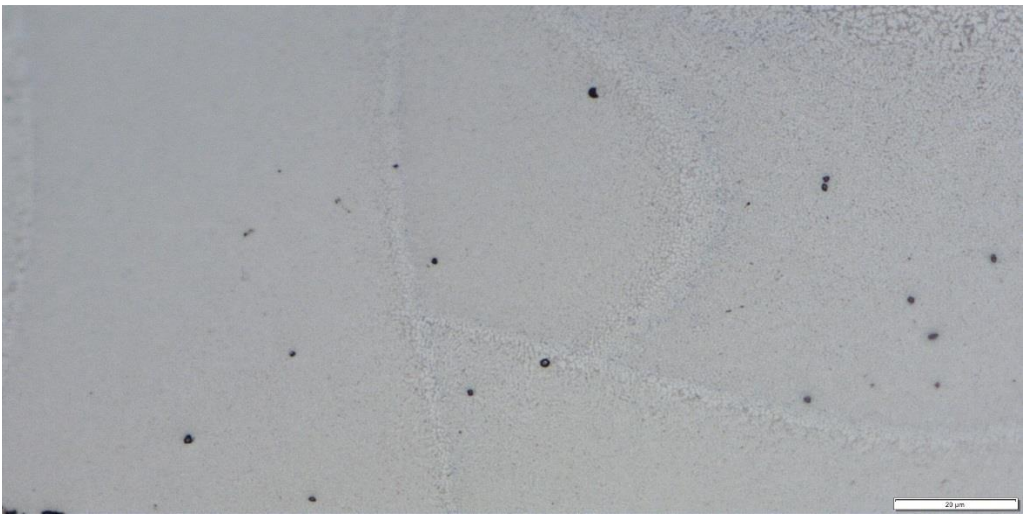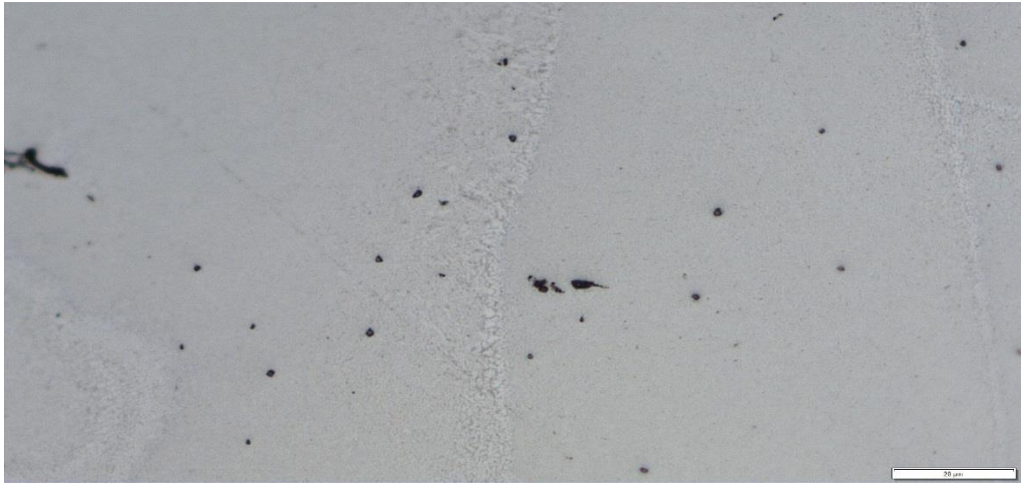
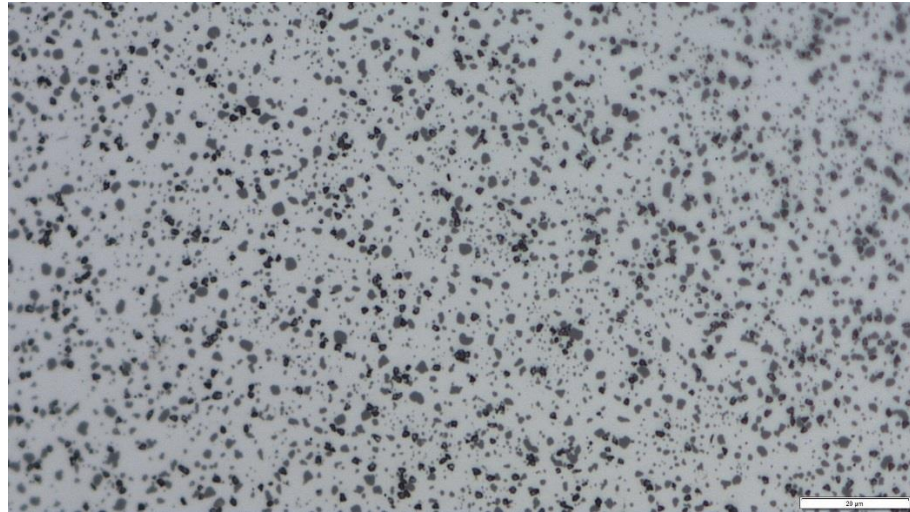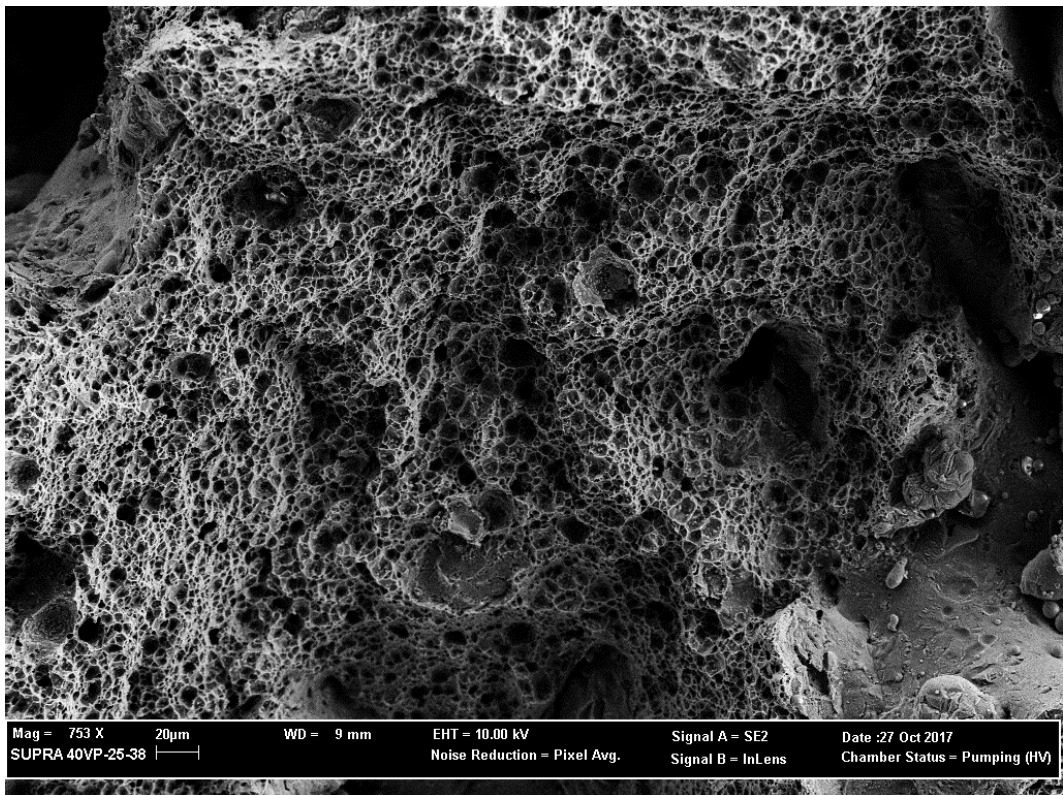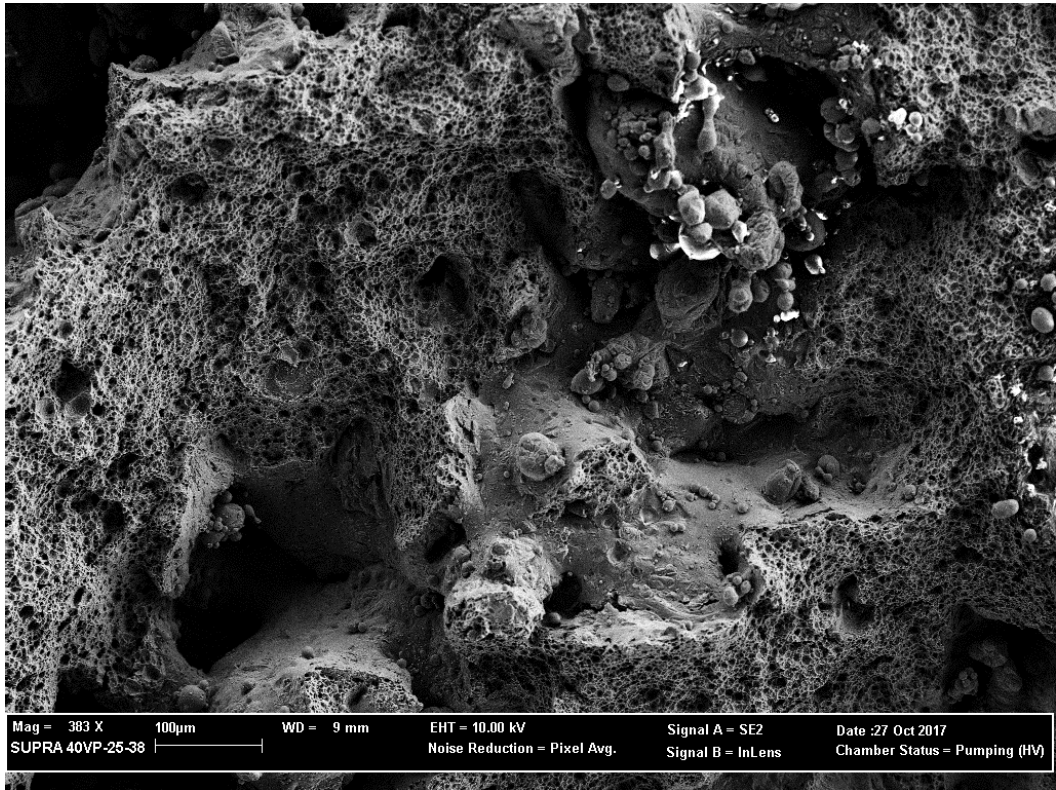Figure 1 OM micrographes of as-build condition of SLM- microstructures
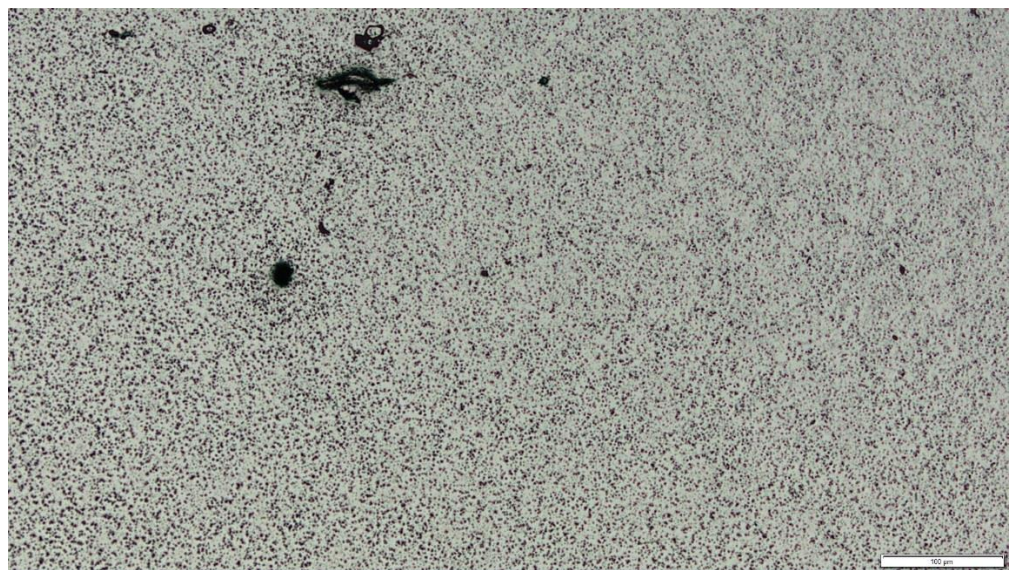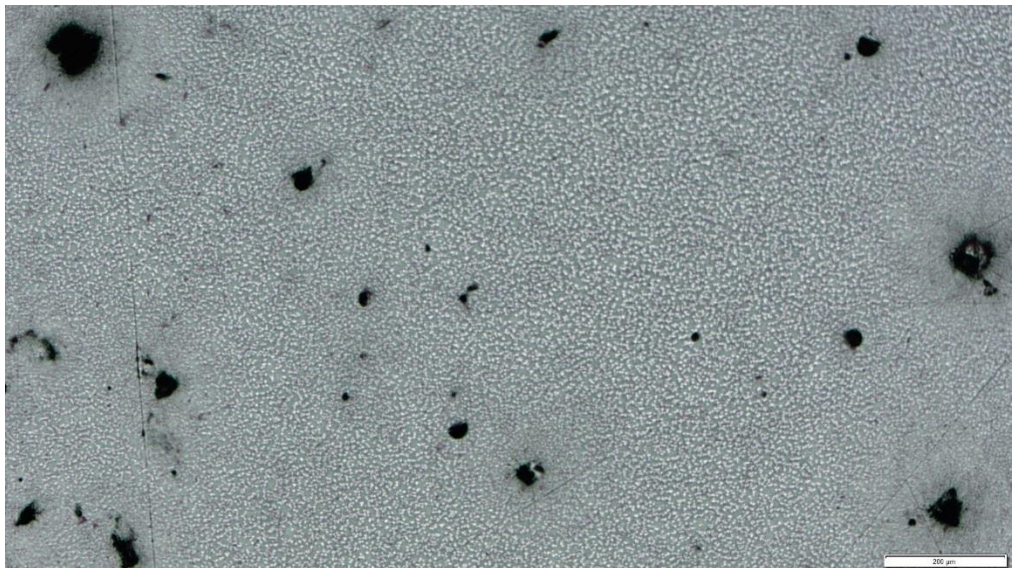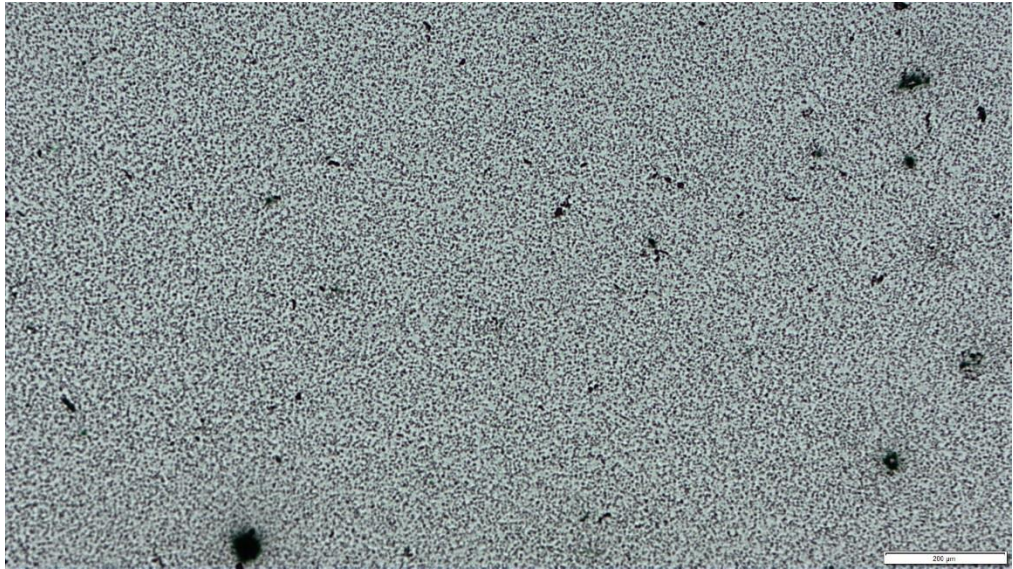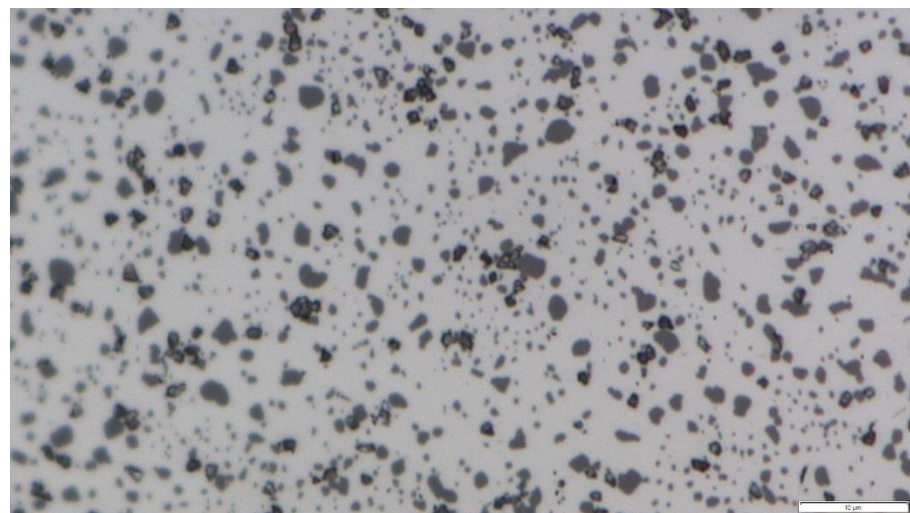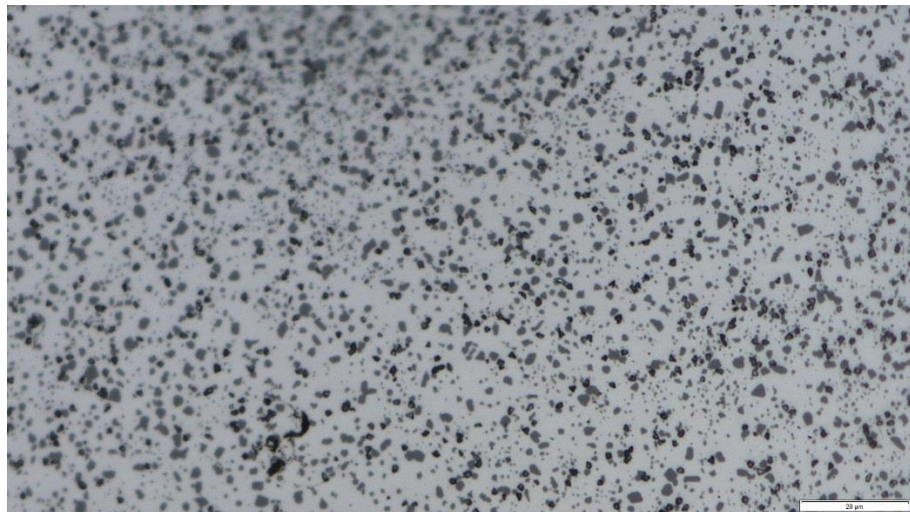
Figure 2 OM micrographes of heat - treated condition of SLM- microstructures

Appendix E

Mag = 383 X 100µm WD = 9 mm EHT = 10.00 kV Signal A = SE2 Date :27 Oct 2017
SUPRA 40VP-25-38 Noise Reduction = Pixel Avg. Signal B = InLens Chamber Status = Pumping (HV)

Mag = 753 X 20µm WD = 9 mm EHT = 10.00 kV Signal A = SE2 Date :27 Oct 2017
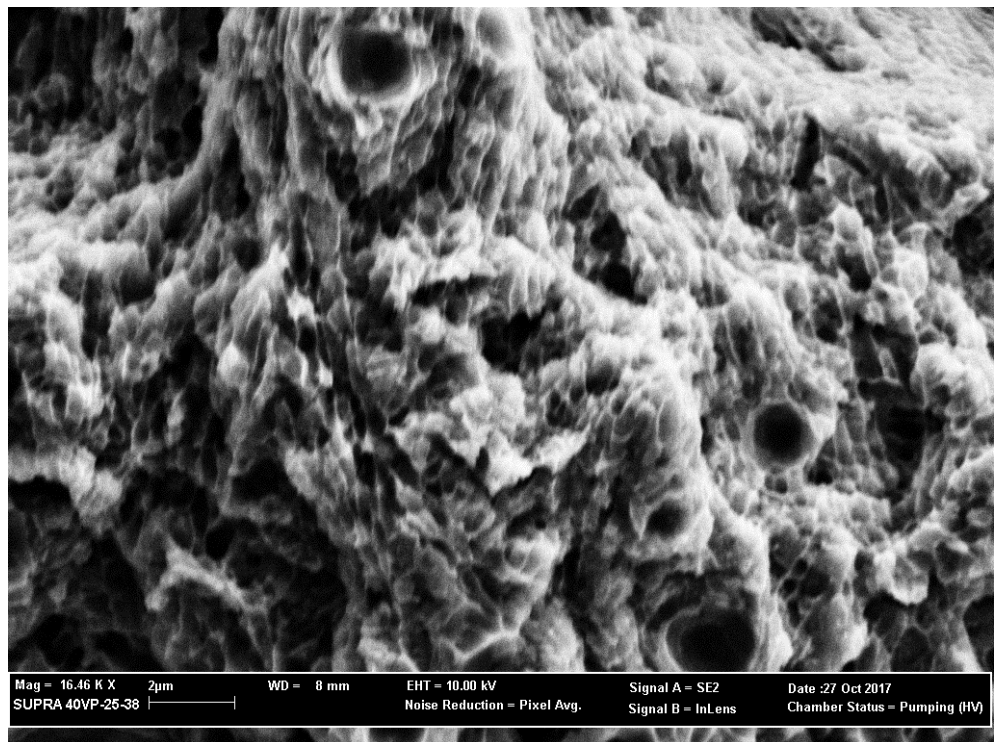SUPRA 40VP-25-38 Noise Reduction = Pixel Avg. Signal B = InLens Chamber Status = Pumping (HV)
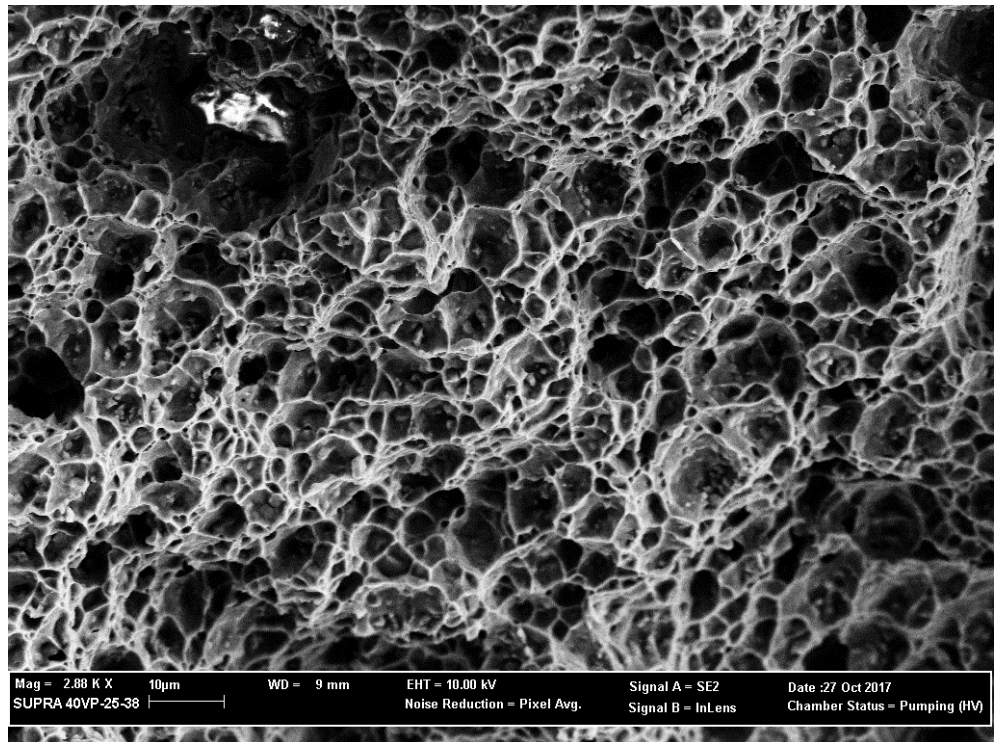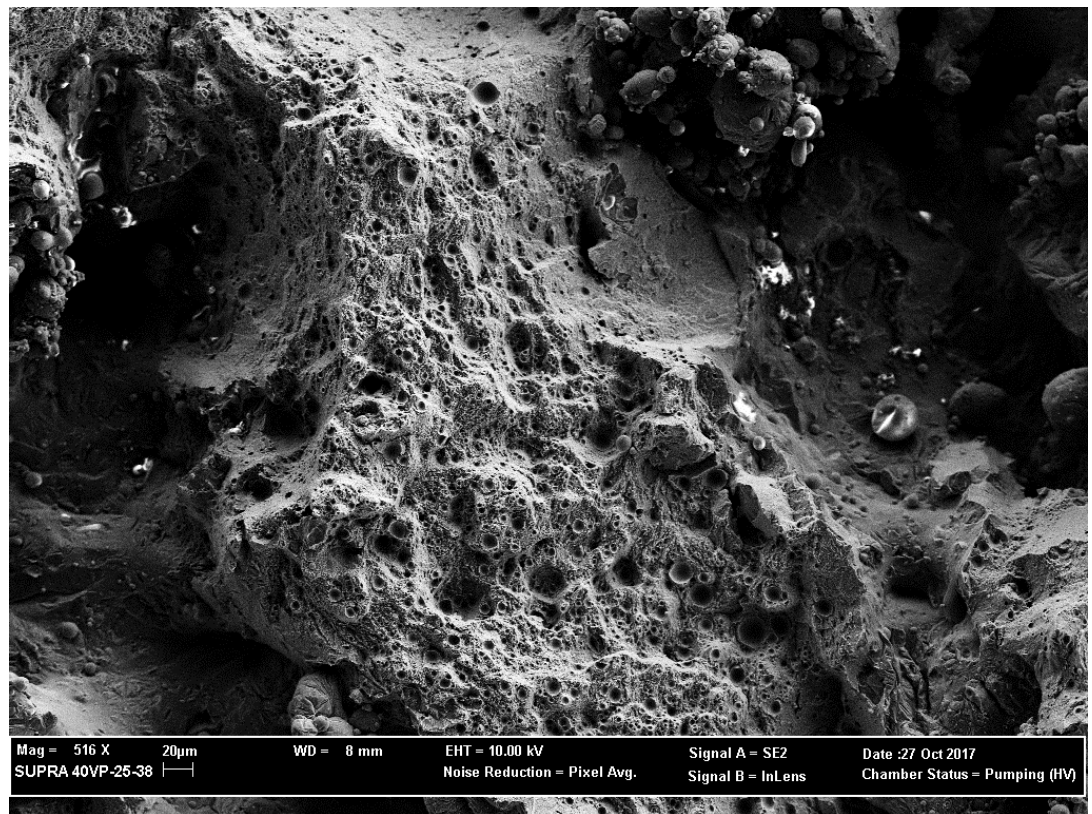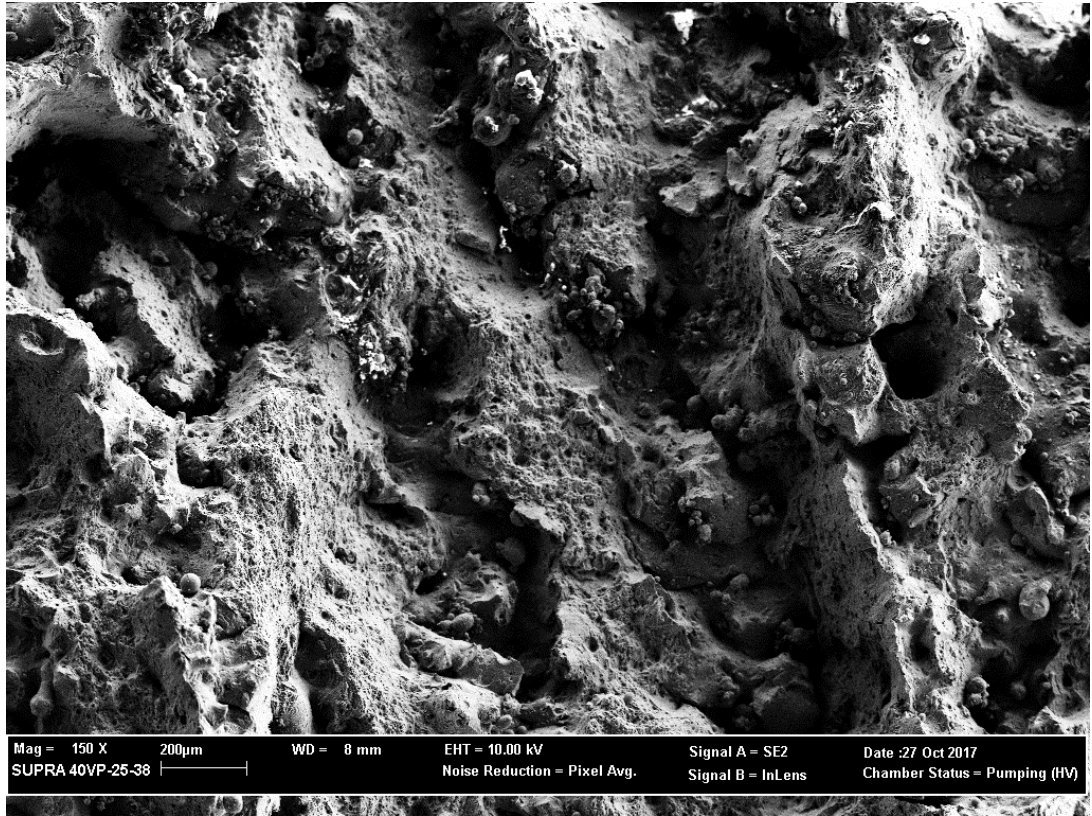
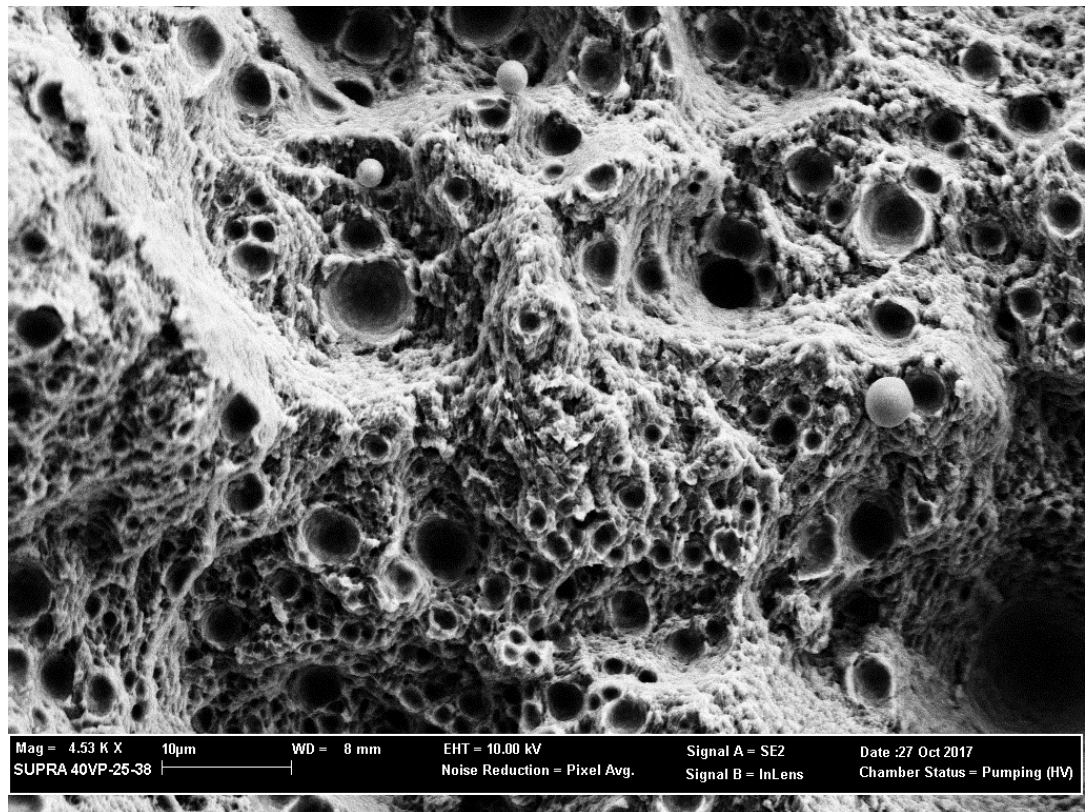Figure 1 SEM images of fracture surface for heat-treated condition sample

Mag = 150 X 200µm WD = 8 mm EHT = 10.00 kV Signal A = SE2 Date :27 Oct 2017
SUPRA 40VP-25-38 Noise Reduction = Pixel Avg. Signal B = InLens Chamber Status = Pumping (HV)

Mag = 516 X 20µm WD = 8 mm EHT = 10.00 kV Signal A = SE2 Date :27 Oct 2017
SUPRA 40VP-25-38 Noise Reduction = Pixel Avg. Signal B = InLens Chamber Status = Pumping (HV)

Mag = 2.15 K X   20µm   WD = 8 mm   EHT = 10.00 kV   Signal A = SE2   Date :27 Oct 2017
SUPRA 40VP-25-38   Noise Reduction = Pixel Avg.   Signal B = InLens   Chamber Status = Pumping (HV)

Mag = 4.53 K X   10µm   WD = 8 mm   EHT = 10.00 kV   Signal A = SE2   Date :27 Oct 2017
SUPRA 40VP-25-38   Noise Reduction = Pixel Avg.   Signal B = InLens   Chamber Status = Pumping (HV)
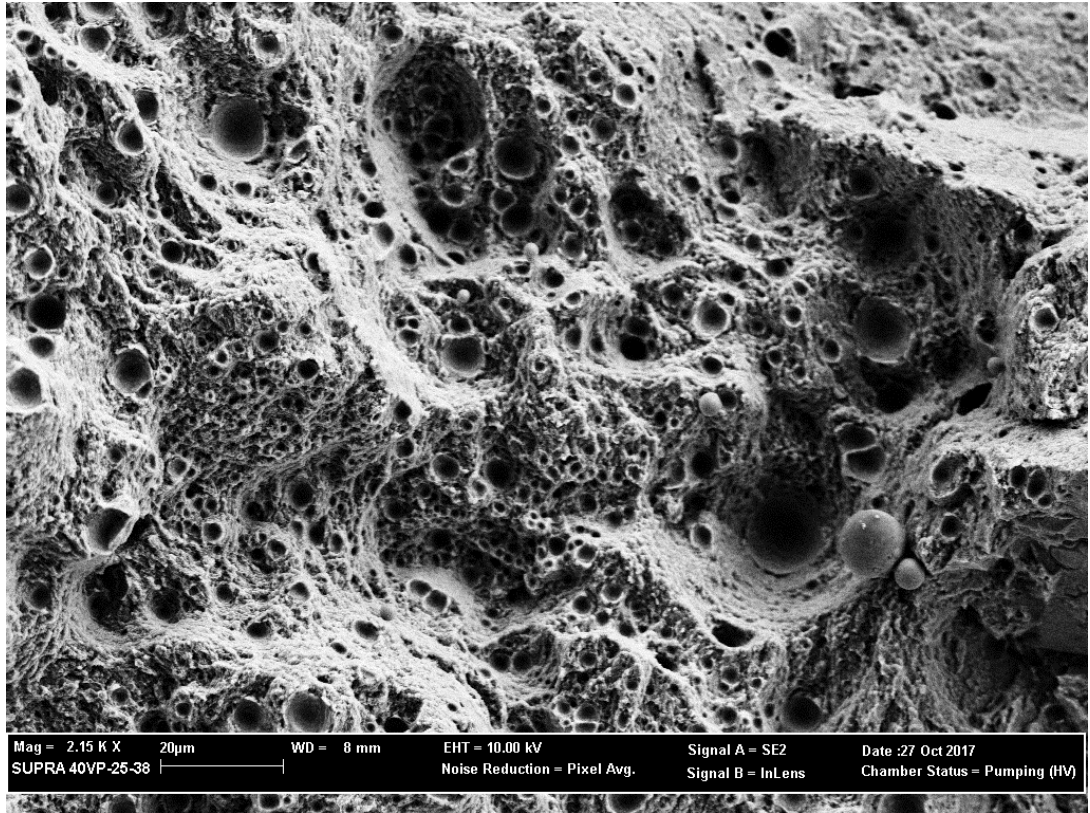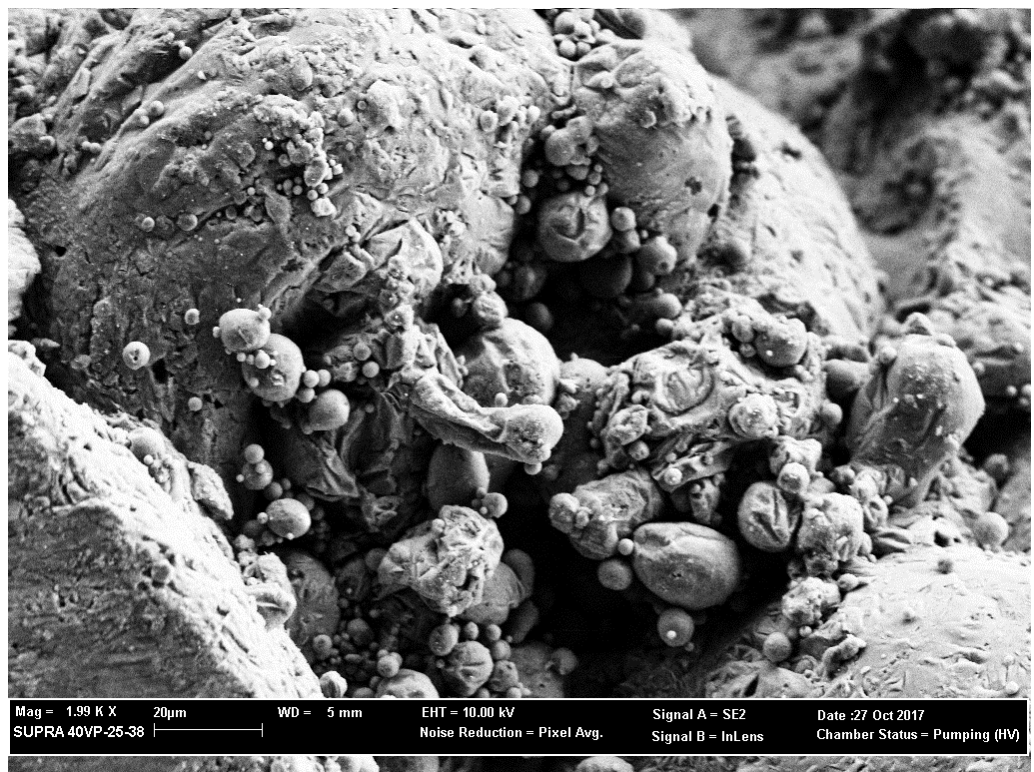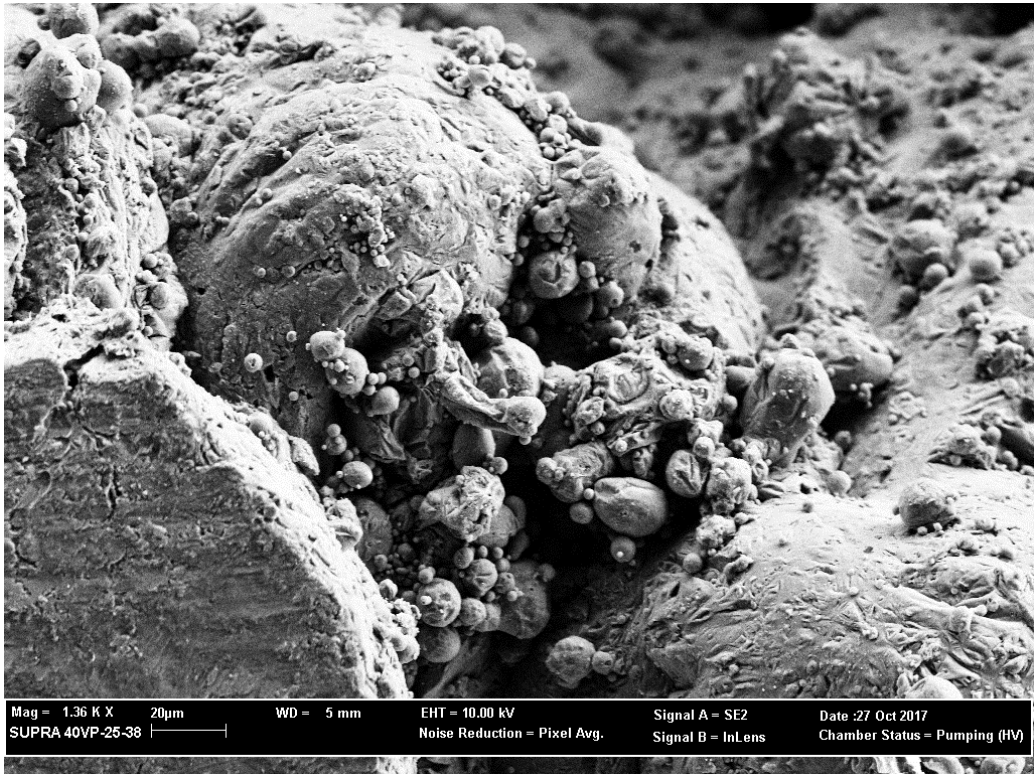
Figure 1 SEM images of fracture surface for as-build condition sample

Appendix F

Mag = 1.36 K X   20µm   WD = 5 mm   EHT = 10.00 kV   Signal A = SE2   Date :27 Oct 2017
SUPRA 40VP-25-38   Noise Reduction = Pixel Avg.   Signal B = InLens   Chamber Status = Pumping (HV)

Mag = 1.99 K X   20µm   WD = 5 mm   EHT = 10.00 kV   Signal A = SE2   Date :27 Oct 2017
SUPRA 40VP-25-38   Noise Reduction = Pixel Avg.   Signal B = InLens   Chamber Status = Pumping (HV)
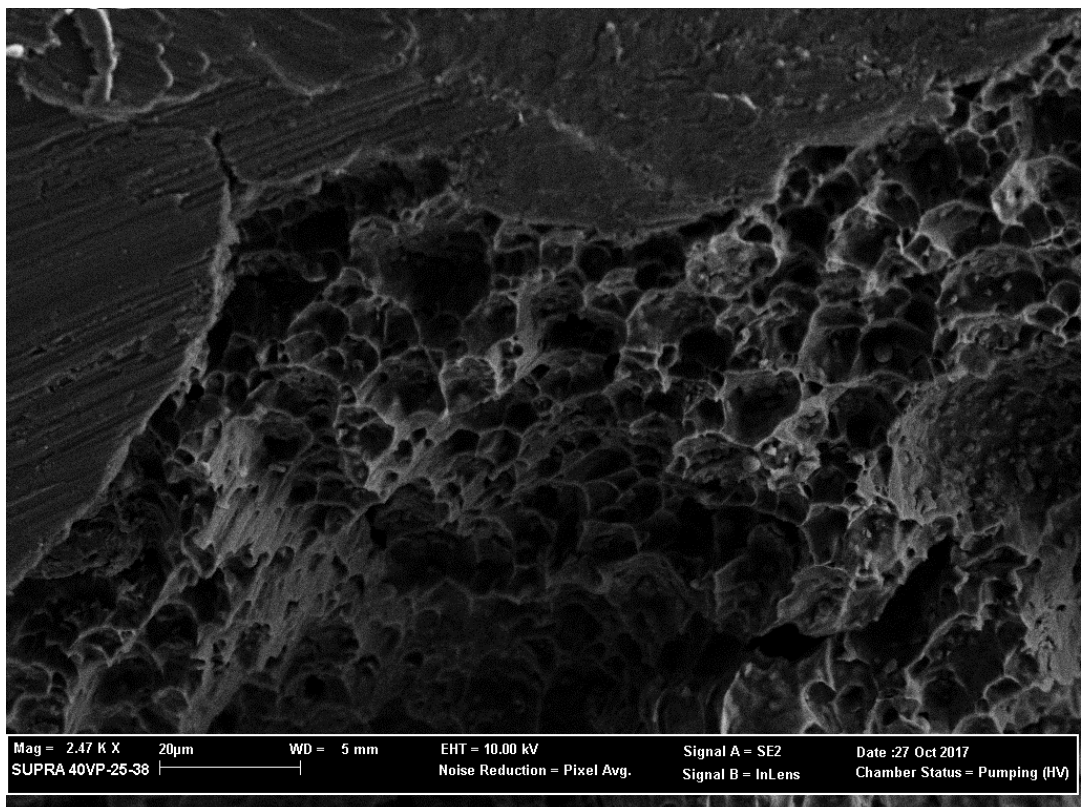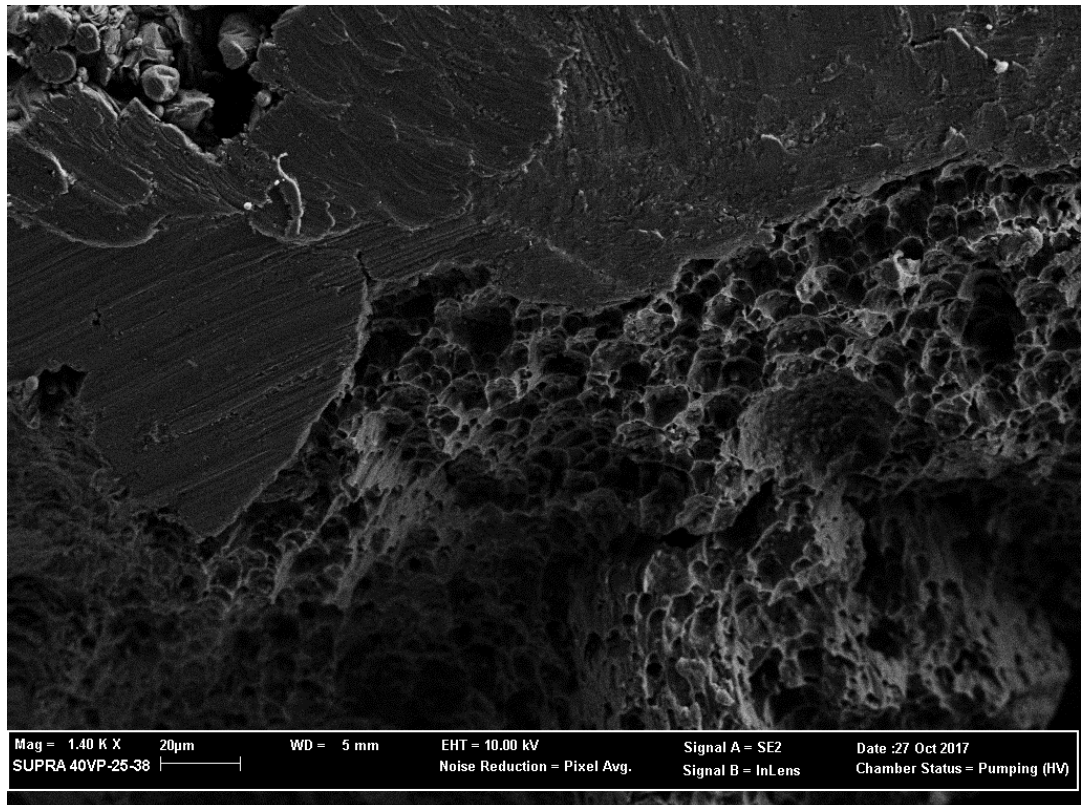
122

Figure 1 SEM images of surface fracture morphology for heat-treated lattice structures